Genetic Modifiers in Response to Ischemia

by

Sehoon Keum

University Program in Genetics and Genomics

Duke University

Date: April 5, 2010

Approved:

_____
Douglas A. Marchuk, Supervisor

_____
Blanche Capel

_____
Greg Crawford

_____
Howard A. Rockman

_____
Beth A. Sullivan

Dissertation submitted in partial fulfillment of
the requirements for the degree of Doctor
of Philosophy in the University Program in
Genetics and Genomics in the Graduate School of
Duke University

2010

ABSTRACT

Genetic Modifiers in Response to Ischemia

by

Sehoon Keum

University Program in Genetics and Genomics

Duke University

Date: April 5, 2010

Approved:

_____
Douglas A. Marchuk, Supervisor

_____
Blanche Capel

_____
Greg Crawford

_____
Howard A. Rockman

_____
Beth A. Sullivan

An abstract of a dissertation submitted in partial fulfillment of
the requirements for the degree of Doctor
of Philosophy in the University Program in
Genetics and Genomics in the Graduate School of
Duke University

2010

Abstract

In a mouse model of ischemic stroke, infarct volume is highly variable and strain dependent, but the natural genetic determinants responsible for this difference remain unknown. To identify genetic determinants regulating ischemic neuronal damage and to dissect apart the role of individual genes and physiological mechanisms in infarction in mice, we performed forward genetic mapping analyses of surgically induced cerebral infarct volume. We have identified multiple quantitative trait loci (QTL) that modulate infarct volume, with a major locus (*Civq1*) on chromosome 7 accounting for over 50% of the variation, with a combined LOD score of 21.7. Measurement of infarct volume in chromosome substitution strains (CSS) and two additional intercrosses validate that *Civq1* on chromosome 7 is present in multiple inbred strains. Interval-specific ancestral SNP haplotype analysis for *Civq1* results in 5 candidate genes. A causative gene underlying *Civq1* may regulate collateral artery formation and genetic variations in the gene may result in the differential outcome of cerebral infarction. Additionally, we have identified a novel infarct volume locus of large effect, *Civq4*, not associated with collateral circulation. In conclusion, the extent of ischemic tissue damage after distal middle cerebral artery occlusion (MCAO) in inbred strains of mice is regulated by genetic variation mapping to at least 4 different loci. A single locus on chromosome 7 determines the majority of the observed variation in the trait in multiple mouse strains. *Civq1* appears to be identical to *Lsq1*, a locus conferring limb salvage and reperfusion in hindlimb ischemia. The identification of the genes underlying these loci may uncover novel genetic and physiological pathways that modulate cerebral infarction and provide new targets for therapeutic intervention in ischemic stroke, and possibly other human vascular occlusive diseases.

Dedication

To the ones I love: my family who is far away and my friends near and far.

Contents

List of Tables

List of Figures

Acknowledgements

I wish to thank my Ph.D. advisor, Dr. Douglas Marchuk, for his excellent mentorship. Throughout my entire graduate school career, he has given me direction, opportunity, and encouragement to refine and build upon the critical scientific thinking necessary to be a scientist. His wealth of knowledge, training, and even friendship inside and even outside of the laboratory has been invaluable to me. I wish to thank all of my thesis advisory committee, Dr. Beth Sullivan, Dr. Howard Rockman, Dr. Greg Crawford, and Dr. Blanche Capel for valuable guidance, diverse perspectives and support in science as well as in my career development during my dissertation research. I would like to thank Dr. Howard Rockman for giving me the opportunity to learn the MCAO surgery and Dr. Lan Mao for all the instructions and techniques on the surgery. I wish to thank Dr. Nina Sherwood and her lab members for advice and encouragement for my project. I also would like to thank Dr. Brian Annex for collaboration and contribution to our joint work that identified chromosome 7 locus for hindlimb ischemia. Thank you to all my current and former fellow lab members for being supportive and fostering a rich environment for scientific development: Carol Gallione, Pei-Lun Chu, Dave McDonald, Hao Tang, Chris Clayton, Dae Un Phillip Lee, Stephanie Li, Katie Qin, Tracy Hadnott, Amy Akers, and Ferrin Wheeler. Lastly, I would like to thank the American Heart Association for my predoctoral fellowship that contributed funding to the work described in this dissertation.

1.

Ischemic Stroke: Disease Pathophysiology, Cerebral Infarction, and Animal Models

1.1 Overview of Ischemic Stroke

Stroke caused by an embolus or local thrombosis results in cerebral ischemia with subsequent brain injury (infarct) in the perfusion territory of the occluded cerebral artery. In general, the severity of tissue damage depends on several factors related to the cerebrovascular circulation including the duration of occlusion, the site of occlusion along the affected vessel, the size of the territory perfused by the vessel, and the extent of the collateral circulation.

Stroke is the third most common cause of death and the most common cause of disability in adults in developed countries. According to the recent statistics released from the American Heart Association, annual mortality from new and recurrent stroke is over 200,000. The national incidence of first stroke is estimated at 750,000 per year in the United States, of which 80% are ischemic and the remainder is due to intracranial hemorrhage. The prevalence of ischemic stroke increases with age and affects approximately 5-6% of individuals 65 to 74 years old and 9-12% of individuals over the age of 75. Women appear to be less susceptible to stroke damage and the risk of stroke is lower in premenopausal women compared to men of the same age [2]. However, the incidence of stroke in women rapidly increases after menopause [3].

1.2 Genetic risk factors – stroke susceptibility

Epidemiologic studies have documented that approximately two-thirds of the population-attributable risk for stroke is due to genetic factors [4]. However, due to genetic and phenotypic heterogeneity and multiple stoke subtypes, the most significant genetic components of human stroke risk have yet to be explained [5]. Two independent family-based genome-wide linkage analyses have identified two causative genes (PDE4D and ALOX5AP) conferring susceptibility to common ischemic strokes [6,7], but the roles of these genes in other populations remain unclear [8,9]. In addition, through a large-scale case–control association study in the Japanese population, protein kinase C-eta (PRKCH) and angiotensin receptor like-1 (AGTRL1) genes were identified as risk factors for brain infarction [10,11] The exact biological roles of these genes were not elucidated but are likely related to atherosclerotic risk.

1.3 Genetic risk factors – stroke outcomes

Although significant progress has been made in the identification of genetic risk factors for human ischemic stroke, identification of genetic risk factors for stroke outcomes has been severely limited. There have been few studies of the genetic determinants of stroke outcomes in humans but most studies have focused on apolipoprotein E (ApoE) as a possible influence on outcomes in ischemic and hemorrhagic strokes. In a large meta-analysis, ApoE ε4 polymorphism carriers showed significantly smaller infarct volumes compared with non-carriers after acute ischemic onset [12]. These findings have been partly validated in mouse models. Infarct volume after middle cerebral artery occlusion (MCAO) was significantly larger in ApoE4/4 homozygous knock-in mice [13]. However, the association between the ApoE4 polymorphism and cerebral infarction is not seen in other populations and the exact role of ApoE/4 in the risk of stroke is uncertain [14, 15].

To date, forward genetic approaches in rodent models of stroke have likewise provided only limited understanding of stroke outcomes. The stroke-prone spontaneous hypertensive rat (SHRSP) has been used to map three loci Str1 (Chr 1), Str2 (Chr 4), and Str3 (Chr 5) which modify the time to stroke onset in SHRSP fed a stroke-permissive diet [16]. The Str2 locus was later identified in an independent study as a genetic determinant of infarct volume after permanent distal MCAO [17]. The Str2 locus accounts for 67% of the total variance in infarct volume and co-localizes with arterial natriuretic peptide (ANP). Although the effect of the ANP marker on infarct volume was shown to be stroke-specific and independent of systolic or mean arterial blood pressure, the role of the ANP gene in ischemic stroke is still unclear in both rats and in humans. Moreover, the genetic variants underlying Str1, Str2, and Str3 have yet to be identified.

1.4 Ischemic Outcome: Cerebral infarction

An acute occlusion of cerebral arteries results in cerebral ischemia with subsequent cell death within the perfusion territory of the affected vessels. The damage that occurs in crucial central brain regions causes profound permanent disability in many patients. The severity of tissue injury depends on the duration of occlusion, the site of occlusion along the vessel, and the amount of collateral circulation. Complex pathophysiologic processes are involved in the final determination of long-term neurologic outcome (infarction), including excitotoxicity, peri-infarct depolarization, inflammation, and apoptosis [18].

In central areas of the stroke, blood flow deficits were severe and cells died rapidly. But in peripheral areas of the stroke, blood flow deficits were milder. This moderate ischemic zone (ischemic penumbra) remains metabolically active but electrically

dysfunctional [19]. The disruption of cellular homeostasis in the penumbra then leads to slow cell death and a step-by-step growth of the lesion. Both clinical and experimental animal studies demonstrate that early on after stroke onset, the penumbra can account for up to 50% of the volume that will later progresses to infarction. Two broad pathophysiological mechanisms have been known to determine the final outcome of cerebral infarction in ischemic stroke: the level of residual blood flow and signals of death mediators corresponding to penumbra (Figure 1). The processes that lead to cell death within the penumbra are the subjects of intensive research as the targets of acute stroke therapy [20]. The salvage of the penumbra depends on both vascular collateral circulation and endogenous neuroprotective factors, but the relative importance of each is the subject of debate [21].

1.4.1 Vascular factors contributing to infarction

A collateral vessel is a branch of artery that interconnects adjacent major arterial trees (arteriole-to-arteriole anastomoses). Pre-existing collateral arteries interconnecting these major arteries have been identified in the coronary, cerebral, and peripheral circulation of various species [22]. The number and the size of these collateral arteries varies between species and tissues. Thus, its has been postulated that these difference in collateral circulation may result in different degree of protection after arterial occlusion.

There are two major collateral systems interconnecting the main supplying arteries of the brain: the circle of Willis and leptomeningeal anastomoses [18,23]. The circle of Willis is responsible for the redistribution of blood supply under conditions of extra-cranial vascular occlusion. The pial network of leptomeningeal anastomoses play roles in the redistribution of blood supply when the constricted artery lies distal to the circle of

Willis. When critical narrowing or occlusion of the main artery causes a pressure drop across the collaterals, the increased flow/shear stress triggers an active outward remodeling of the vascular wall, leading to an increase in vascular diameter and conductance [24]. These anastomoses build up the highest perfusion pressure in the peripheral branches of the brain arteries, resulting in the preferential protection of the penumbra. Individual variability of these anastomoses has been suggested to contribute to a wide range of tissue damage from small lesions located in the central region to large infarcts involving the total vascular supplying territory [18,23]. However, whether the collateral circulation in the pial area of the brain significantly modulates infarct volume is still controversial mainly due to apparently variable presence of these vessels plus absence of good imaging methods in humans.

1.4.2 Endogenous neuroprotective factors contributing to infarction

The mammalian brain can adapt to cerebral ischemia to promote cell survival in the face of subsequent injury. Tolerance to ischemia in the brain refers to a state in which cells become resistant to the damaging effect of a period of cerebral ischemia through a noxious stimulus, resulting in reduced cell death. A number of different mechanisms including vessel occlusion, heat shock, depolarization, and hypoxia, have been found to trigger protective effects against tissue damage from cerebral ischemia [25].Significantly, the cells within the penumbra receive the most benefit from ischemic tolerance, as their chances of survival are increased [19]. The effectors involved in these preconditioning-protective responses are either produced *de novo* as a result of changes in gene expression or induced by post-translational modification of existing proteins. Even prior to ischemia, preconditioning establishes a latent cerebroprotective phenotype. In particular, the inhibition of programmed cell death and augmentation of programmed c-

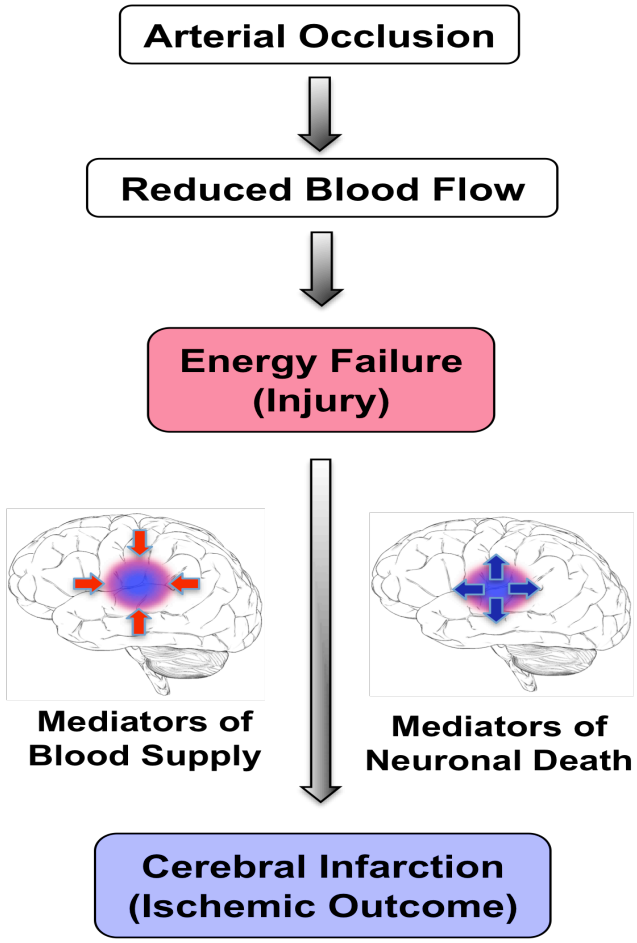

Figure 1. Two broad mediators determining severity of cerebral infarction in ischemic stroke. After initial injury by obstructed blood flow, the level of residual blood flow and signals of death mediators corresponding to the penumbra determine the final outcome of ischemic tissue damage in the brain.

-ell death and augmentation of programmed cell survival pathways have been found to contribute to ischemic tolerance [25].

Different responses to preconditioning have been observed in rodent models of stroke. The stroke-prone rat strains showed a lower response to ischemic preconditioning and a larger infarct size than rats that were not prone to stroke [26]. Moreover, transgenic mice for several hypoxia or apoptosis-induced genes involved in ischemic tolerance, such as heat shock protein (Hsp)-70, Bcl-2, Bcl-XL, and Bag1 showed substantially reduced infarct volume after MCA occlusion [27-30]. Consistent with this idea, differences in gene expression or protein activity between B6 and BALB/c strains were postulated to be involved in the induction of ischemic tolerance for protection against ischemic insults after permanent MCA occlusion [31].

1.5 Animal Models of Stroke

Animal models of ischemic stroke have been used to investigate the pathophysiologic events occurring after cerebral ischemia. In particular, two major approaches have been attempted to treat ischemic stroke: recanalization and neuroprotection. For this reason, most stroke models induce cerebral ischemia within the MCA territory in order to be most relevant to human thrombo-embolic stroke (Figure 2). Table 1 illustrates that MCA occlusion models vary both in the extent of occlusion (permanent vs. temporal occlusion) and the site of occlusion (proximal vs. distal portion of the vessel). Pathophysiological mechanisms and size of the ischemic lesion vary according to the model. Direct surgical methods that occlude distal MCA have been shown to produce more restricted and reproducible damage to the cerebral hemisphere (frontal and pariet-

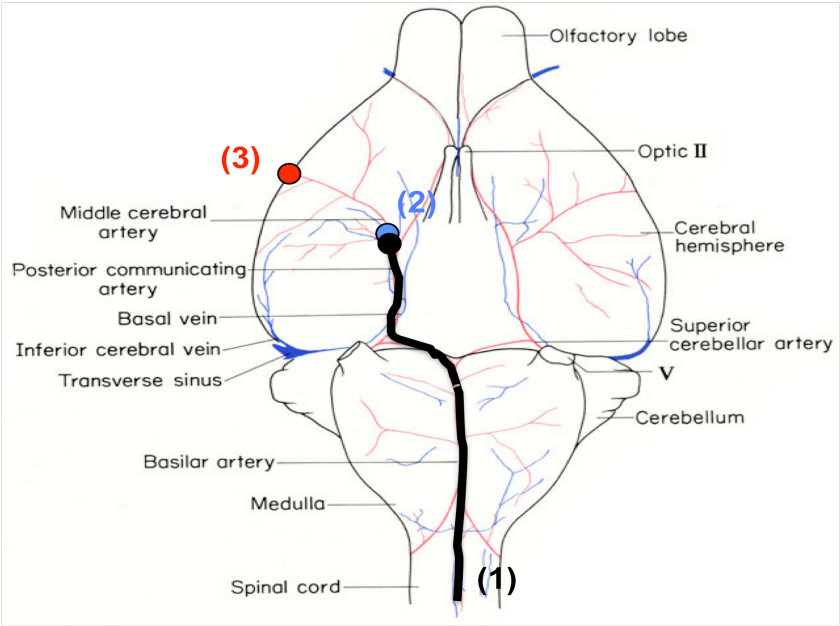

Figure 2. Three major surgical MCAO methods to induce focal cerebral ischemia in animal models of ischemic stroke. (1) Intraluminal suture insertion, (2) proximal cauterization, and (3) distal cauterization. The original image in the mouse anatomy atlas of the Jackson laboratory was modified.

Table 1. Three major surgical methods for MCAO

	Intraluminal Suture (1)	Proximal (2)	Distal (3)
Occlusion	Transient	Permanent	Permanent
Size of infarction	Variable/ Large	Reproducible/ Large	Reproducible/ Small
Infarcted area	Most ipsilateral cerebral hemisphere	Most ipsilateral cerebral hemisphere	Only cerebral cortex
Mortality	High	High	Very low
Advantage	Reperfusion	-	-
Disadvantage	Hyperthermina/ Hemorrhage	Hyperthermina/ Hemorrhage	Cranietomy

-al cortex) without hyperthermia than common intraluminal suture and proximal MCA occlusion models [32,33]. Permanent occlusion of distal MCA method shows some advantages to temporal occlusion, as it does not directly affect flow in any other major artery [34-37]. Furthermore, electrocauterization permanently and exclusively shuts off blood flow and avoids the variable size of the cortical infarct that can result from the suture ligation method [35,37].

1.6 Proposal of Research

Experimental studies in stroke in rodents have provided an extensive body of the current understanding of the pathophysiological mechanisms underlying cerebral infarction and have spurred the investigation of the potential therapeutic effects of those mechanisms. Many genes and biochemical pathways that regulate the size (volume) of the infarct when ischemia is induced have been identified in genetically manipulated mouse models. Unfortunately, evidence based solely on gene knockout or transgenic mice does not always provide insight into mechanisms involved in the natural (innate) disease state [38,39]. Despite many potential therapeutics have been shown to alleviate severity of cerebral infarction in animal models of experimental stroke, very few have been found to have similar beneficial effects in clinical trials. Experimental gene deletion or transgenic over-expression creates an artificial genetic and physiologic state that can be far removed from that found in naturally occurring disease. Genetic risk factors and the pathophysiological differences that determine the outcome of ischemic stroke in the natural state remain uncertain.

In a well-established surgically induced model of stroke, we and others have reported [34-37,40] that innate sensitivity to focal cerebral ischemia is highly variable and strain

dependent. Here we have extended these observations to 16 inbred mouse strains, where we found a wide range of phenotypic variation in infarct volume after permanent MCAO, providing further evidence that the innate response to focal cerebral ischemia is under strong genetic control [41]. Despite the ongoing debate on mechanisms (vascular/anatomic vs. neuronal), experimental proof is lacking for any of the hypotheses, since all data supporting each view derives from correlative studies, lacking any genetic support. Thus, the pathophysiological mechanisms responsible for the differential stroke outcomes between inbred strains are not understood yet. The observed phenotypic differences among strains may be attributable to multiple mechanisms, each driven by sequence variation at distinct genes.

Therefore, to identify genetic determinants critical to ischemic tissue damage and to dissect apart the role of individual genes and physiological mechanisms in infarction in mice my research described in this dissertation has employed a forward genetic quantitative trait locus (QTL) mapping approach.

Specific Aim 1: To genetically map chromosomal loci determining the infarct volume. In the well-established mouse model of focal cerebral ischemia, innate sensitivity to focal cerebral ischemia has been shown to be highly variable and strain dependent. We have extended these observations to 16 inbred mouse strains, where we found a wide range of difference in infarct volume after permanent distal MCAO, providing further evidence that the innate response to focal cerebral ischemia is under strong genetic control. We have exploited these differences to a natural genetic determinant of infarct volume. In an F1 intercross between B6 and BALB/c, we have

mapped a locus on distal chromosome 7 (LOD score = 11.9) that contributes over 50% of the observed variation in infarct volume.

Specific Aim 2: To identify a causative gene underlying the ischemic tissue damage QTL and establish the mechanism of action for the chromosome 7 locus. We identified that the chromosome 7 locus has shown a large effect on infarct volume, accounting for over 50% of phenotypic variation, which would be the most likely locus to study to lead to underlying gene identification. Comparison of the infarct volume data with the ancestral SNP haplotype sharing pattern in the 5 strains used for mapping has enabled us to fine-map the chromosome 7 QTL. Interestingly, during the course of my research we have found that cerebral infarction QTL (*Civq1*) maps to the identical genomic position of chromosome 7 as a limb salvage QTL (*Lsq1*) identified in a mouse model of hindlimb ischemia. These results lead us to hypothesize that genetic variation in a gene underlying the chromosome 7 locus determines ischemic outcome in multiple tissues through the same physiological mechanism.

The research outlined in my dissertation will provide insight into the biochemical pathways modulating ischemic tissue damage based on natural endogenous variation in a genetically tractable mammal. These genes are not likely to be identified directly in human vascular occlusive disease patients, but the pathways controlling ischemic tissue injury are likely to be conserved across related species. Identification of novel genes modulating infarction will provide new and physiologically relevant insight into the pathways and mechanisms involved in tissue damage. In the long-term, this work may provide novel targets for therapeutic intervention of ischemic stroke and other vascular diseases.

2.

Identification of Natural Genetic Determinants of Cerebral infarction

1. Introduction/ Rationale

In a well-established surgically induced model of stroke, we and others have reported [34-37,40] that innate sensitivity to focal cerebral ischemia is highly variable and strain dependent. Here we have extended these observations to 16 inbred mouse strains, where we found a wide range of phenotypic variation in infarct volume after permanent MCAO, providing further evidence that the innate response to focal cerebral ischemia is under strong genetic control [41]. Despite the ongoing debate on mechanisms (vascular/anatomic vs. neuronal), experimental proof is lacking for any of the hypotheses, since all data supporting each view derives from correlative studies, lacking any genetic support. Thus, the pathophysiological mechanisms responsible for the differential stroke outcomes between inbred strains are not understood yet.

We reasoned that the observed phenotypic difference among the strains might result from multiple mechanisms, each driven by different genetic loci. To identify a genetic determinant regulating ischemic infarct outcome and to dissect apart the role of individual genes and pathophysiogical pathway in cerebral infarction, we performed QTL mapping with selected multiple inbred strains and identified the genomic locations contributing to these phenotypic differences. By genetically isolating the loci in congenic animals, we sought to dissect apart the role of individual genes and physiological pathways in infarction.

2.2 Results

2.2.1 Variability in the volume of cerebral infarction in different genetic backgrounds

Five studies have shown differences in infarct volume between B6 and BALB/cByJ (hereafter BALB/c) mice [34-37,40]. We first sought to determine whether the published differences in infarct volume between the 2 strains were reproducible in our hands. As described earlier in Chapter 1, in order to maximize survival and the reproducibility of the extent of ischemic tissue damage that is critical for any measurement of a quantitative trait, we chose direct occlusion of the right distal MCA, which exclusively and permanently eliminates blood flow to tissue distal to the occlusion [34-37]. In contrast to proximal artery occlusion models, disruption of the distal MCA limits ischemic tissue damage to frontal and parietal cortex, reducing ischemia-associated death and providing a compact territory of tissue damage for quantitative measurements [29]. Distal occlusion of the MCA beyond the circle of Willis also eliminates any potential effects of anatomic variation in the anterior and posterior commissural arteries. Moreover, this method does not directly affect flow in any other major artery, maximizes postsurgical survival, and avoids the variable size of the cortical infarct that can result from the suture ligation method [34-37]. Infarct volume was measured at 24 hours, the time point showing the maximum size [29]. Other study also showed that with each successive day beyond this, the size of the infarct gradually decreases due to resorption of the infarcted tissue [42]. We observed that infarct volumes 24 hours after MCAO were significantly different between inbred strains B6 and BALB/c (Figure 3).

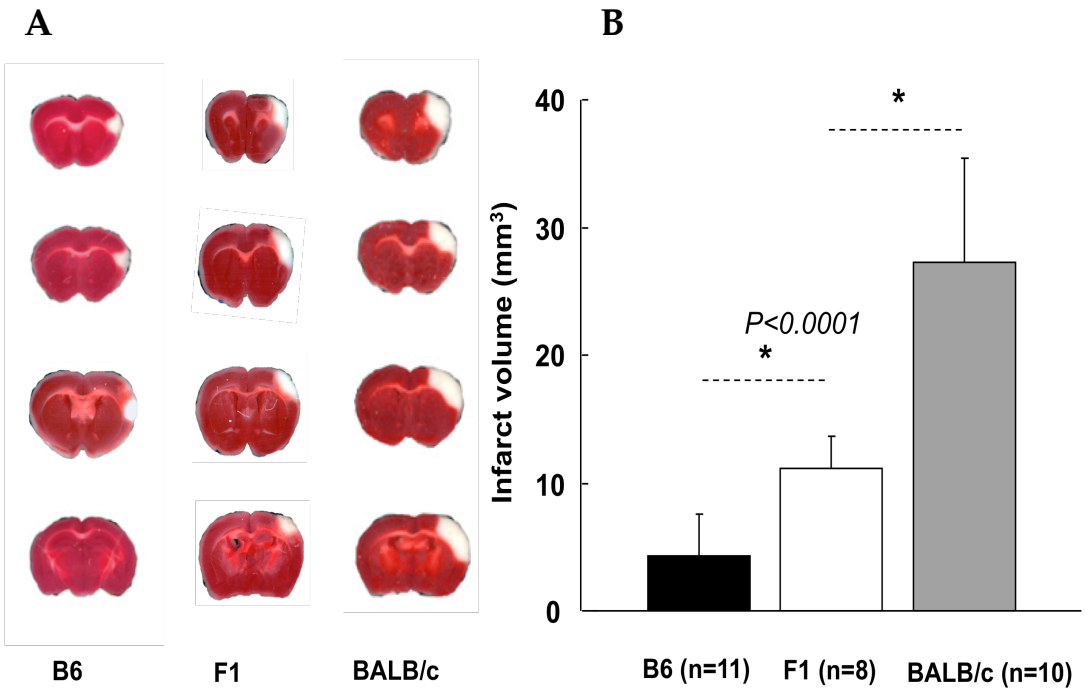

Figure 3. Distinct outcomes of cerebral infarction from surgically-induced focal cerebral ischemia in strain C57BL/6 (B6), BALB/c, and F1 (B6XBALB) mice. (A) Focal cerebral ischemia was induced and tissue damage was measured by TTC staining 24 hours after permanent distal MCAO (white = damaged tissue). The posterior faces of representative 1mm coronal sections from the three mouse strains are shown. (B) Mean infarct volumes (±SD) in the three strains of mouse. F1 mice exhibit significantly different infarct volumes from B6 as well as from BALB/c at the * *P<0.001* level.

Infarct volume of BALB/c mice was 6-fold larger (27.3 mm^3) than B6 mice (4.4 mm^3). F1 mice show an intermediate infarct size compared to the extremes of the parental strains. We then determined infarct volumes for an additional 12 inbred strains encompassing the classical inbred strains recently used for mouse genome resequencing [43,44]. Infarct volumes were highly reproducible among individual animals of the same inbred strain. Across strains, we observed a wide range of infarct volume (Figure 4), with as much as 30-fold difference between the strain pair at the phenotypic extremes (C57BLKS/J versus BALB/c). Heritability (H^2) of the trait of infarct volume after permanent middle cerebral artery occlusion was estimated to be 0.88. Postsurgical survival did not vary among strains, as only a single animal from a total of more than 100 did not survive the ischemic insult.

2.2.2 A chromosome 7 locus contributes the predominant effect on infarct volume

These marked differences in sensitivity to focal cerebral ischemia between inbred strains confirm a strong genetic influence on underlying mechanisms of cerebral infarction. To exploit these differences for identification of natural genetic determinants of infarct volume, we performed a reciprocal F1 intercross between strains B6 and BALB/c. Infarct volumes in F2 progeny exhibited a large variance, ranging from 0.2 to 43.6 mm^3 (Figure 5A). Infarct volume was not correlated with either body size or sex in the F2 cohort (Figure 5B). Similarly, infarct volume was not correlated with the strain origin of the males or females in the (F1) cross, indicating that neither the mitochondrial genome nor the Y-chromosome contributes to the phenotypic differences.

A total of 105 F2 mice were genotyped for 239 SNP markers that were informative in this cross. The average spacing between fully informative SNP markers was 6.8 ± 1.6 cM, aff-

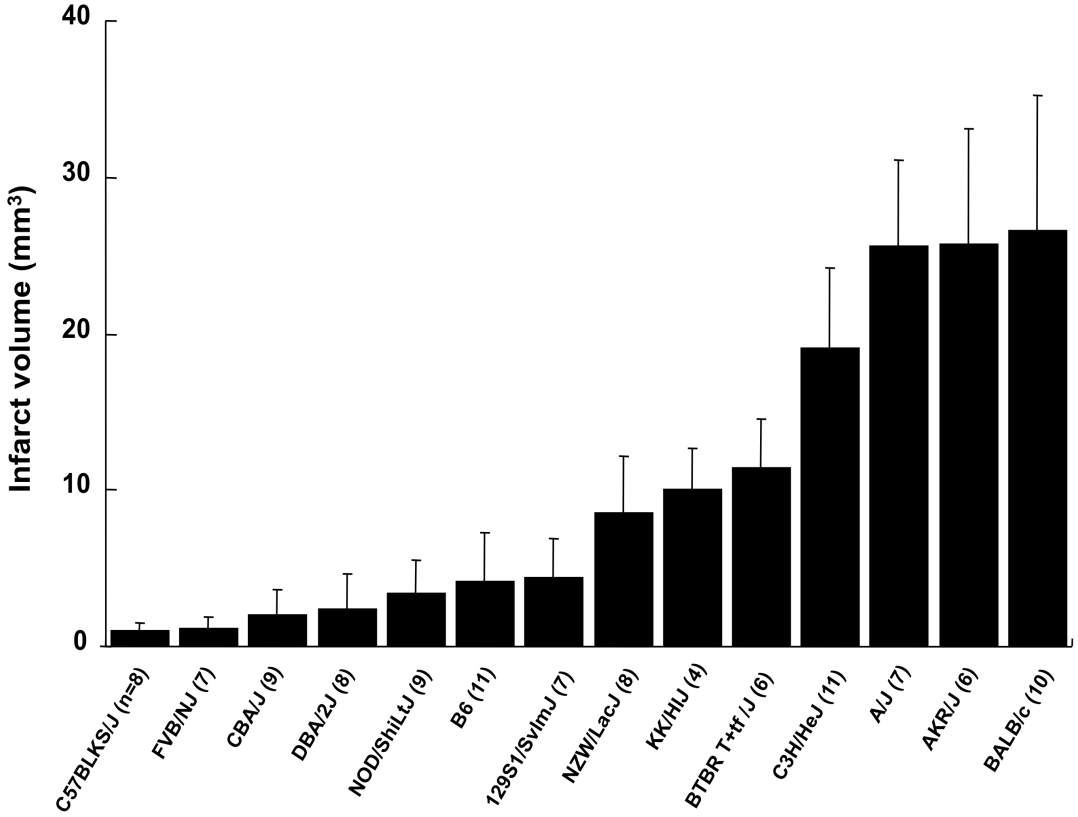

Figure 4. Distribution of infarct volumes across 14 inbred strains of mice. The value in parentheses refers to number of animals used per strain. Values represent mean ± SD.

-ording complete coverage of the mouse genome. We identified a highly significant locus (LOD score=11.9) mapping to distal chromosome 7 influencing infarct volume. In addition, we identified 2 suggestive QTL mapping to chromosome 1 and 8 (Figure 6). We designated these loci *Civq* (Cerebral infarct volume QTL). Table 1 shows the characteristics of the 3 QTL, including peak SNP marker location, LOD score, effect size, and mode of inheritance. *Civq1* is the strongest QTL that accounts for 56% of the observed variance in infarct volume. As predicted from the parental and F1 strain phenotypes, the B6 allele shows a co-dominant protective effect on infarct volume. To determine the allelic contribution of the effect of *Civq1*, infarct volumes were evaluated against genotype at the highest LOD score among all of the informative SNP markers (Figure 7). There was no statistical difference in infarct volume between F2 animals homozygous for the B6 and BALB/c allele at rs13479513 when compared with that of the parental strains. There was also no difference between F2 animals heterozygous at rs13479513 and F1 (B6/BALB) animals. Therefore, even though other loci are also present across the genome, *Civq1* alone is able to explain nearly all of the phenotypic difference in infarct volume observed between the 2 inbred strains.

The two other QTL located on chromosome 1 (*Civq2*) and 8 (*Civq3*) explain 7% and 12%, respectively, of the variation in the trait. At *Civq2*, the B6 allele displayed a dominantly acting protective effect on infarct volume. By contrast, although the BALB/c strain shows larger infarct volume, the BALB/c allele at *Civq3* conferred a protective additive effect to the trait (Table 2). These opposing phenotypic effects of the B6 (or BALB/c) alleles at the minor loci would counteract each other in the parental strains, and this may explain the robust correlation between overall phenotype in the F2 cohort and genotype

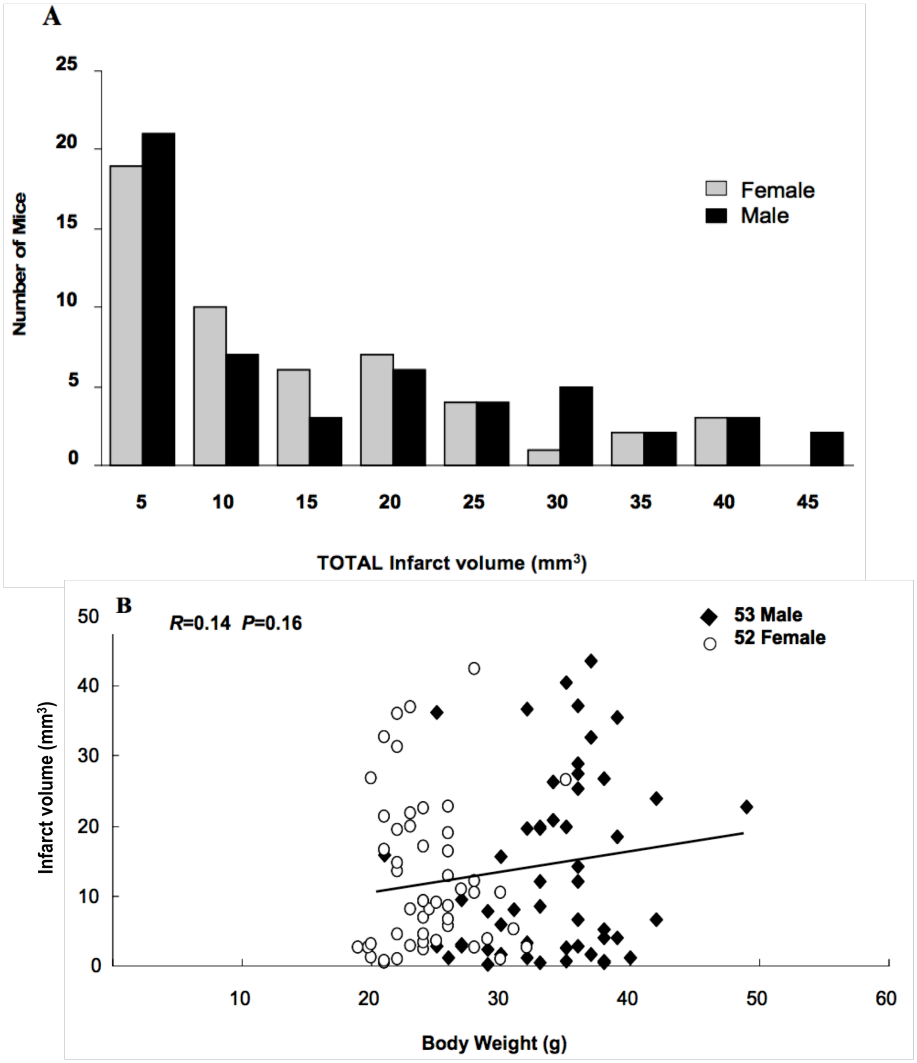

Figure 5. Infarct volume is not influenced by the sex or body weight of the F2 (B6×BALB/c) animals. **A.** The graph shows the distribution of infarct volumes between male and female F2 animals. A total of 53 male and 52 female F2 progeny were analyzed to examine gender effects on the differential outcomes of focal cerebral ischemia. The nonparametric Kruskal-Wallis statistical analysis shows no significant difference between male and female mice. **B.** Infarct volume does not correlate with body size of F2 (B6×BALB/c) animals. A scatter plot shows the relationship between infarct volumes and body weights in 53 male and 52 female F2 animals. Each point indicates an individual value of a F2 mouse. The correlation coefficient (R) and significance (P) are shown. Body weight was not correlated with the volumes of cortical infarct in the cross.

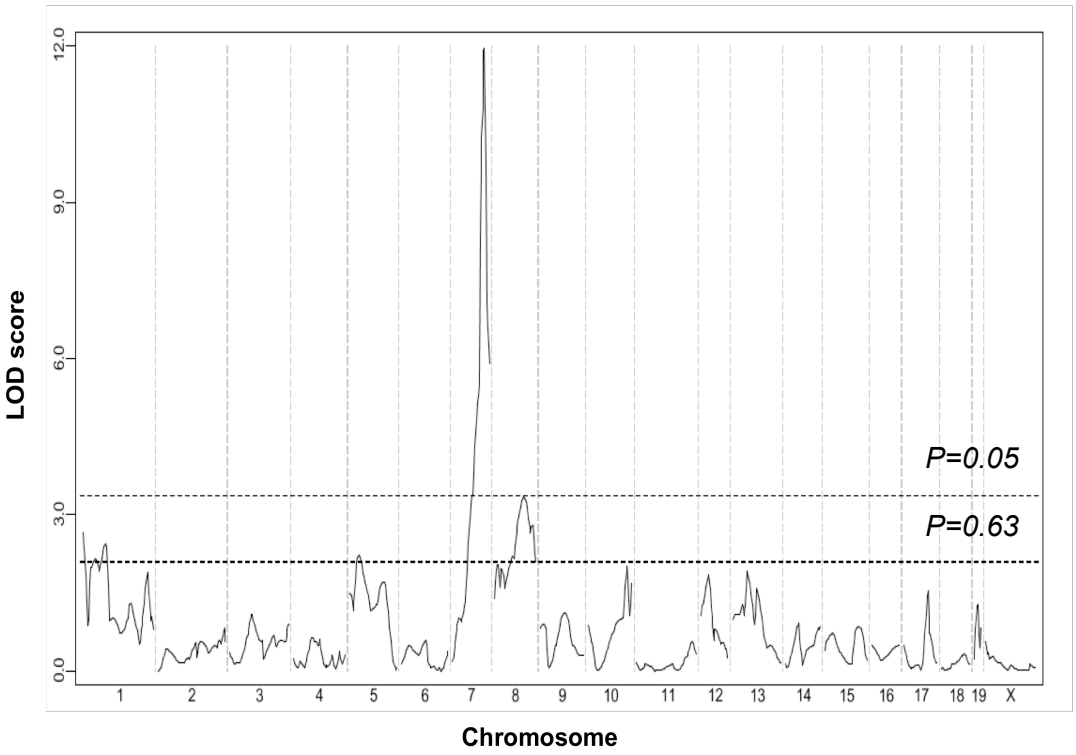

Figure 6. A major locus for infarct volume maps to distal chromosome 7. The graph presents the results of a genome-wide linkage scan for infarct volume 24 hours after permanent MCAO in 105 (B6xBALB/c) F2 progeny. Chromosomes 1 through X are represented numerically on the x-axis. The relative width of the space allotted for each chromosome reflects the relative length of each chromosome. The y-axis represents the LOD score. The significant (*P=0.05*) and suggestive (*P=0.63*) levels of linkage were determined by 1000 permutation tests. One region of the genome, distal chromosome 7, displays highly significant linkage to the trait, with a LOD score of 11.9. Two loci mapping to chromosome 1 and 8 only reached the *P=0.63* suggestive level.

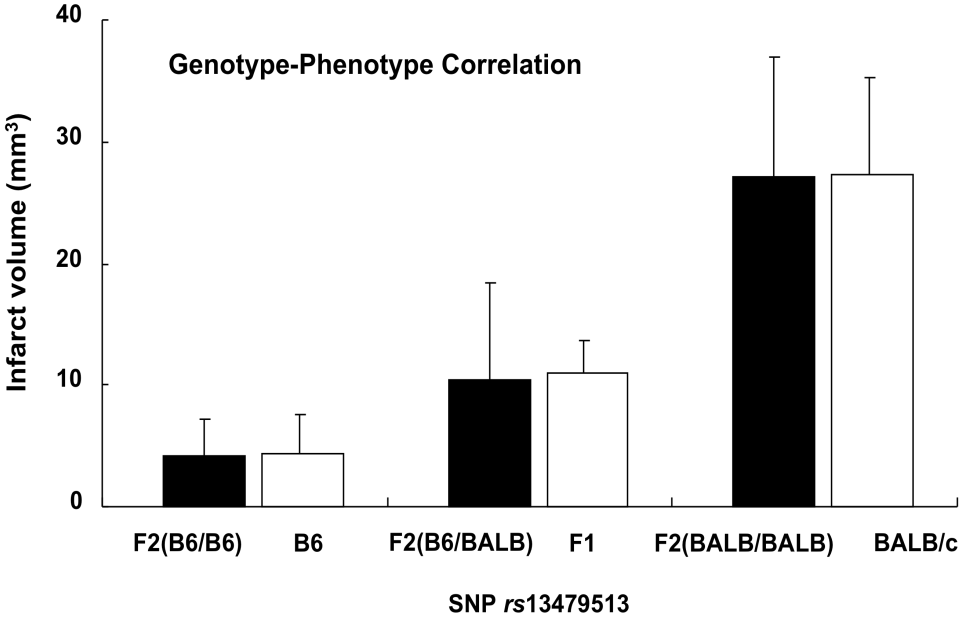

Figure 7. The chromosome 7 QTL contributes the predominant effect to the infarct volume trait. The histogram displays the phenotypic effect of the allele at SNP rs13479513 (in parenthesis) on infarct volume in comparison with the overall phenotype of the parental strains. F2 animals homozygous for the BALB/c allele (n=29) exhibit higher mean infarct volume than mice homozygous for the B6 allele (n=32). Infarct volumes for F2 animals heterozygous at the SNP (n=44) are intermediate to those of the homozygous animals. Significantly, there is no difference in infarct volume between F2 animals homozygous for the B6 or BALB alleles at rs13479513 when compared with that of the respective B6 or BALB/c parental strains. Similarly, there is no difference between F2 heterozygotes at rs13479513 and F1 (B6/BALB) animals. Thus, the parental origin of the allele at this locus effectively determines infarct volume, regardless of the genotype throughout the remainder of the genome. Error bars represent SD.

Table 2. Summary of the three QTLs identified in an intercross (B6x BALB/c)

Location	LOD score	Effect size (%) †	Protective allele	Mode of Inheritance	Marker at peak	Overlapping QTL‡
Chr 1 (*Civq2*)	2.7*	7	B6	Dominant	rs13475783	
Chr 7 (*Civq1*)	11.9	56	B6	Additive	rs13479513	LS-q1(Dokun et al., 2008)
Chr 8 (*Civq3*)	3.0*	11	BALB/c	Additive	rs8253516	

* Suggestive QTL
† The percentage of the total trait variance attributable to this locus
‡ Overlapping QTL identified in previous studies

at the major locus, *Civq1*. None of these *Civq* loci exhibit epistatic interactions with other regions of the genome.

2.2.3 Chromosome Substitution Strains between validate *Civq1* and *Civq2*

To confirm the presence of an infarct volume locus mapping to mouse chromosome 7, we used the C57BL/6J-Chr7A/J/NaJ chromosome substitution strain (hereafter CSS7) in which strain A/J chromosome 7 has been substituted into the B6 background [45]. We first examined infarct volume of the donor A/J strain. A/J mice exhibited an infarct volume 6-fold larger than that of B6 but not statistically different from that observed for BALB/c (Figure 8). Based on this finding, we next determined the phenotype of the CSS7 mice. The CSS7 mice displayed large infarct volumes identical to the A/J parental strain that provides chromosome 7. This confirms that chromosome 7 harbors a locus with a large effect on cerebral infarction, with the B6 allele providing a protective effect. Additionally, this suggests that the A/J and BALB/c alleles at the chromosome 7 locus may be identical because of ancestral relatedness.

To verify existence of the B6 protective allele on *Civq2* responsible for 7% of phenotypic variance, we also measured infarct volumes of CSS1 mice. As predicted, CSS1 exhibited a significantly larger infarct volume than B6 (Figure 8). In the CSS1 line, the contribution of chromosome 1 to the phenotype seems larger than would be predicted by the effect size of *Civq2* calculated from the F2 intercross. This was not unexpected, because a locus that is isolated from the effects of other loci across the genome by chromosome substitution can often show stronger effects than that predicted from a mapping cross [46]. Because we did not map an infarct volume locus to chromosome 18, the CSS18 was used as a negative control for the CSS validation approach. The CSS18 mice showed infarct volumes identical to the B6 parental mice, confirming the negative mapping data and

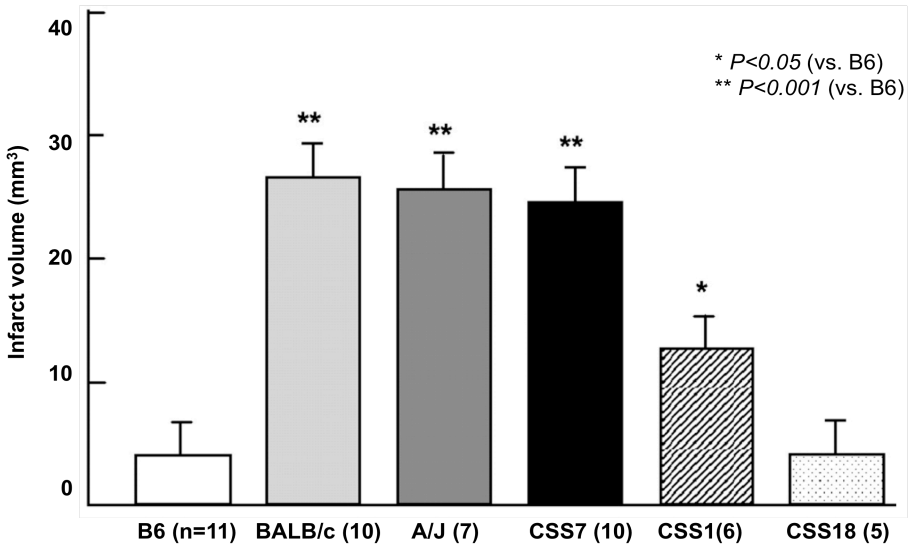

Figure 8. The B6 chromosome 7 confers a strong protective effect on ischemic infarct volume in a chromosome substitution strain. Similar to BALB/c strain, A/J mice display larger infarct volumes than B6 mice. The C57BL/6J-Chr7A/J/NaJ (CSS7) mice which have an A/J chromosome 7 substituted into the B6 genomic background, show a similar infarct volume as A/J (the source of chromosome 7) and BALB/c, but significantly different than B6 mice (the genomic background). The CSS1 mice, where a minor locus was mapped, also exhibit larger infarct volumes than B6, but consistent with the lower effect size, smaller than BALB/c, A/J, and CSS7 mice. CSS18 mice, substituting a copy of A/J chromosome 18, where no infarct volume locus was mapped, show no difference with B6 mice, consistent with the QTL mapping data. Error bars indicate SD.

the use of CSS mice for locus validation for this phenotype.

2.2.4 Genome-wide haplotype association analysis failed to replicate the mapping results

The number of recombinants in a mapping cross provides insufficient crossovers for mapping a complex trait, and our case is no exception, as the portion of the linkage peak above the highly significant threshold extends over 42 Mb of chromosome 7. A commonly used cutoff for a more precise localization of the underlying gene would be the 1.5-LOD interval, which in our case encompasses 10 Mb and covers more than 200 potential candidate genes. This provides a much tighter location for the causative gene, but still contains a large number of candidates.

Although the increased availability of SNP data for many inbred strains has led to *in silico* genome-wide haplotype association mapping of mouse QTL and several groups have successfully identified the QTLs using the method [47-49], many studies have reported that QTL identified by genome-wide haplotype analysis in inbred mouse strains are ofttenspurious associations due to the problem of complex population structure among strains and this method must be carried out in conjunction with linkage analysis to detect relevant loci. Intriguingly, Pletcher *et al*. and others have demonstrated that the genome-wide haplotype association analysis can be a powerful tool to narrow down a QTL when used with a experimentally derived genetic linkage locus [50,51]. The authors focused on candidate genes within the associated haplotype interval and identified a plausible candidate gene containing a non-synonymous sequence polymorphism.

Since we identified a linkage locus on chromosome 7 in an experimental cross and validated the existence of *Civq1* using CSS7 mice, we hypothesized that the locus on

chromosome 7 of a large effect on infarct volume might be present in multiple strains and haplotype association mapping might help to reduce the *Civq1* interval. We carried out a genome-wide haplotype association for the infarct volumes of the 16 inbred mouse strains. We performed genome-wide haplotype association using the SNPster algorithm, incorporating our phenotype data for 16 inbred strains program (http://snpster.gnf.org) and we have identified 3 QTLs over the significant threshold mapping to chromosome 3 (143.12 ~ 143.42 Mb), chromosome 7 (16.04 ~ 16.32 Mb), and chromosome 1 (77.81 ~ 78.07 Mb). However, the QTLs on chromosome 7 and chromosome 1 were mapped in completely different genomic positions not overlapping with *Civq1* and *Civq2*, and chromosome 3 was not discovered in our mapping analysis, indicating that all three loci obtained from the SNPster are false-positive spurious associations. This is not surprising because association mapping in the population of inbred mouse strains is characterized by a high false-positive rate. In agreement with previous studies [49], it would be highly probable that the number of mouse strains used in our analysis was not enough to result in a true association result. Although a suggestion was made that genome-wide association mapping must be carried out with a large number of strains (i.e., 40 to 150), there is substantial controversy about the minimum number of mouse strains and SNPs , and statistical approach used in the original *in silico* QTL analysis [52,53]. Thus, despite the three QTLs were identified in the haplotype association mapping, these *in silico* analyses did not help narrow down the *Civq1* interval.

2.2.5 Interval-specific haplotype association reduced the interval to 6 genes

Although the false-positive results from the genome-wide association mapping might be due to a small number of inbred strains and SNPs, or complex population structure among the strains, we hypothesize that the infarct volume data for the 14 inbred mouse strains still enable us to combine the data from ancestral haplotype association with our

own mapping cross data to fine-map the locus. In this light, we next sought to use an alternative method for applying haplotype analysis to the QTL: interval-specific haplotype association analysis [52]. To perform interval-specific haplotype analysis, we grouped the genotype data covering the *Civq1* 2-LOD interval into the strains that carry the large infarct allele and those that carry the small infarct allele. Any region with genotypes that are shared between the large allele strains and different from the small allele strains is considered a haplotype region likely to contain the causative gene. We searched for haplotype blocks shared between strains C3H, A/J, AKR, and BALB/c (large infarct volume) but for which a distinct haplotype is shared between strains FVB, DBA, NOD, 129S1/SvlmJ and B6 (small infarct volume). The three strains that show intermediate infarct volume phenotypes (NZW, KK, and BTBR) and strain C57BLKS/J and CBA with low-density SNP in the database were not used in interval-specific haplotype association analysis. We identified three genes that fall within clear haplotype blocks matching the phenotype pattern of the strains. When we relaxed the definition of haplotype block to include "mixed haplotype" blocks, another 3 genes fall within the interval. This analysis results in 3 strong and 3 weaker candidate genes to consider for *Civq1* (Figure 9).

The largest shared haplotype block of approximately 210 kb contains only two genes, *Bag3* and *Inpp5F*. *Bag3* is the Bcl2-associated athanogene 3, a member of a family of proteins sharing the BAG domain. Bag proteins compete with Hip for binding to the Hsp70 ATPase domain to promote substrate release, and are thought to be regulators of the chaperon activity of Hsp70 [54,55]. Numerous studies suggest that *Bag3* is an anti-apoptotic factor for stress-induced apoptosis. *Bag3* is broadly expressed across tissues and organs, but expression is particularly high in brain, heart and muscle. *Bag3*-deficient

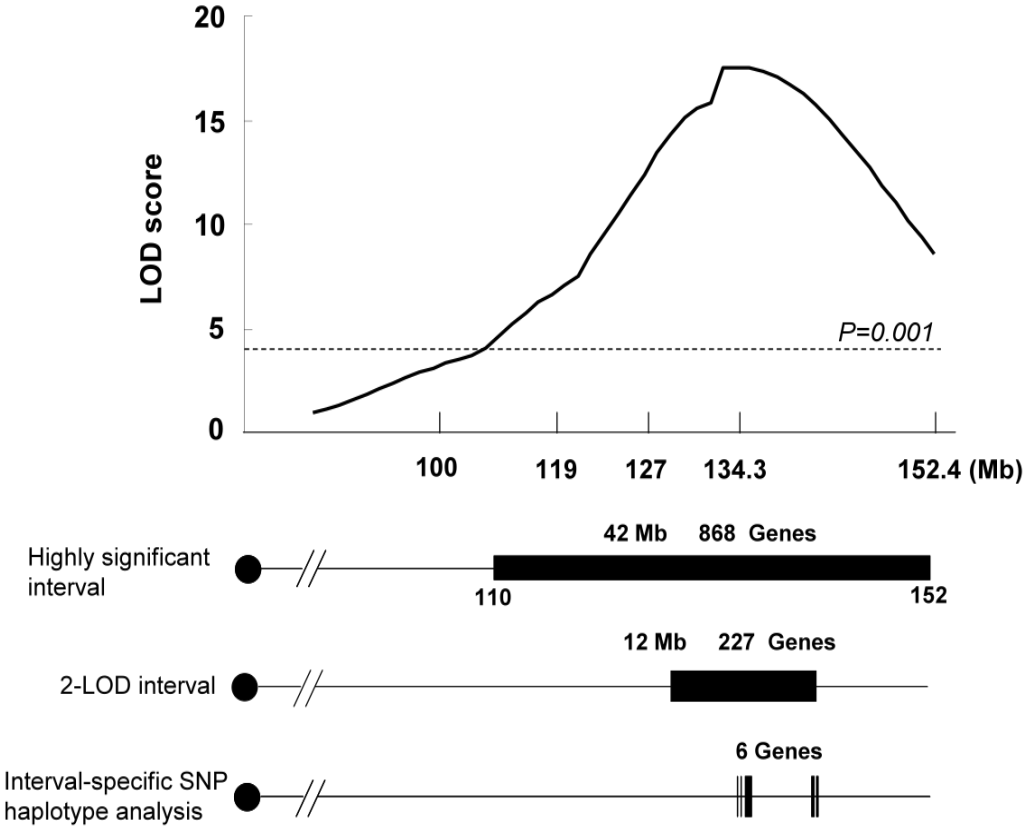

Figure 9. Interval-specific haplotype association analysis reduced the number of potential candidate genes to only six genes.

mouse shows in fulminant myopathy and death by 4 weeks [56].

Inpp5F, inositol polyphosphate-5-phosphatase F, is a member of a large family of phosphoinositide phosphatases. It contains a Sac (Suppressor of actin) domain required for its phosphatase activity. Although this particular protein has not been well characterized, other family members are involved in a diverse array of cellular functions including insulin signaling, endocytosis, cell proliferation and activation, and actin polymerization. Another family member, inositol polyphosphate 5-phosphatase OCRL-1, is mutated in Lowe syndrome, an X-linked disease characterized by psychomotor retardation, behavioral problems, cataracts, glaucoma, and renal tubule dysfunction [57]. Expression of *Innp5F* is restricted to the brain (http://symatlas.gnf.org/SymAtlas/). Recently, Zhu *et al*. have generated *Inpp5f* knockout mice and cardiac specific *Inpp5f* overexpression transgenic mice [58]. The knockout mice have augmented hypertrophy and reactivation of the fetal gene program in response to stress and cardiac overexpression of Inpp5f in transgenic mice reduces hypertrophic responsiveness, suggesting that Inpp5f is a functionally important endogenous modulator of cardiac myocyte size and of the cardiac response to stress.

A smaller haplotype block of approximately 10 kb, supported by multiple contiguous SNPs, maps entirely within the third intron of the *Adam12* gene. ADAM is an acronym for "a disintegrin and metalloproteinase domain", a family of multi-domain proteins with structural homology to snake venom metalloproteases. *Adam12* possesses extracellular metalloprotease and cell-binding functions, as well as intracellular signaling capacities [59]. The protein regulates cell differentiation, proliferation, migration,

and invasion. It is also thought to modulate cell-cell and cell-extracellular matrix contacts through its interaction with cell surface receptor integrins and syndecans, and through these interactions re-organize the actin cytoskeleton [59]. *Adam12* expression appears to be restricted to placenta, umbilical chord, and uterus (http://symatlas.gnf.org/SymAtlas/). This organ-specific expression pattern suggests that the gene is primarily expressed in vascular endothelium or smooth muscle, which could be relevant to the infarct phenotype. *Adam12* knockout mice are mostly viable (30% lethality by 1 week of age), but the surviving homozygotes are fertile and appear grossly normal, with defects in adipogenesis and myogenesis [60]. A putative non-coding RNA (AK143656) was recently added to the annotation of the mouse genome databases. Most of this single-exon transcript maps within this 10 kb block, and therefore was subjected to the same expression analyses as outlined for the other genes.

If the causative SNP underlying the locus acts at a distance to modulate gene expression, then we must expand our search to include genes that flank these two haplotype blocks, even when no known part of the gene lies within the block. One well-known example of this phenomenon is the common SNP underlying adult onset lactose intolerance (in humans), which maps within an intron of the gene flanking the lactase gene, modulating the expression of lactase into adulthood [61,62]. In line of this, we identified the 210 kb haplotype block at the chromosome 7 locus that contains the two flanking genes, *Tial1* and Riken clone 1110007A13. Tial1 is the cytotoxic granule-associated RNA binding protein-like-1 gene, was recently shown to regulate alternative splice site usage at U-rich intronic motifs across the genome [63]. It is widely expressed in organs and tissues including the brain. Riken 1110007A13 is an uncharacterized gene, highly expressed in oocytes, but also expressed in other organs and tissues including brain.

For the 10 Kb haplotype block within intron 3 of *Adam12*, the two flanking genes are *Fank1* and RIKEN cDNA 4933400E14 gene. *Fank1*, Fibronectin type 3 and ankyrin repeat domains 1, appears to be exclusively expressed in testes [64] and (http://symatlas.gnf.org/SymAtlas/). Riken clone RIKEN cDNA 4933400E14 is an uncharacterized gene whose organ and tissue expression pattern is also not well characterized.

In order to be even more conservative in our approach to candidate genes, we next relaxed our definition of shared haplotype blocks. These additional haplotype blocks were not recognized by the Perlegen Haplotype Browser (http://mouse.perlegen.com/mouse/hapBrowser_doc1.html), but were only identified by exhaustive re-examination of the entire list of SNPs mapping under the linkage curve using the Jackson laboratory's Mouse Phenome Database (http://phenome.jax.org/pub-cgi/phenome/). Generally, these blocks were supported by several SNPs, but also showed numerous SNPs within the block that violated the sharing pattern among phenotypically similar strains – resulting in a "mixed haplotype" pattern. From this analysis, three other genes can be considered - *Cox6a2*, *Rgs10*, and *Dock1*.

Cox6a2 encodes the heart- and skeletal muscle-specific isoform of cytochrome c oxidase (COX) subunit VIa. This protein participates in a complex in the last enzymatic reaction of the respiratory electron transport chain, transferring protons to oxygen to create water. Expression is mostly restricted to heart and skeletal muscle (http://symatlas.gnf.org/SymAtlas/). There are no published reports of a gene knockout.

Dock1 (also Dock180), dedicator of cytokinesis, functions as a guanine nucleotide exchange factor for Rac1. *Dock 1* is plays a role in cytoskeletal rearrangements required for phagocytosis of apoptotic cells [65]. *Dock1* is broadly expressed in multiple organs and tissues including brain (http://symatlas.gnf.org/SymAtlas/). Morpholino antisense-oligonucleotide-mediated knockdown of *Dock1* in the zebrafish embryo results in a defect in the fusion of embryonic fast-twitch myoblasts [65,66]

Rgs10, "regulator of G protein signaling", is one member of a family of proteins that modulate G-protein signaling at the G alpha subunit. Many have been shown to have GTPase accelerating activity. Rgs10 is broadly expressed in multiple organs and tissues including brain, but is most highly expressed in T cells, B cells and monocytes (http://symatlas.gnf.org/SymAtlas/). Murine knockout of Rgs10 results in severe osteoporosis and impaired osteoclast differentiation and death within the first 3 weeks after birth [67]. Further analysis of the knockout mice has suggested a role for Rgs10 in modulating the sensitivity of dopaminergic neurons against inflammation-mediated cell death [68].

2.2.6 The identified 6 candidate genes do not differentially express

Broadly speaking, the gene underlying the infarct volume locus might either harbor a non-synonymous cSNP(s) that alter protein function, or regulatory SNPs that alter the expression, translation, or stability of the transcript. This latter class might include binding sites for regulatory microRNAs. Our strategy for further analysis of all of the above-mentioned genes includes studies of transcript level differences between the strains as a proxy for underlying regulatory changes, and studies of differences in the coding capacity for each of the genes, by exon re-sequencing.

Under the assumption that the gene underlying *Civq1* acts intrinsically within the brain tissue to alter the metabolic response to ischemia, we hypothesize that the neural tissue is itself the critical tissue that mediates the differential response to ischemia. We first sought to determine whether the 6 candidate gene underlying *Civq1* express differentially in the brain. The mRNAs were isolated from the cerebral cortex in B6 and BALB/c mice and quantitative RT-PCR was performed for the 6 genes. Figure 10 shows analysis of brain mRNA for the 6 genes identified by interval-specific haplotype association. Only two genes appear to show even marginal differences in transcript levels (*Adam12* and Cox6a2).

2.2.7 A non-synonymous coding SNP in *Bag3* co-segregates with infarct volume phenotypes in 14 inbred mouse strains.

Alternatively, to cover the possibility of coding SNPs in the candidate genes, we have performed *in silico* sequence analysis using multiple SNP databases. This *in silico* survey shows that only two of the genes exhibit a non-synonymous coding SNP that differs between B6 and BALB/c. The *Bag3* gene harbors a cSNP that creates an Ile81Met polymorphism in the *Bag3* protein. This residue is not conserved across species, but this fact alone is of limited significance, since non-synonymous coding SNPs for complex genetic traits tend not to fall within highly conserved residues/regions of proteins [69]. Significantly, the Ile81Met polymorphism clearly segregates with the infarct volume phenotype (Figure 11). Strains that exhibit small infarcts encode the Ile81 isoform, whereas strains that exhibit larger infarcts encode the Met81 isoform, with a clean demarcation between the two groups. Given the co-segregation of this cSNP with the infarct phenotype across 14 inbred strains, its robust expression in a variety of tissues

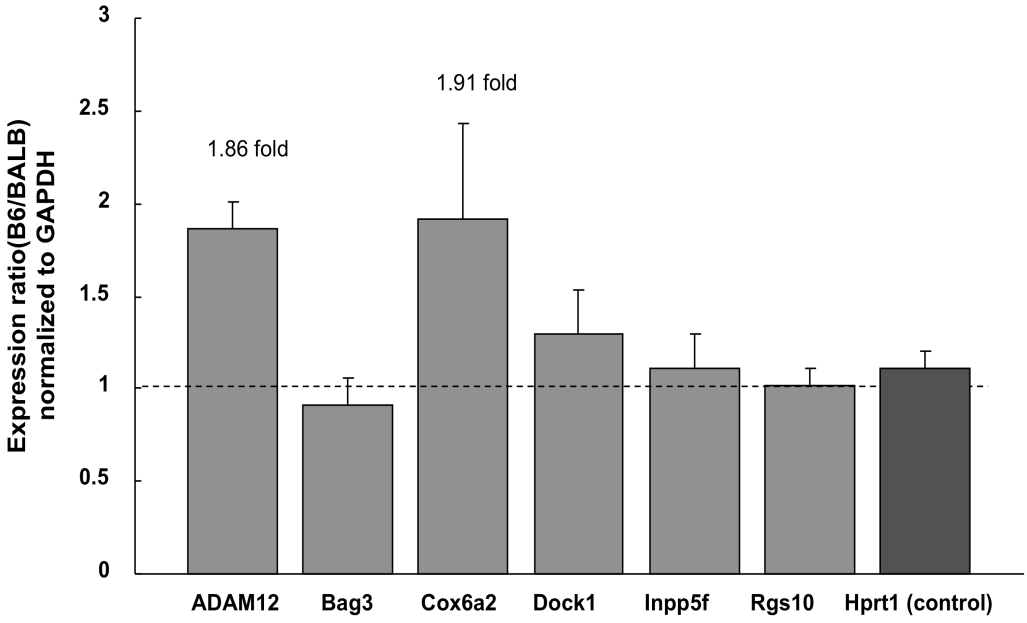

Figure 10. The B6/BALB expression ratio of six genes identified by interval-SNP haplotype association analysis. The expression level of each gene was normalized to GAPDH. Normalization to the *Hprt1* gene as a different control gave similar results.

including brain, and a potential role as an anti-apoptosis regulator, *Bag3* becomes a compelling candidate for the chromosome 7-infarct volume locus.

Adam12 also harbors a non-synonymous coding SNP between B6 and BALB/c, creating a Thr40Ala polymorphism in the protein. Amino acid residue 40 in the protein is not conserved across species. However, this cSNP does not segregate with the infarct volume phenotype, especially at the low end of the phenotype (Figure 11). Strains showing smaller infarcts somewhat randomly encode either the Thr40 or the Ala40 isoform. The lack of segregation with the phenotype was predicted, since this cSNP does not map within the small, entirely intronic haplotype block that implicates the *Adam12* gene. We would surmise that if *Adam12* were the causative gene, it would harbor a regulatory sequence variant mapping within the associated haplotype block in intron 3 of the gene.

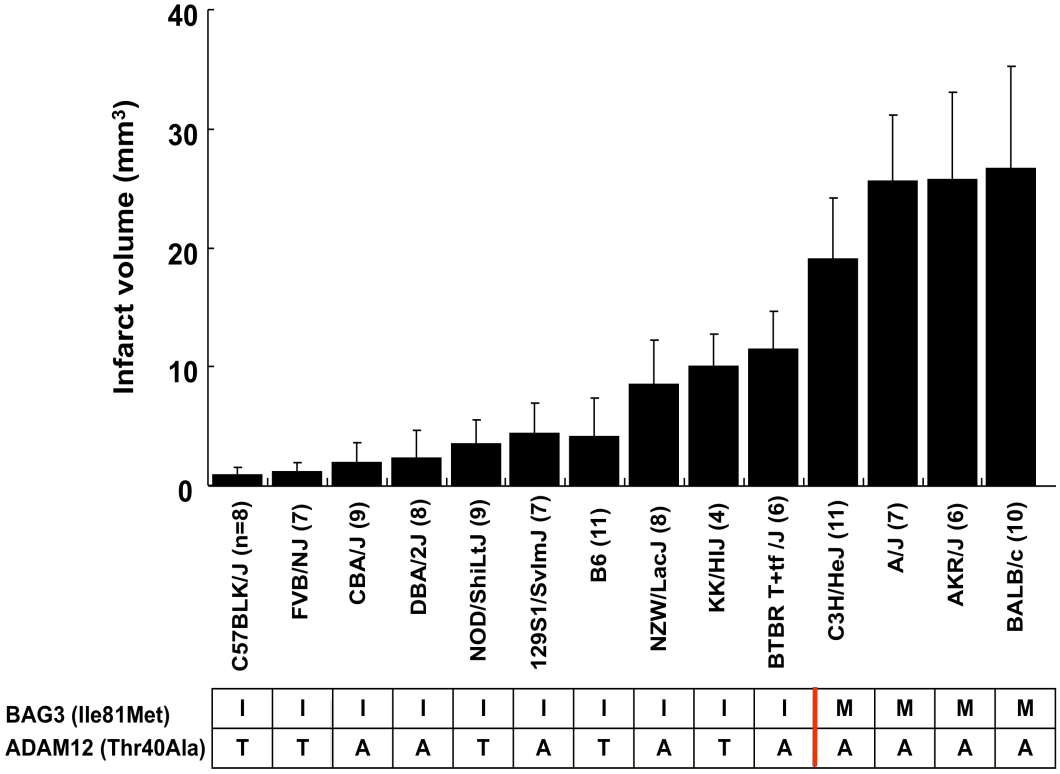

Figure 11. Segregation of the infarct volume phenotype and the two non-synonymous cSNPs in *Bag3* and *Adam12*. The Ile81Met SNP in *Bag3* segregates (red line) with infarct volume in 14 inbred strains, whereas the Thr40Ala SNP in *Adam12* segregates randomly with infarct volume.

2.2.8 *Bag3* protects neuronal cells from ischemic insult

Of the candidate genes discussed previously, the existing molecular genetic data points to *Bag3*. This gene also has strong biological plausibility. Antisense reduction of *Bag3* transcript levels in two distinct cell types (cancer cell line and human mononuclear cells) increases the apoptotic response to oxidative stress (elevated reactive oxygen species). Conversely, over-expression of *Bag3* reduces oxidative stress-induced apoptosis in 293T cells [70,71]. These data place *Bag3* at the crossroads of the apoptotic response, and would suggest that infarct volume differences between B6 and BALB/c may be due to differential apoptotic response of neurons to ischemia. However, other groups reported that *Bag3* itself exerts only weak anti-apoptotic activity. *Bag3* transfection into HeLa cells exhibited little or no anti-apoptotic activity alone, although it synergized with over-expressed Bcl-2 in preventing Bax-induced and Fas-mediated apoptosis [72]. Similarly, murine myeloid progenitor cells over-expressing *Bag3* slightly reduced the level of cytokine-induced (IL3) apoptosis, but the effect is considerably weaker than that reported for its relative, *Bag1* [73]. Moreover, MEFs (mouse embryonic fibroblast) from *Bag3* deficient mice do not show increased sensitivity to a variety of apoptosis-inducing agents [74].

However, of significance, none of previous studies have investigated the role of *Bag3* in ischemia-induced apoptosis in neuronal cells. We propose that if *Bag3* underlies the chromosome 7 locus, as our genetic data would suggest, then it may play a significant role in modulating neuronal apoptosis induced by ischemia. To investigate the role of *Bag3* in the neuronal cell death induced by ischemia, we knocked down expression of *Bag3* in human SH-SY5Y neuroblastoma cells with human *Bag3*-specific siRNAs and compared the viability with control groups after 2 hr oxygen-glucose deprivation. To

monitor silencing of *Bag3* by RNA interference, we performed western blot analysis. In comparison with nonspecific-siRNA transfected cultures, the *BAG3* protein level was significantly lowered by application of *Bag3* siRNAs (Figure 12B). Interestingly, inhibition of *Bag3* expression significantly increased the extent of OGD-triggered cell death as compared with the mock-transfected cells (Figure 12A). This data suggests that *Bag3* may have a potent cytoprotective effect in the OGD model of ischemia. In parallel, we sought to further investigate the role of *Bag3* in focal cerebral ischemia using the *Bag3* knockout mice. Since the *Bag3*-deficient mice die by 4 weeks after birth due to fulminant myopathy [56], we tested the infarct volume of the heterozygote mice. The phenotype was significantly variable between mice and showed no correlation with the genotypes. We determined that the mice were of mixed genomic backgrounds using the whole genome SNP genotyping. The heterozygous mice in the B6 background will be tested.

2.2.9 Strain SJL and SWR mice harbor the *Bag3* allele (Ile81Met) not correlated with their infarct volume phenotypes

Haplotype analysis can be applied to any number of crosses that detect a QTL approximately at the same position, but it has been known that the analysis is most effective when applied only to the strains used for experimental crosses [52,53,75,76]. Only those regions where the strain carrying the protective allele share common ancestral DNA and differ from strains carrying the sensitive allele are likely to contain the causative gene. Thus, increasing number of crosses and strains available for haplotype analysis of a particular QTL improved the ability to reduce the QTL interval. For this purpose, we also determined the phenotype of two additional inbred mouse strains (SJL and SWR) to increase our power for haplotype association fine mapping.

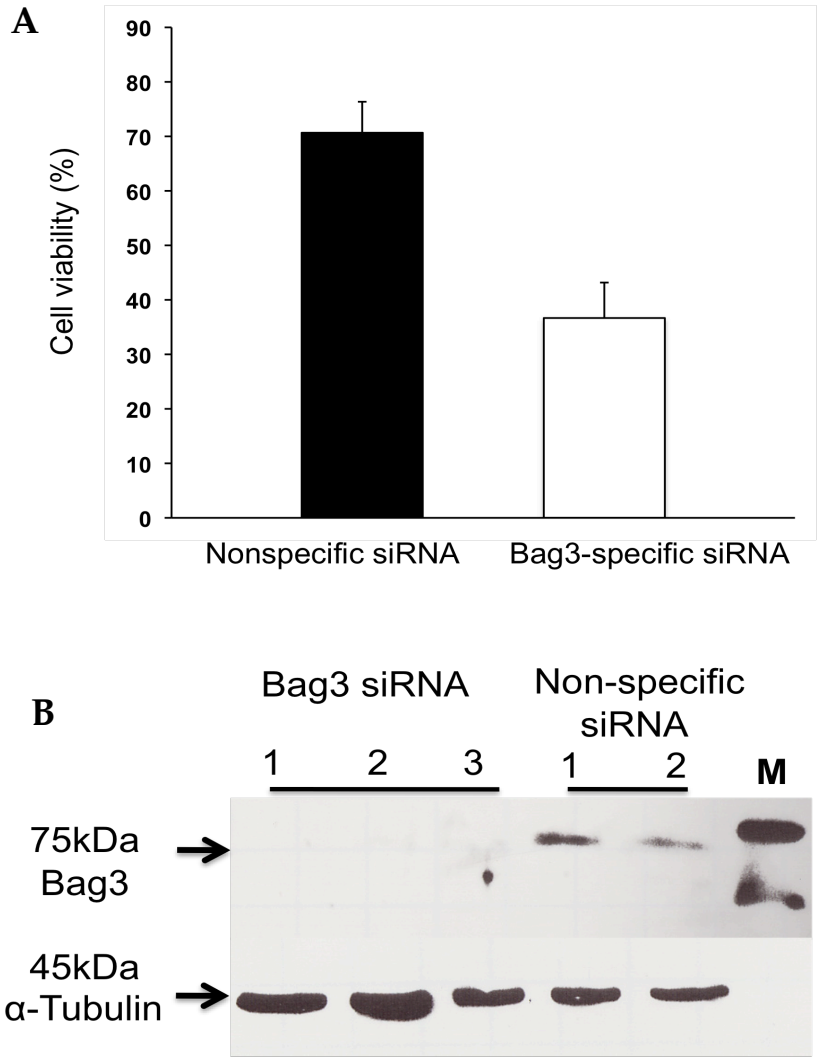

Figure 12. *Bag3* shows a cytoprotective effect on cell death induced by OGD. **A.** Knockdown of *Bag3* expression significantly increases the extent of cell death in human SH-SY5Y neuronal cells. Viability was determined as the percent of total cells that excluded trypan blue in comparison with control cells not exposed to OGD. **B.** Functional knockdown of Bag3 protein was confirmed by western blot.

To further validate whether the Bag3 coding SNP (I81M) co-segregate with the infarct volume phenotypes in these strains. We performed the sequencing analysis of Bag3 gene in both SJL and SWR strains. Interestingly, both strains harbor the coding SNP not matching the infarct volume phenotype of the other 14 mouse strains. Figure 13 illustrates infarct volumes of the strains in comparison to B6 and BALB/c mice. Strain SJL shows a very small infarct volume, nearly identical to that seen for B6, and yet this strain shares the sensitive BALB/c allele (Met81) in *Bag3*. Thus, we hypothesize that even though SJL has the susceptible haplotype and therefore, the susceptibility allele at the chromosome 7 gene, this strain must harbor at least one protective allele at a different locus or gene. Similarly, strain SWR/J shows a very large infarct volume, nearly identical than that seen for BALB/c, and yet this strain shares the protective B6 allele (Ile81) in *Bag3*. Thus, since B6 and SWR strains show a 700% difference in infarct volume even though SWR has the protective B6 allele at *Bag3*, we hypothesized that this strain must harbor at least one sensitive gene/allele at a different locus that exhibits a large effect on the infarction phenotype. Conversely, if we map the chromosome 7 locus in this cross, it is most likely that genetic variation in a different causal gene, but not the coding SNP (Ile81Met) in *Bag3*, causes the phenotypic difference in infarct volume after MCAO between the strains. Thus, by performing this cross, we also sought to prove that *Bag3* is the causative gene underlying *Civq1* for infarct volume.

2.2.10 An intercross between Strain B6 and SWR re-identifies *Civq1* and suggests that Bag3 is not the causative gene

We conducted a second intercross between inbred strains B6 and SWR/J, which also differ 6-fold in infarct volume (*P<0.001*; Figure 13). Infarct volumes were measured in both sexes for a total of 78 F2 intercross progeny. F2 mice were genotyped for 215 SNP

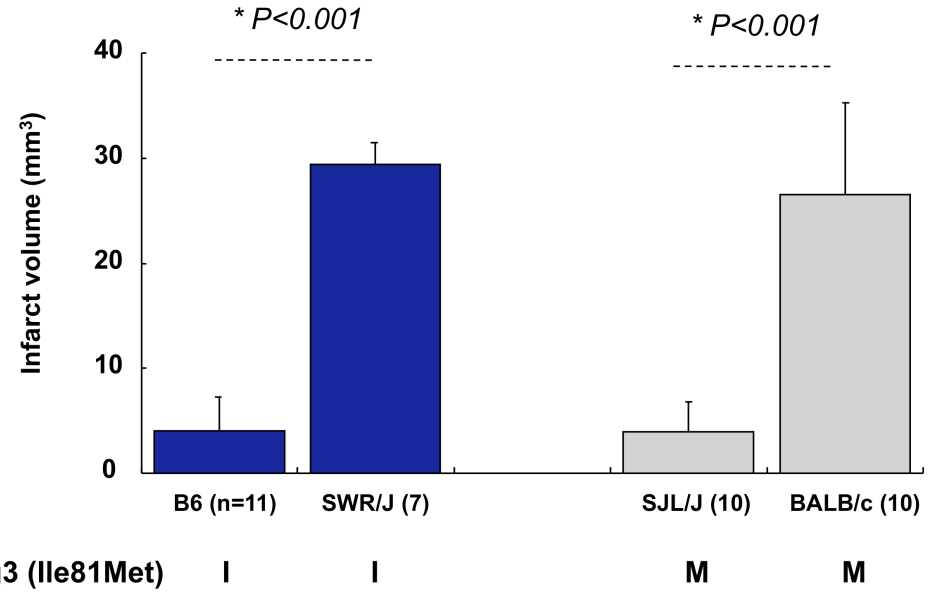

Figure 13. SWR and SJL strains harbor the Bag3 coding SNP (I81M) that does not co-segregate with the infarct volume phenotype. Inbred mouse strains that differ greatly in their infarct volumes but which harbor the same Bag3 coding SNP.

markers that were informative between the B6 and SWR/J strains. From this cross, we identified a highly significant locus (LOD=9.7) that mapped to the identical position (peak LOD at rs13479513) on chromosome 7 as that of *Civq1* (Figure 14). Similar to *Civq1* mapped in the original B6×BALB/c cross, *Civq1* identified in this second cross also explains the majority of the effect (57%) of the total variance of infarct volume and shows the same genotype-phenotype correlation. Of importance, this data validates the importance of *Civq1* in the determination of infarct volume in common inbred mouse strains. Furthermore, it also provides strong evidence that a different gene and genetic variation underlying *Civq1*, but not the Ile81Met polymorphism in *Bag3*, determines the differential infarct volumes between the strains.

2.2.11 *Civq1* was remapped in an intercross between FVB and BALB/c strains

Since we identified *Civq1* in two different genetic crosses and in the CSS series, each of which include B6 as one of parental strain, it is potentially possible that the mutation causing *Civq1* might have occurred only in B6 strain after the strains were separated from common ancestors approximately 100 years ago. To determine that allelic variation at *Civq1* is not unique to B6 strain but due to a gene that maps within ancestral SNP haplotype block, we performed an additional intercross between the large infarct strain BALB/c and another small infarct strain FVB/J, which exhibit 10-fold difference in infarct volume. Because it was not our goal to identify a new locus in this cross, we measured infarct volumes in a small number of F2 (BALB/c×FVB/J) progeny (n=33). F2 mice were genotyped for 165 SNP markers that were informative between the FVB/J and BALB/c strains. We identified a significant locus (LOD=2.78) that mapped to the identical position (peak LOD at rs13479513) on chromosome 7 as that of *Civq1*. Similar to *Civq1* mapped in the B6×BALB/c and B6×SWR/J crosses, *Civq1* identified in this third c-

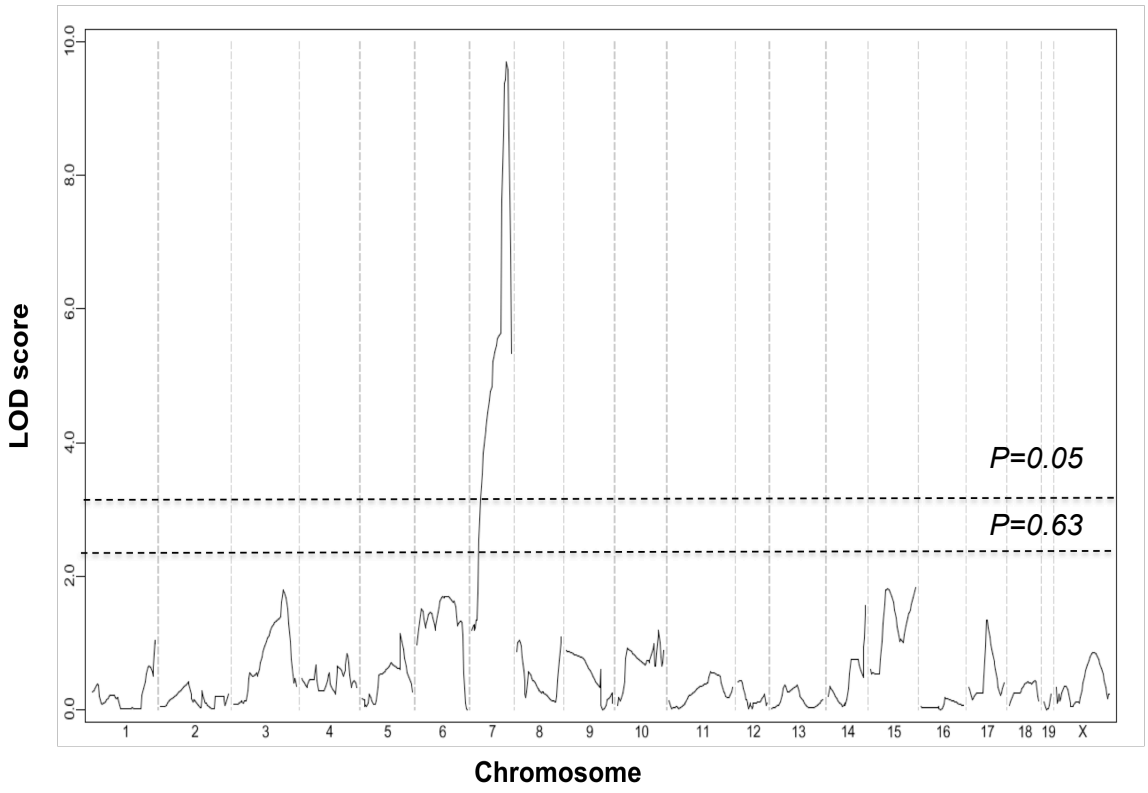

Figure 14. *Civq1* is re-identified in a second intercross between B6 and SWR/J inbred mouse strains. The graph presents the results of a genome-wide linkage scan for infarct volumes in 78 (B6×SWR/J) F2 progeny. The y-axis represents the LOD score. The significant (*P=0.05*) and suggestive (*P=0.63*) levels of linkage were determined by 1000 permutation tests. One region of the genome, distal chromosome 7, displays significant linkage to the trait, reaching a LOD score of 9.7. This linkage peak completely overlaps *Civq1* originally mapped in the B6 BALB/c intercross.

-ross also explains the majority of the effect of the total variance of infarct volume and shows the same genotype-phenotype correlation. These data further validate the importance of *Civq1* in the determination of infarct volume in common inbred mouse strains. More importantly, it also strongly suggests that the sequence variation for *Civq1* causing the phenotypic difference in infarction is located within an ancestral haplotype block between inbred strains, not within a minority of the sequence variation being only unique to strain B6.

2.2.12 Combined cross analysis to reduce 1.5-LOD interval of *Civq1*

The number of recombinants in a mapping cross provides insufficient crossovers for mapping a complex trait, and our case is no exception, as the portion of the linkage peak above the significant threshold ($p=0.05$) extends over 42 Mb of chromosome 7. This provides a much tighter location for the causative gene, but still contains a large number of candidates. The limited number of crossovers in a traditional mapping cross results in a large confidence interval for the typical QTL. Similarly, in our crosses the portion of the linkage peak above the significance threshold extends over 42 Mb of chromosome 7 in the B6×BALB/c and 32 Mb in the B6×SWR crosses, implicating hundreds of genes as potential candidates. Recently, Churchill and colleagues have shown that by combining and analyzing data from multiple crosses, the number of crossovers is increased and the QTL interval can be reduced [77]. Thus, we merged the genotype and phenotype data from the 3 intercrosses and performed genome-wide linkage analysis on the combined data. The combined animals from both intercrosses yielded an overall LOD score of 21.7 (Figure 15). This analysis significantly reduced the 1.5-LOD interval to 9.9 Mb encompassing 225 potential candidate genes [78].

2.2.13 Interval-specific SNP haplotype analysis further narrowed *Civq1*

The combined cross analysis provides a much tighter location for the causative gene, but it still contains a large number of candidate genes. Thus, to further dissect the interval, we compared ancestral SNP haplotype patterns within the inbred mouse lineages. Interval-specific SNP haplotype analysis can refine confidence intervals by identifying high-priority regions within a QTL interval that are likely to harbor the causal polymorphism [52,79]. Approximately 97% of the genetic variation between inbred laboratory mouse strains is found in ancestral haplotype DNA regions that seem to be identical by descent with a minority of the sequence variation being unique to any individual strain [80,81]. Because *Civq1* was identified in 3 different genetic crosses (B6×BALB/c, B6×SWR, and FVB×BALB/c) and in the CSS (B6×A/J) series, allelic variation at *Civq1* is therefore most likely due to a gene that maps within an ancestral haplotype block that is shared between BALB/c, A/J, and SWR, but that is different from B6 and FVB strains.

We examined all haplotypes throughout the 1.5-LOD interval of *Civq1*, defining a haplotype block to be 3 or more adjacent consecutive shared SNP alleles [52,79]. We searched for a SNP haplotype shared between strains BALB/c, A/J, and SWR/J (large infarct volume) but for which a distinct haplotype is shared between strains B6 and FVB (small infarct volume). Figure 15 illustrates that only five genes fall clearly within haplotype blocks matching the phenotype pattern of the strains (Table 3). Two genes, *Qprt* and *Itgal*, are located within two different shared haplotype blocks of approximately 29.3kb and 22.4kb, respectively, at the peak of the *Civq1* interval.

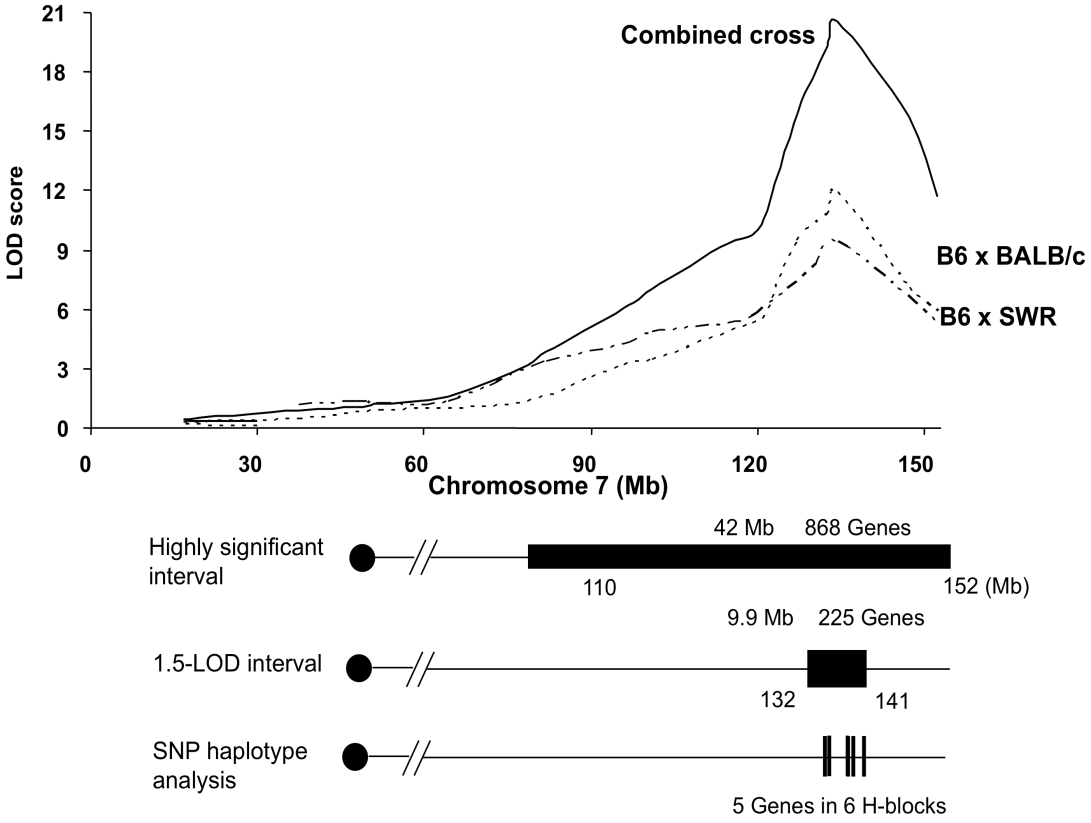

Figure 15. Fine mapping of the *Civq1* interval using combined cross and interval-specific SNP haplotype analysis. The top graph presents the LOD score plots on chromosome 7 in B6×BALB/c (dashed line), B6×SWR/J (dotted line), FVB×BALB/c, and combined cross (solid line). The combined cross approach narrowed 1.5-LOD interval of *Civq1* to 9.9 Mb. Interval-specific SNP haplotype sharing patterns among the strains further reduced the interval to 5 possible candidate genes.

Itgal (CD11a) encodes an alpha subunit of leukocyte β2-integrin Lymphocyte function-associated antigen-1 (LFA-1) that mediates adhesion and migration of leukocytes [82]. *Itgal* is highly expressed in microglia, spleen, bone marrow, and most leukocyte populations. In addition to the role in inflammatory-mediated tissue injury in the pathogenesis of ischemic stroke [83], the αLβ2-integrin has been known to modulate adhesion of monocytes to collateral endothelium involved in arteriogenesis [84-86]. *Itgal*, thus, represents an attractive candidate gene based on its putative function both in stroke and in collateral vessel formation.

Qprt, quinolinate phosphoribosyltransferase, is a key enzyme in catabolism of quinolinate, an intermediate in the tryptophan-nicotinamide adenine dinucleotide pathway [87]. Quinolinic acid acts as a potent endogenous exitotoxin to neurons. *Qprt* is present primarily in glial cells, some of which resemble the dendritic, antigen-presenting cells in the immune system, and could also resemble represent cells infiltrating the brain from the periphery. QPRT is secreted to destroy excessive and potentially harmful amounts of quinolinic acid. Elevation of quinolinic acid levels in the brain has been linked to the pathogenesis of neurological disorders such as stroke, epilepsy, Alzheimer's disease, and Huntington's disease [87]. Interestingly, a recent study has reported that the injection of quinolinic acid causes a time-dependent change in vascular remodeling in rat brains [88]. To date the phenotype of a *Qprt* knockout mouse model has not been reported.

A large haplotype block of approximately 133kb, supported by multiple contiguous SNPs, maps entirely within Dock1 (also Dock180), dedicator of cytokinesis, which functions as a guanine nucleotide exchange factor for Rac1. Dock1 plays a role in

cytoskeletal rearrangements required for phagocytosis of apoptotic cells [65]. Dock1 is broadly expressed in multiple organs and tissues including the brain. Morpholino antisense oligonucleotide-mediated knockdown of Dock1 in the zebra fish embryo results in a defect in the fusion of embryonic fast-twitch myoblasts [65,66]. Interestingly, Dock1 was also identified in the interval-specific SNP haplotype association mapping using the 9 inbred mouse strains.

Two uncharacterized genes, 4933440M02Rik and 1500016O10Rik were also identified within the shared haplotype blocks. 4933440M02Rik is highly expressed only in testis. Recently, the 150006O10Rik gene was annotated as gene Fam57b (family with sequence similarity 57, member B) and is highly expressed in the retina, but is also expressed in other organs and tissues including brain and skeletal muscle. Its cellular function has not yet been studied.

As we discussed earlier, it is potentially possible that the regulatory genetic variations within a shared haplotype block influence the transcript level of a gene outside of the haplotype block. If the causative SNP underlying the locus acts at a distance to modulate gene expression, then we must expand our search to include genes that flank these two haplotype blocks, even when no known part of the gene lies within the block. Thus, in order to be even more conservative in our approach to candidate genes, we included genes located within 10 kb away from the borders of all shared SNP haplotype blocks. From this analysis, two other genes, 1810010M01Rik (Zymogen granule protein 16) and zfp768 (Zinc finger protein 768), can be considered.

Table 3. Candidate genes within the shared SNP haplotype blocks for *Civq1*

Genomic position (Build 37)	Gene	Description
132473157–132493286	4933440M02Rik	RIKEN cDNA 4933440M02 gene
133941182–133974050	Fam57b	RIKEN cDNA 1500016O10 gene
134250176–134266022	Qprt	Quinolinate phosphoribosyltransferase
134438374–134478651	Itgal	Integrin alphaL subunit
141860759–142365780	Dock1	Dedicator of cytokinesis 1

2.2.14 Candidate gene identification

Generally, functional polymorphisms underlying a causative gene could be classified into either non-synonymous coding SNPs that alter protein function, or regulatory SNPs that alter the expression, translation, or stability of the transcript [89]. This latter class might include binding sites for regulatory microRNAs. To identify the causal gene for *Civq1*, we sought to determine whether there are differences in transcript level or differences in the coding capacity for each of the 5 genes between the mouse strains used in our experimental crosses.

2.2.14.1 Expression level of *Itgal* correlates inversely with infarct volumes

First, to identify genes differentially expressed between the two strains, we performed quantitative RT-PCR to analyze levels of brain mRNA for the 5 genes identified by shared SNP haplotype analysis. Only one gene, *Itgal*, shows a 7-fold higher transcript level in the brain in B6 strain than in BALB/c brain. Since we are only interested in those candidate genes that harbor *cis*-acting elements near the candidate gene that alter its expression, we have performed the allele-specific SNapShot gene expression analysis to verify whether *cis*-acting variation is determining this difference. Similar to the qRT-PCR result in parental strains, allele-specific gene expression analysis has confirmed that the level of *Itgal* transcript is approximately 6-fold higher than BALB/c transcript in the cerebral cortex in F1 animals (Figure 16A).

We next sought to determine whether the differential expression level of the *Itgal* is correlated with the infarct volume phenotype between the 4 mapping strains. Indeed, the expression level of *Itgal* in B6 was higher (>8 fold) than those in the 3 large infarct strains (BALB/c, A/J, and SWR/J), providing further evidence that regulatory genetic

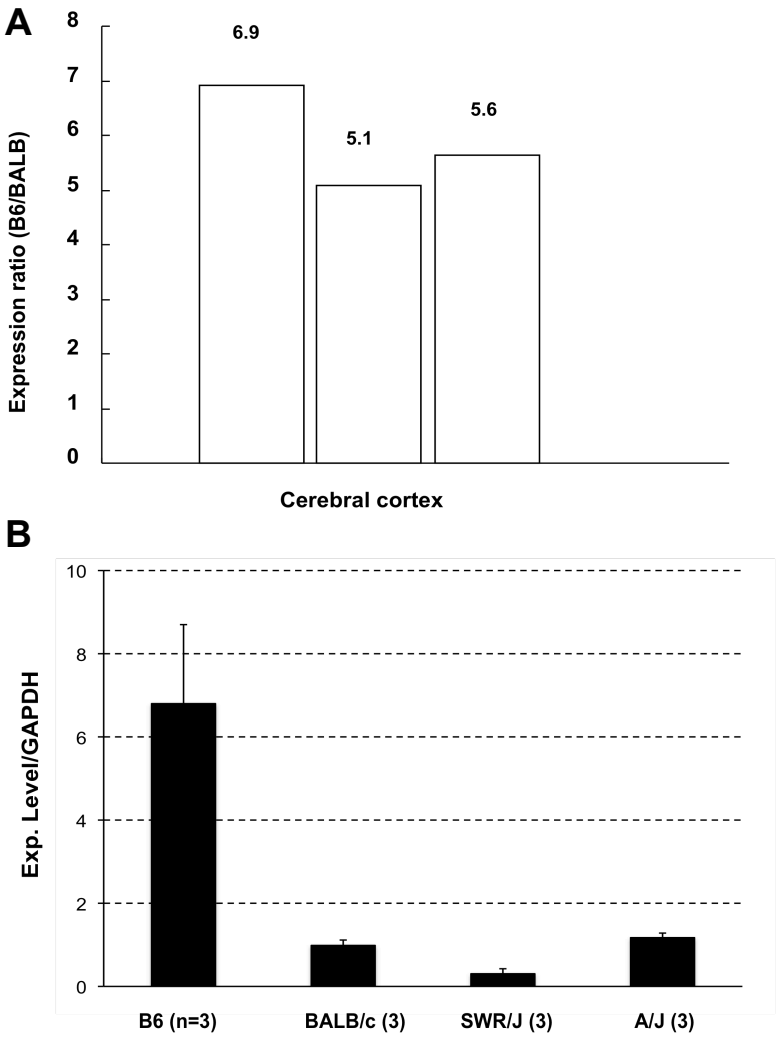

Figure 16. *Itgal* is differentially expressed in the brain between the strains. **A.** The allele-specific expression ratio of *Itgal* transcript levels in F1 (B6xBALB) mice. A coding SNP in exon 32 was used to monitor the B6-allele and BALB/c-allele transcripts of *Itgal* in the cerebral cortex. Each bar represents the allele-specific expression ratio (B6/BALB) of the *Itgal* transcript in a single F1 animal. **B**. The difference in *Itgal* transcript level in the cerebral cortex is correlated inversely with the infarct volumes between the 4 mapping strains. The relative expression of mRNA of *Itgal* was normalized to GAPDH. Values represent average± SD.

variation resulted in the difference in *Itgal* mRNA abundance in the brain between the 4 strains (Figure 16B).

2.2.14.2 Coding SNPs in *Itgal* and *Qprt* co-segregate with infarct volumes

To cover the possibility of coding SNPs in the candidate genes, we have done the complete re-sequencing of all of the coding exons (including at least 50 bp of flanking intron) for the 5 candidate genes within the shared DNA haplotype blocks. Through sequencing analysis and an *in silico* SNP database survey, we have found that *Qprt* and *Itgal* harbor coding SNPs that correlate with the infarct volume phenotypes between the 5 mapping inbred mouse strains (Figure 17).

The *Itgal* harbors two coding SNPs that create a Trp972Arg and a Pro978Leu polymorphisms in the protein. Strains B6 and FVB that exhibit small infarcts, encode the Trp972 and Pro978 isoform, whereas BALB/c, A/J, and SWR/J strains that exhibit large infarcts, encode the Arg972 and Leu978 isoform (Figure 17A). Interestingly, the Trp972Arg change was predicted to cause deleterious effect on the protein by *in silico* amino acid substitution analysis in the three different databases, PolyPhen (http://genetics.bwh.harvard.edu/pph/), PMut (http://mmb2.pcb.ub.es:8080/PMut/), and Panther (http://www.pantherdb.org/).

Qprt also harbors two coding SNPs co-segregating with the infarct volume phenotypes: Glu205Lys and Asp253Asn. Strains B6 and FVB that exhibit small infarcts, encode the Glu205 and Asp253 isoforms, whereas BALB/c, A/J, and SWR/J strains that exhibit larger infarcts, encode the Lys205 and Asn253 isoform. Interestingly, except rodents all the other mammalian species have Glutamine (Q) at position 205 (Figure 17B). Both cha-

A. ***Itgal***

	972									978			
B6 and FVB	G	V	P	**W**	P	H	S	E	D	**P**	I	T	Y
BALB/c, A/J, and SWR	G	V	P	**R**	P	H	S	E	D	**L**	I	T	Y
Rat	E	V	P	**Q**	P	H	S	E	G	**P**	I	A	H
Human	G	V	P	**Q**	P	P	S	E	G	**P**	I	T	H
Chimpanzee	G	V	P	**Q**	P	P	S	Q	G	**P**	I	T	H
Pig	G	V	P	**Q**	P	H	P	K	G	**P**	I	T	H
Horse	G	V	P	**W**	P	H	S	K	G	**P**	I	M	H
Dog	G	V	P	**V**	S	H	S	E	G	**P**	I	T	H
Rabbit	G	V	P	**V**	P	H	G	E	E	**P**	I	T	Y
Cow	R	V	P	**R**	V	H	S	E	G	**L**	I	T	H
Sheep	R	V	P	**R**	V	H	S	E	G	**L**	I	T	H
Opossum	V	V	P	**R**	S	Q	M	G	G	**F**	F	T	R

B. ***Qprt***

	205												253		
B6 and FVB	S	S	L	**E**	E	A	F	R	~	~	V	T	L	**D**	N	L
BALB/c, A/J, and SWR	S	S	L	**K**	E	A	F	R	~	~	V	T	L	**N**	N	L
Rat	S	S	L	**K**	E	A	L	Q	~	~	V	T	L	**D**	N	L
Human	S	S	L	**Q**	E	A	V	Q	~	~	I	T	L	**D**	N	L
Chimpanzee	S	S	L	**Q**	E	A	V	Q	~	~	I	T	L	**D**	N	L
Cow	S	S	L	**Q**	E	A	V	E	~	~	V	R	L	**D**	N	L
Horse	S	S	L	**Q**	E	A	V	E	~	~	I	T	L	**G**	N	L
Rabbit	S	S	L	**Q**	E	A	V	R	~	~	V	T	L	**G**	N	L
Dog	S	S	L	**Q**	E	A	V	E	~	~	I	T	L	**A**	N	L
Opossum	S	S	L	**Q**	E	A	L	K	~	~	I	T	L	**Q**	N	L

Figure 17. The coding SNPs in *Itgal* and *Qprt*. **A.** W972R and P978L amino acid substitutions in *Itgal* are variable among mammalian species. **B.** E205K and D253N coding changes in *Qprt* are not conserved among mammalian species. Glutamine (Q) at position 205 is conserved in mammalian species except rodents.

-nges were predicted to be benign for the protein by *in silico* database analysis.

In silico SNP database analysis has not found any coding SNPs in *Fam57b*, *4933440M02Rik,* and *Dock1* that show the appropriate patterns matching the infarct volume phenotypes. Sequencing analysis of these genes to identify an unknown non-synonymous SNP is underway.

2.3 Summary and Discussion

My research described in this chapter has employed a forward genetic QTL mapping approach to identify genetic determinants critical to cerebral infarction and to dissect apart the roles of individual genes and physiological mechanisms in infarction in mice. The work described here has significantly expanded upon the initial observation on the strain-specific difference in infarct volume, by defining and identifying genetic loci, thus providing a new insight into the pathophysiological mechanisms modulating infarction, based on natural, endogenous genetic variation. The identification of new genes regulating infarct volume will provide additional insight into the biochemical pathways involved in ischemic tissue damage, and in the long-term, provide novel targets for therapeutic intervention of ischemic stroke.

A novel genetic locus for infarct volume was identified

Although significant progress has been made in the identification of genetic risk factors for human ischemic stroke susceptibility, identification of genetic risk factors for stroke outcomes has been severely limited [5]. Because variation in the anatomic location of the occluded artery, extent/ duration of occlusion, time until treatment, and other contributing factors cannot be controlled in patients, few genetic factors have been identified that contribute to the severity of tissue damage in human ischemic stroke. By contrast, these same factors are readily controlled using experimental animal model systems. Importantly, our *Civq*1 does not map to regions of conserved synteny for any of the loci mapped for human stroke susceptibility, illustrating distinct genetic contributions to stroke susceptibility versus stroke outcomes.

In a MCA occlusion study using the spontaneous hypertensive stroke-prone rat (SHRSP), a QTL modulating infarct volume has been mapped to rat chromosome 5 [17]. The major locus we have mapped in the mouse, *Civq1*, is not the region of conserved synteny for the rat locus on chromosome 5. Furthermore, we did not uncover a significant locus on mouse chromosome 4, the genomic region of conserved synteny for rat chromosome 5. Therefore, the same gene cannot be responsible for these 2 loci. Interestingly, we have identified a new infarction locus (*Civq4*) mapping to chromosome 4 in another intercross between B6 and C3H strains. The significant region of Civq4 is the region of conserved synteny for the rat chromosome 5 locus.

In an intercross between SHRSP with WKR rats, blood pressure was influenced by 5 different loci across the genome. One of these, mapping to rat chromosome 1, also influenced infarct volume after distal MCA occlusion [90]. Intriguingly, congenic animals for this locus also showed increased cerebral blood flow, providing genetic evidence for the importance of the regulation of cerebral blood flow in the modulation of infarct volume in this species. We note that a portion of *Civq1* on mouse chromosome 7 is partially overlapping with the region of conserved synteny for the rat chromosome 1 linkage peak. However, the width of the linkage peaks in both species precludes further conjecture on the relationship between the 2 loci.

Civq1 identified in multiple strains has a predominant effect on infarction

Our study confirms that the differences in the severity of ischemic tissue damage after distal MCAO in the common inbred mouse strains are highly heritable because of natural genetic variation. Through the use of different inbred strains and genetic crosses, we present evidence of 3 distinct QTLs that modulate the volume of cerebral infarction.

In particular, a single locus, *Civq1*, which maps to distal mouse chromosome 7, accounts for the major portion of variation in infarct volume in multiple inbred lines. These data demonstrate that natural variation in infarct volume in this species is predominantly due to sequence variation at a single locus, and possibly at a single gene.

Ancestral haplotype analysis greatly facilitated candidate gene identification

Despite successful detection of many QTLs and the important roles of QTL genes in diseases and traits in rodents and humans, identification of causal genes underlying QTLs has been a major obstacle because of a large confidence interval for the typical QTL. Recently, Paigen and colleagues discussed the difficulties associated with identifying causal genes underlying QTLs and presented a complementary bioinformatics strategy for narrowing down QTLs made possible by the recent public sequence and genotype database [52].

Through the use of SNP haplotype analysis we have employed three different ways to capitalize on the structure of the mouse genome to narrow the *Civq1* interval: (1) genome-wide haplotype association, (2) interval-specific haplotype association analysis, and (3) interval-specific haplotype analysis only with the 5 mapping strains used in the experimental crosses. In both genome-wide and interval-specific haplotype association studies, we obtained false-positive results not overlapping with any of our linkage results and the phenotypes. This may be due to a small number of inbred mouse strains in our studies, limited number of SNP used in SNPster algorithm, or complex population structure among the strains.

By contrast, the identification of the same QTL in multiple different crosses significantly facilitated the use of interval-specific ancestral SNP haplotype analysis to substantially reduce the number of potential candidate genes in our locus. Because *Civq1* was detected in multiple experimental crosses, we hypothesize that an ancestral allele of the causative gene on chromosome 7 determines the outcome of focal cerebral ischemia only in the 5 mapping mouse strains. Through the combined analysis of bioinformatics and the public SNP database, the *Civq1* interval was most effectively reduced to only 5 candidate genes that clearly fall within shared SNP haplotype blocks. By DNA sequencing analysis for the 5 possible candidate genes, we have identified that two genes, *Itgal* and *Qprt*, have non-synonymous coding SNPs co-segregating with infarct volume phenotypes. Additionally, *Itgal* exhibited differential gene expression in the brain between the 4 mapping strains, which also correlated with the infarct volume phenotypes.

A major pathophysiological mechanisms underlying *Civq1*

The identification of *Civq1* has raised the question of its associated physiological mechanism and the role of the causative gene in pathophysiology of ischemic stroke. Two broad hypotheses have been put forth to explain the strain-specific effects in infarct volume. The first proposes that differences in infarct volume reflect variation in pre-existing vascular anatomy (i.e. collateral artery) between the strains. A second suggests that the difference in infarct volume is due to a variation in intrinsic ischemic tolerance or protection pathways in the neural tissue.

Hsu and coworkers examined the size of cortical infarct after permanent distal MCA occlusion in 3 different inbred strains; B6, BALB/c, and 129X1/SvJ. BALB/c mice had significantly larger infarcts than B6 and 129X1/SvJ strains[34]. The authors postulated that

the greater susceptibility of BALB/c to ischemic damage was not associated with a greater reduction in flow to the MCA territory because blood flow before and after occlusion was nearly identical in all 3 strains. Similarly, although some strains had a poorly developed posterior segment of the circle of Willis, this anatomic difference did not strictly correlate with either distal blood flow or infarct volume. Thus, Majid *et al* suggested that the differential ischemic outcomes after permanent MCA occlusion are not caused by interstrain differences in cerebrovascular anatomy, but may instead be related to intrinsic differences in ischemic tolerance or protection pathways in neural tissue [34].

By contrast, many other groups have proposed a competing hypothesis that compensatory collateral circulation is a critical anatomic factor responsible for restoration of blood flow after arterial occlusion. However, despite different mouse strains show difference in collateral density in large number of different tissues, whether the collateral circulation in the pial area of the brain significantly modulates infarct volume in stroke is still controversial mainly due to apparently variable presence of these vessels plus absence of good imaging methods in humans. Furthermore, little is known about the genetic determinants and pathways regulating collateral vessel formation and its relationship with severity of cerebral infarction.

In support of this hypothesis, Dr. James Faber's group in communication with our laboratory has recently suggested that the differential tissue damage after MCA ligation might result from differences in preexisting vascular anatomy between B6 and BALB/c strains. They have shown that B6 mice have a well-developed collateral vessel network in the pial area of the brain leading to robust perfusion after MCA ligation, whereas

BALB/c showed almost no collateral vessels and greatly impaired perfusion after ligation. Their data suggest that the observed differences in infarct volume between strains may be due to sequence variation in genes regulating collateral vessel formation [91].

More recently, his group has further demonstrated that the extent of pial collateral circulation in the brain is strongly correlated inversely with our infarct volume data for the 15 inbred mouse strains (Figure 18) [92]. They suggest that variability in collateral vessel number might be a major contributor to variation in infarct volume observed in multiple inbred mouse strains. More importantly, using a total of 243 F2 (B6xBALB/c) progeny, they have identified a significant QTL for collateral vessel number mapping to the identical genomic position of chromosome 7 as *Civq1* maps [92]. Taken together, these data lead us to hypothesize that a causative gene for *Civq1* may regulate collateral vessel development, and that genetic variation in the gene may cause the different extent of compensatory collateral circulation after arterial occlusion resulting in the differential infarct volumes.

To test that hypothesis that *Civq1* for infarct volume regulates collateral vessel density, we have created congenic mouse lines that genetically isolate *Civq1* from B6 background in the genetic background of BALB/c strain. We have also generated the reciprocal congenic line, containing the BALB/c haplotype for *Civq1* on a B6 background. The reciprocal congenic lines retaining the infarct volume locus will be used in the analysis of collateral vessel number in order to test whether *Civq1* for infarct volume is solely determined by collateral vessel formation.

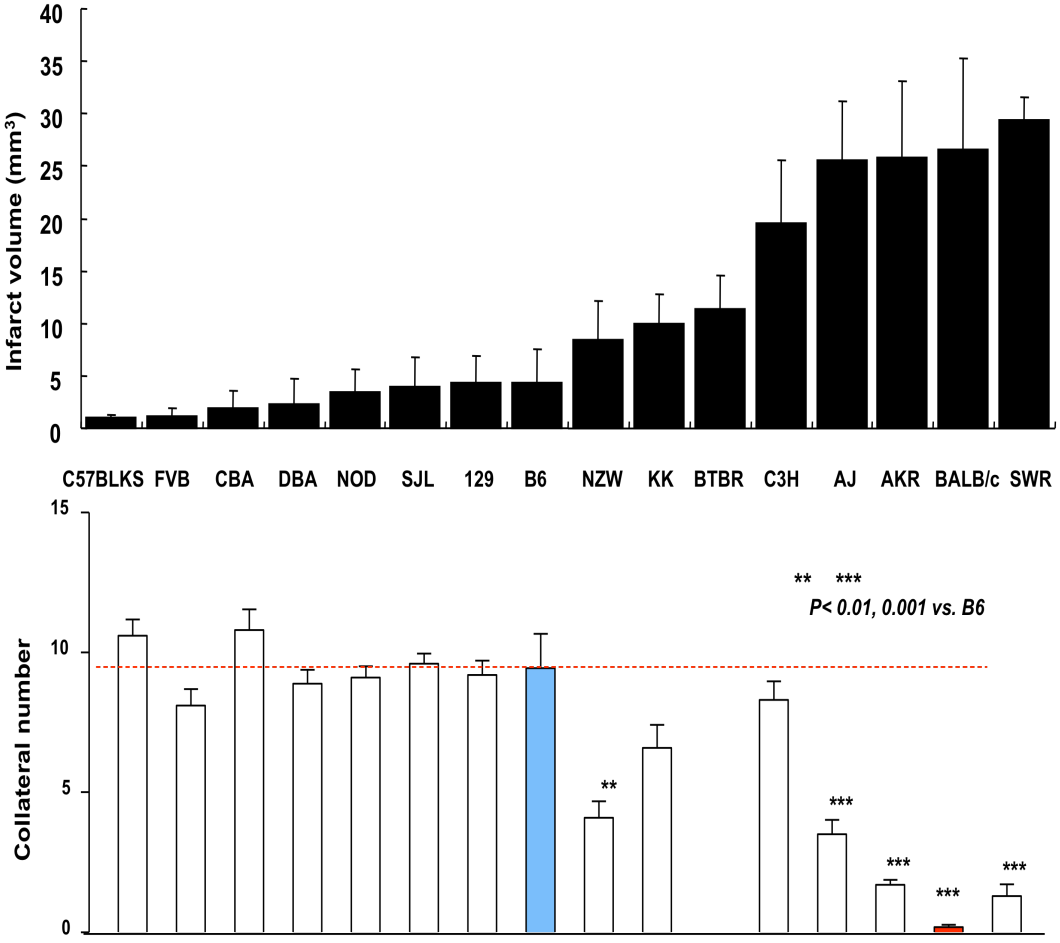

Figure 18. Infarct volume is correlated inversely with collateral vessel number in the pial area of the brain among common inbred mouse strains [90].

Functional validation of candidate genes as a causal gene for *Civq1*

The identification of a QTL for collateral artery number mapping to chromosome 7 is now evidence to strongly suggest that a causative gene underlying *Civq1* may regulate collateral vessel formation. In line with this, we hypothesized that the role of a candidate gene may be important in the leukocyte-endothelial interaction that has been implicated as a critical cellular process for collateral artery formation and remodeling [22,93]. Furthermore, inflammatory response in the brain also has been known to mediate ischemic neuroprotection[94,95]. Of interest, previously several studies have shown that both of the two potential candidate genes, *Itgal* and *Qprt*, play roles in inflammation-mediated vascular growth. Specifically, *Itgal* is highly expressed in microglia, spleen, bone marrow, and most leukocyte populations. In addition to the role in mediating leukocyte inflammation and associated tissue injury, the LFA-1 (αLβ2-integrins)-integrins has been known to modulate adhesion of monocytes to collateral endothelium involved in arteriogenesis [22,83,84]. Thus, *Itgal* represents an attractive candidate gene based on its putative function both in ischemic cell death and in collateral vessel formation.

Interestingly, Arumugam *et al*. showed that due to reduced leukocyte and platelet adhesion to endothelium, *Itgal*-deficient mice exhibited significant reduction in infarct volumes after transient MCAO (1hr occlusion and 24 hr reperfusion) [83]. The authors suggest that LFA-1 (αLβ2-integrins) contribute to the inflammation-mediated brain injury and blood cell-vessel wall interactions associated with transient focal cerebral ischemia. Intriguingly, these data are in contrast to our hypothesis that the higher transcript level of *Itgal* in B6 mice may contribute to the enhanced collateral vessel development, resulting in less severe brain damage in focal cerebral ischemia. In our preliminary experiment, we observed that *Itgal*-deficient mice in a B6 genomic

background showed significantly larger infarct volumes than control B6 mice after permanent distal MCAO model. Further investigation is required to resolve the discrepancy between two different surgical models as well as the role of *Itgal* in collateral formation and ischemic tissue damage.

Besides the quantitative difference of *Itgal* in the brain between mouse strains, we have also identified qualitative changes of the protein caused by two coding SNPs. These two changes (Trp972Arg and Pro978Leu) are located in the calf-2 domain of LFA-1 integrin. These two changes are not conserved across species (Figure 11A) but this alone is of limited significance, though, since non-synonymous coding SNPs for complex genetic traits tend not to fall within highly conserved residues/regions of proteins [69]. Furthermore, although the exact role of the calf-2 domain is not fully understood, the domain is known to be important for stabilizing the bent conformation of integrin proteins [82]. Specifically, Tadokoro *et al*. have demonstrate that a point mutation calf-2 domain of integrin $\alpha_v\beta 3$ in Glazmann thrombasthenia patients disrupts the normal contacts between alpha and beta subunits, resulting in impaired cellular transport from the endoplasmic reticulum [96]. Thus, it is possible that the two amino acid substitutions in the calf-2 region of ITGAL may have an effect on $\alpha-\beta$ complex formation and stabilization of LFA-1 integrin. The functionality of these sequence changes remains to be determined. Studies using Itgal-deficient mice to test the differential gene expression and cell-based assay to test the coding polymorphisms will be carried out to investigate the role of this gene in leukocyte-endothelial interaction.

Although *Qprt* does not appear to be differentially expressed between the mouse strains, it harbors two coding SNPs (Glu205Lys and Asp253Asn) correlated with the infarct

volume phenotypes. *Qprt* is a key enzyme for catabolism of quinolinic acid, a strong neuroendotoxin in the body [87]. Interestingly, several recent studies have demonstrated that the elevated level of quinolinic acid is associated with severity of infarct volume in stroke patients [57]. Furthermore, Ryu *et al*. recently demonstrated that the elevated level of quinolinic acid causes a time-dependent change in vascular growth and remodeling in rat brains [88,97]. Thus, it is possible that the different enzymatic activity of *Qprt* caused by the coding SNPs between the mouse strains might be involved in collateral vessel formation and result in the differential ischemic outcomes. The functional outcome of these two coding polymorphisms also needs to be determined in an enzymatic assay for quinolinic acid metabolism.

2.4 Materials and Methods

Permanent distal MCAO

Focal cerebral ischemia was induced by direct occlusion of the distal MCA as detailed in previous publications [34-37] with the following modifications. Briefly, mice were anesthetized with ketamine (100 mg/kg) and xylazine (5 mg/kg), and the right MCA was exposed by a 0.5-cm vertical skin incision midway between the right eye and ear. After the temporalis muscle was split, a 2-mm burr hole was drilled at the junction of the zygomatic arch and the squamous bone. While visualizing with a stereomicroscope, the right MCA distal to the lenticulostriate branches was electrocauterized using a microcauterizer. The coagulated MCA segment was then transected with microscissors to verify that the occlusion was permanent. The surgical site was closed with 6-0 sterile nylon sutures, and 4% lidocaine cream was applied. Animals were maintained at 37°C during and after surgery until fully recovered from anesthesia, when they were returned to their cages and allowed free access to food and water. All mice were housed in an air-ventilated room with ambient temperature maintained at 24±0.5°C.

Measurement of infarct volume

Twenty-four hours after surgery, the animal was euthanized and the brain was chilled at -70°C for 3 min to slightly harden the tissue. The brain was sliced into 1-mm coronal sections using a brain matrix. Each brain slice was placed in 24 well plates and incubated for 20 min in a solution of 2% TTC in PBS at RT. The sections were then washed twice with PBS and fixed with 10% PBS-buffered formalin. The sections are stored at 4°C. Twenty-four hours after fixation, the caudal face of each section is scanned using a flatbed color scanner. The scanned images are used to determine the infarct volume [98]. ImagePro software is used to calculate the infarcted area of each slice by subtracting the

remaining area of the infarcted hemisphere from the area of the uninfarcted hemisphere to minimize the error that is introduced by edema. The total infarct volumes were calculated by measuring infarct areas on the separate slices, multiplying areas by slice thickness, and summing all slices; this "indirect" morphometric method corrects for edematous swelling [98,99].

Statistical analysis

Infarct volumes were expressed as mean ± SD and compared among mouse strains using 1-way ANOVA or nonparametric Kruskal–Wallis tests. Heritability H^2 [(genetic (interstrain) variance)/(genetic variance + environmental (intrastrain) variance)] was estimated using 1-way ANOVA.

SNP genotyping

A standard high salt procedure is used to isolate genomic DNA from mouse tails. SNP genotyping is performed using the GoldenGateTM genotyping assay. The Illumina mouse low-density (LD) linkage panel is used, consisting of 377 SNPs covering the entire mouse genome, chosen to be maximally informative in crosses between B6 and other inbred strains. Reported genetic map positions were retrieved from the SNP database (Build 37.1) of NCBI.

Linkage analysis

Genome-wide scans were plotted using the J/QTL mapping program, version 1.2.1 (http://research.jax.org/faculty/churchill/). Suggestive ($P=0.63$) and significant ($P=0.05$) thresholds were established empirically for each phenotypic trait by 1000 permutation tests using all informative markers [100]. QTL over suggestive threshold value

were named in accordance with the International Committee on Standard Genetic Nomenclature for Mice (http://www.informatics.jax.org/mgihome/nomen). The percentage of total trait variance attributable to each locus was determined using the Fit QTL function provided within the J/QTL software.

Combined cross analysis

The genotype data for all three intercrosses (B6xBALB/c, B6xSWR/J, and FVBxBALB/c) were merged and a genome-wide scan analysis was run on the combined data using J/QTL mapping program [77]. An indicator variable, cross, was created and included along with any other covariates. The genotype data were merged using a binary encoding that reflected the expected allele types of a shared QTL ("A" genotype - protective strain (B6); "B" genotype - sensitive strains (BALB/c and SWR)). This encoding was based on the parental phenotypes. A combined-cross genome scan was carried out using cross as an additive covariate (Comb1:B6xBALB/c, Comb2: B6xSWR/J, Comb3: FVBxBALB/c) to detect the shared QTL.

Interval-specific SNP haplotype analysis

For the 31.2-Mb interval on chromosome 7, SNP data were obtained from the Mouse Phenome Database (http://phenome.jax.org/), Perlegen mouse SNP haplotype analysis browser (http://mouse.perlegen.com/mouse/mousehap.html), and the Center for Genome Dynamics (http://cgd.jax.org). Physical map position was based on the genomic sequence from the NCBI build 37. Haplotype blocks were defined by 3 or more adjacent informative SNPs [52,79] shared between the large infarct strains (BALB/c, A/J, and SWR/J), which differed from the haplotype for B6 and FVB (REF).

Quantitative real time-PCR

Quantitative RT-PCR was performed using SYBR green dye to determine relative gene expression level of each candidate gene in the cerebral cortex. Quantification of an RT-PCR product was measured by examining the increase in fluorescence that was caused by SYBR green binding to dsDNA. The reaction was analyzed on an ABI 7700 Sequence Detection system (Applied Biosystems) using the following conditions: 95ºC for 10 minutes followed by 40 cycles of 95ºC for 15 seconds and 60ºC for 1 minute. All samples were run in triplicate and additional assays for endogenous controls (GAPDH and/or Hprt1) were performed to control for input cDNA template quantity. Relative quantification was determined for each sample by calculating the mean Ct (the cycle number at which the fluorescence crosses a statistically determined threshold) for each sample and the difference (ΔCt) between the mean Ct values of the samples for each of the target genes and the Ct of the endogenous control. One sample act as the calibrator (the standard to which all other samples are compared). The ΔΔCt, which was the difference between the ΔCt values of the samples for each target and the mean Ct value of the calibrator, was calculated and the relative quantification was expressed as 2-ΔΔCt. Sequence detection software (SDS version 2.1.1, Applied Biosystems) was used for this analysis.

Allele-specific gene expression analysis (SNapShot)

This approach requires at least one SNP in the transcript to distinguish the alleles of the two strains. PCR was performed using an appropriate dilution of cDNA generated from the cerebral cortex of F1 (B6/BALB) animals as described above. Amplicons containing coding SNPs were amplified by conventional PCR, and 15 ul of PCR products were

treated with 1U exonuclease I (New England Biolabs) and 5 U of Shrimp Alkaline Phosphatase (SAP) (Promega). Purified PCR products were used in combination with a conventional primer designed to sit at the nucleotide to the immediate 5′ position of a coding SNPs in the transcript. In SNapShot reaction, 2uM of Itgal Forward primer 5′-CTCCTGGGAAGACTTCGT-3′ or 5′-CAGTGCACAGTGCCATTCAGCTC-3′, 1x PCR buffer, 0.5mM $MgCl_2$ were included. Cycling conditions were as follows: 40 cycles of 95C° for 10s, 50C° for 5s, and 60C° for 30s. The primer became labeled with a fluorescently tagged dideoxynucleotide through a single base pair extension (SNaPshot kit from ABI). These products were treated with 1U of SAP prior to running on an ABI 3130 sequencer and the labeled primer was separated on an ABI 3130 capillary sequencer, and peak heights were logged using Gene Mapper (ABI). To determine conditions under which the SNaPshot assays were quantitative, genomic DNA from the F1 animals was amplified (Primers: F 5′-CTTGAGAGTTAGTGGCCTCTGG-3′ and R 5′-AAGGACACCCAGATGGAAGG-3′) and also analyzed by SNaPshot using the same extension. The expression ratio of each transcript allele was normalized to the ratio of the two alleles in genomic DNA.

Sequencing analysis

Genomic DNA was extracted from mouse tissue using standard procedures. The coding exons and flanking intronic regions of the gene of interest were PCR amplified from genomic DNA. The primers used were designed using the Primer 3 program (http://frodo.wi.mit.edu/cgi-bin/primer3/primer3_www.cgi) to include at least 50 bp of intronic sequence flanking each exon. PCR was performed in thermocyclers using standard conditions. DNA was sequenced using the BigDye Terminator Cycle Sequencing Ready Reaction version 1.1 (Applied Biosystems, Foster City, CA) (1:8).

Excess unincorporated primer and dNTPs were removed using by passage through Sephadex G-50 (Fine) in a microtiter plate format. The cleaned sequencing reaction was then eluted into a 96-well plate compatible with the ABI Prism 3730 (TempPlate III, USA Scientific Plastics). Prepared sequencing reactions were run on an ABI Prism 3730 sequencer (Perkin Elmer, Wellesley, MA). Sequences generated were analyzed using Sequencher software version 4.1.4 (Gene Codes, Ann Arbor, MI) and compared to reference sequences.

Bag3 siRNA knockdown in the OGD ischemia model

Oxygen-glucose deprivation (OGD) in the human SH-SY5Y neuroblastoma cell line is a well-established cell-culture assay for investigation of the role of genes in ischemia (Kogel et al., 2006; Zhu et al., 2007). The short interfering RNA (siRNA) oligonucleotides to knockdown expression of human Bag3 was purchased from Dharmacon (Acell siRNA delivery system). Briefly, human SH-SY5Y cells were trypsinized, plated the cells into a well of a 24-wll plate of 60% confluency, and incubate the cells at 37C° with 5% CO_2 overnight. Next day final 1 μM Bag3 siRNA was treated into the cells and incubated for 72 hours. Functional knockdown of BAG3 protein expression was assessed by western blot. After 72 hour, the growth media was replace with OGD buffer (154 mM NaCl, 5.6 mM KCl, 5.0 mM HEPES, 3.6 mM $NaHCO_3$, 2.3 mM $CaCl_2$), pH 7.4, bubbled with an anaerobic gas mixture (95% N2, 5% CO_2) for at least 2 hr before use. The cell cultures were transferred to a hypoxic pouch (37°C, 95% nitrogen, 5% CO_2, 0.2–0.5% O_2) for 2 hours. Controls are maintained under normal oxygen and glucose concentrations. Cell death was assessed by trypan blue exclusion, which stains nonviable cells.

Western Blot analysis

SH-SY5Y cells were lysed with ice-cold protein lysis buffer (10 mM Tris–HCl, 50 mM NaCl, 5 mM EDTA, plus 1% Triton X-100) containing proteases inhibitors cocktail (Roche) for 20 min. Samples (50 Ag proteins) were then electrophoresed in a 7% polyacrylamide gel and electro-blotted for 4 hours on a nitrocellulose membrane at room temperature. The membrane was then incubated in 5% milk powder in TBST buffer for 1 h. The blot was incubated with the polyclonal anti-Bag3 (1:1000) or anti-Tubulin (1:5000) primary antibody overnight at 4C°, and then with the anti-rabbit (1:10000) horseradish peroxidase-labeled secondary antibody for 1 h. The protein bands were visualized by the chemiluminescence reaction (ECL detection kit), and then densitometrically analyzed by an imaging system.

3.

Identification of the Same Locus on Chromosome 7 in Hindlimb Ischemia

3.1 Introduction/ Rationale

During the course of the work identifying genetic determinants of cerebral infarction after MCAO, we have found that *Civq1* maps in the identical genomic region as a locus that we identified in of hindlimb ischemia, a preclinical animal model of human peripheral arterial diseases (PAD) [1]. Similar to the focal cerebral ischemia model, different mouse strains show differences in limb salvage in surgically induced hindlimb ischemia [1,91,101-103]. After hindlimb ischemia, blood flow was restored to near normal levels by 3 weeks and the limbs exhibited nearly full recovery in B6 mice, whereas BALB/c mice were able to establish only modest levels of blood flow to the ischemic limb, resulting in eventual loss of the limb [1]. This suggests that sequence variation in specific gene(s) in B6 and BALB/c strains may confer the observed phenotypic difference. Thus, we sought to map the genetic loci involved in this differential recovery and test the role of the identified chromosomal region in the observed phenotypic outcome. In a cross between B6 and BALB/c, our laboratory and Dr. Brian Annex's group in the division of cardiology at Duke have identified a very strong locus influencing limb necrosis and recovery of perfusion (*Lsq1*) in the identical position on chromosome 7 as *Civq1* maps.

Given the similarities between the two ischemic models, these data lead us to hypothesize that the chromosome 7 locus protects against the effects of ischemia, regard-

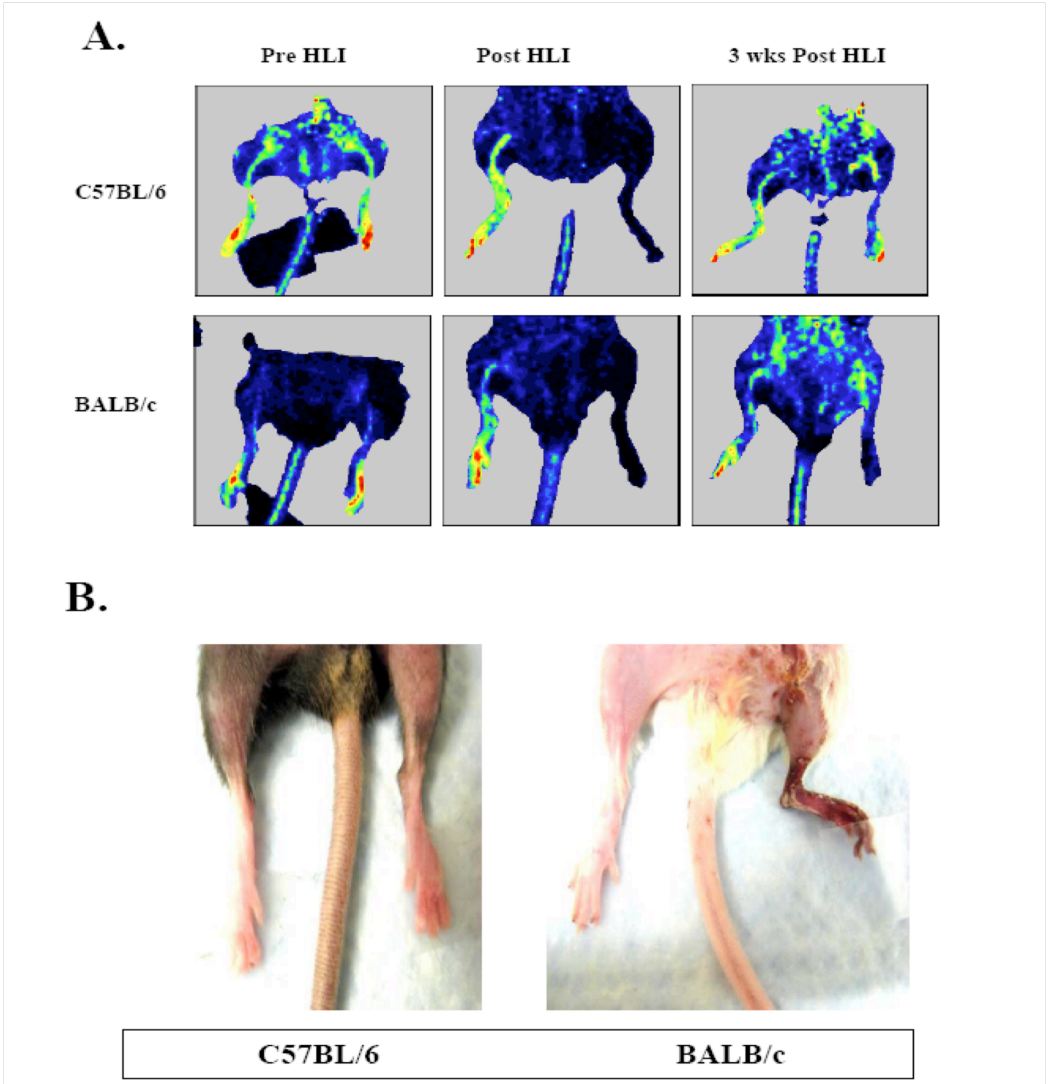

Figure 19. B6 and BALB/c strains differ in response to hindlimb ischemia. **A.** Hindlimb ischemia was induced, and perfusion was measured by laser Doppler perfusion imaging in B6 and BALB/c mice. Representative laser Doppler perfusion images of mice before surgery, immediately after surgery, and 3 weeks into recovery are shown. **B.** BALB/c mice exhibit severe development of necrosis 1 week after induction of hindlimb ischemia [1].

-less of the organ or tissue involved. Thus, the underlying gene, once identified, may have relevance to cerebral ischemia (stroke), limb-ischemia (peripheral arterial disease) and other human vascular occlusive diseases.

3.2 Results

3.2.1 Identification of a QTL mapping to distal chromosome 7

B6 mice showed robust perfusion recovery after ligation, whereas poor blood flow reperfusion was seen in the BALB/c mice (Figure 19A). Necrosis was quite rare in the B6 strain and when present was at a low grade, whereas BALB/c mice were prone to develop necrosis (Figure 19B). The F1 mice exhibited no significant difference in perfusion recovery or necrosis compared to B6 parental strain (Figure 20). This suggests that a dominantly allele(s) in B6 strain could be responsible for the lack of tissue loss.

To map this dominantly acting protective allele in B6 mice, we performed an F1 backcross with BALB/c strain. A total of 105 N2 progeny were genotyped for the 239 SNP markers that were informative in this cross. The average spacing between SNPs was 6.8±1.6 cM, affording full coverage of the mouse genome. Figure 21 illustrates a genome-wide linkage data for the phenotypes of necrosis and perfusion ratio at day 21 after surgery. We identified a single locus on chromosome 7 spanning 31 Mb that exhibited significant linkage to tissue necrosis and day 21 perfusion ratio, with a peak LOD score of 7.96 and 3.71, respectfully, at marker rs13479513 (Figure 21). We designated this QTL *Lsq1* (Limb salvage QTL). We showed the whole genome linkage profile for reperfusion ratio at day 21 because at this time point of measurement chromosome 7 exhibited the highest LOD score. Perfusion ratio was also measured at day 7 and 14 after surgery. For both of these time points, the chromosome 7 linkage reac-

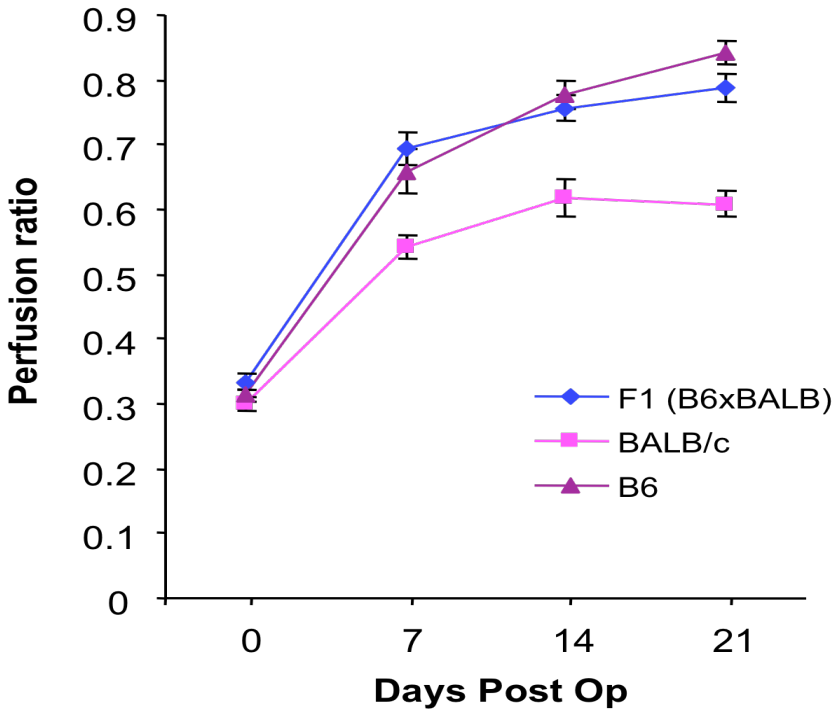

Figure 20. B6 and F1 (B6×BALB/c) mice show similar recovery from hindlimb ischemia. Hindlimb ischemia was induced, and perfusion was measured by laser Doppler perfusion imaging in B6 (n=13), BALB/c (n=9), and F1 (n=18) mice. Immediately after surgery, no difference in perfusion was observed between the three strains. Perfusion in B6 and F1 mice remained similar (*P=0.05*) but was different from BALB/c at later time points (*P=0.05*).

-hed the *P=0.05* significance threshold. Otherwise, across the genome, the linkage profiles for other time points are similar to that seen for the day 21 measurement. Furthermore, the linkage peak for necrosis was even more significant, far surpassing the *P=0.001* threshold. The linkage peaks for perfusion ratio and necrosis were almost identical in chromosomal position, differing only in the magnitude of the strength of linkage (Figure 21).

Because the LOD score for the necrosis trait greatly exceeded that of the perfusion ratio trait, we examined the possibility that the linkage score for the necrosis trait was artificially inflated because of a nonnormal distribution of necrosis scores between heterozygous (B6/BALB) and homozygous (BALB/BALB) animals at *Lsq1*. To exclude this possibility, we recoded the necrosis scores of all the N2 mice on a scale of 0, I, or II (where all scores over II received a value of II) and again as a dichotomous trait (where any level of necrosis received a score of I). Under both recoding schemes, the linkage scores for necrosis were essentially unchanged from the original. Because the MapManager QTX program employs means and not variance components in the analysis, the linkage scores are not unduly influenced by the nonnormal distribution of the values for the trait. Instead, it is likely that these 2 phenotypes are biologically interrelated, with necrosis being the stronger measure of the underlying pathogenesis. The coincident linkage peaks for both traits further support this possibility. No significant gender differences were present in either tissue necrosis or perfusion ratio in either parental background or in the progeny of the backcross.

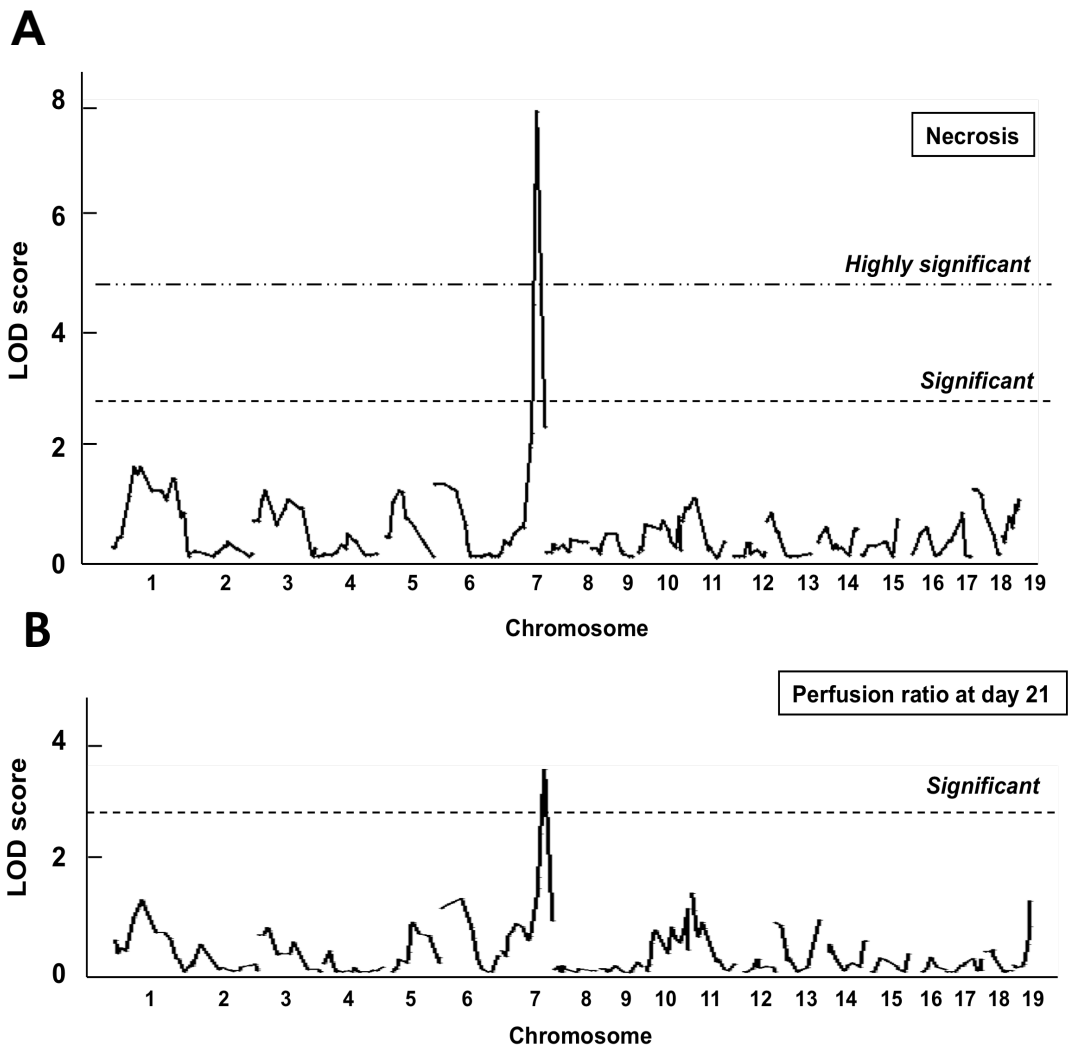

Figure 21. Genome-wide linkage scans for necrosis (A) and perfusion ratio (B) at day 21 after surgery in 105 N2 (F1×BALB/c) progeny. Chromosomes 1 through 19 are represented numerically on the ordinate. The relative width of the space allotted for each chromosome reflects the relative length of each chromosome. The abscissa represents the LOD score. The highly significant (*P=0.001*) and significant (*P=0.05*) levels of linkage were determined by 10,000 permutation tests. Only the chromosome 7 locus showed significant linkage to the 2 phenotypes.

3.2.2 *Lsq1* has a predominant effect on recovery from hindlimb ischemia

To determine the allelic contribution to the effect of the locus between genotype and phenotype data, necrosis and perfusion ratio were evaluated against genotype at *Lsq1* that showed the highest LOD score among all of our SNP markers. The N2 animals with a heterozygous genotype (B6/BALB) at marker rs13479513 showed minimal necrosis and higher perfusion ratio on average than their homozygous (BALB/BALB) littermates (0.37 vs. 1.60 and 0.71 vs. 0.47, respectively; Figure 22). Because the necrosis score was not normally distributed, we used the nonparametric Kruskal-Wallis test, and both necrosis score and perfusion ratio were significantly different between BALB/BALB and B6/BALB animals ($P<0.001$). Moreover, when we examined the correlation between necrosis and perfusion recovery in the N2 progeny, an association was present between poor final perfusion and greater necrosis in these mice (r=-0.628, $P<0.001$; Figure 22C). Results were similar if the perfusion recovery was measured as perfusion at follow-up minus the immediate postoperative value. Taken together, these data provide evidence that B6 chromosome 7 is contributing a dominant protective allele (or alleles) to the recovery phenotype from hindlimb ischemia, and this allele is protective via a mechanism contributing to perfusion recovery.

3.2.3 CSS7 validates existence of *Lsq1* on chromosome 7

To determine whether a B6 protective alleles(s) for tissue recovery from hindlimb ischemia is present on chromosome 7, we used the C57BL/6J-Chr7A/J/NaJ (CSS7) in which the A/J chromosome 7 has been substituted in to B6 genomic background. We first performed unilateral femoral ligation and excision on donor A/J strain to determine its recovery phenotype; A/J mice showed poor recovery compared with B6 and, similar to BALB/c, was prone to developing limb necrosis (Table 4). In light of these finding, we

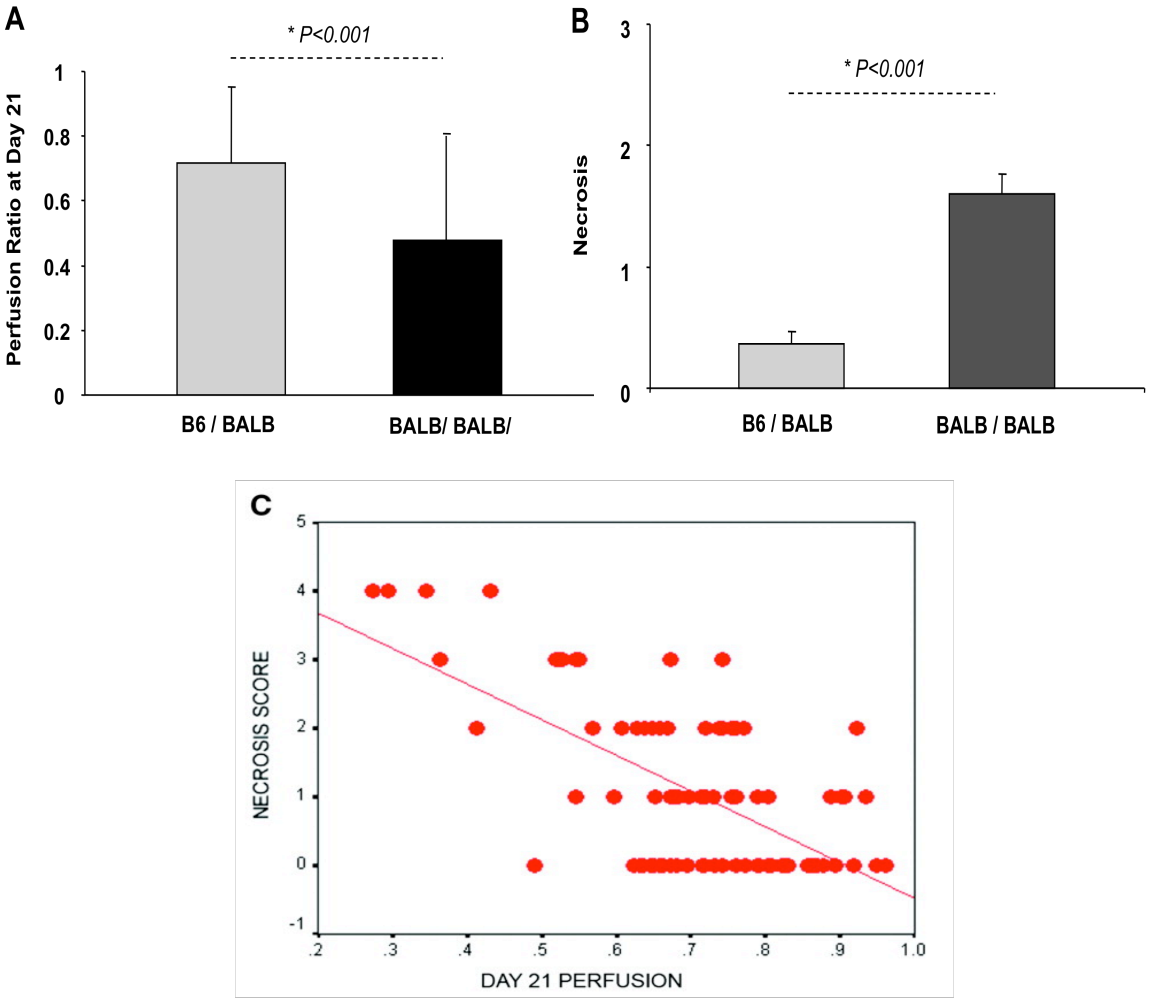

Figure 22. Allelic effects of *Lsq1* on perfusion ratio (**A**) and necrosis (**B**) at SNP marker rs13479513. The heterozygous animals (n=50) with one B6 and one BALB/c allele have higher mean of perfusion ratio and lower mean of necrosis than homozygous BALB/c N2 animals (n=55) (0.72 vs. 0.48 and 0.37 vs. 1.60, respectively), indicating that the heterozygotes show more robust recovery phenotypes after hindlimb ischemia. Each bar represents mean ± SEM. (**P<0.001*). **C.** Necrosis score negatively correlates with perfusion at day 21 in the N2 progeny used for mapping. Statistics was performed by Spearman rank order correlation coefficient, resulting in r= -0.628 and *P<0.001*.

next sought to examine the phenotype in the CSS7 strain and discovered that CSS7 mice also showed poor perfusion recovery (Figure 23) and tendency to develop limb necrosis (Table 3). Furthermore, although no significant difference was observed in capillary density between B6 (0.99±0.07) and A/J (0.91±0.04; *P=0.38*) strains in nonischemic tissues, 5 weeks after induction of limb ischemia, B6 mice showed higher capillary density (1.30 ± 0.06) than the A/J or the CSS strain (0.97± 0.10, *P=0.03* or 1.01± 0.11, *P=0.04*; n=3 per group). Therefore, these data show that the B6 chromosome 7 is required for the lack of tissue loss and greater perfusion recovery phenotype after hindlimb ischemia. Additionally, A/J and BALB/c alleles at the chromosome 7 locus may be identical because of ancestral relateness.

3.2.4 B6 allele(s) at *Lsq1* has no effect on would healing

We next sought to determine the role of B6 allele(s) at *Lsq1* in a nonischemic tissue injury (ie, wound healing). Wounding healing rates were determined over a 2-week period. No significant difference was observed between the 2 strains in the rate of wound healing 1 week after injury (79.8 ± 2.6% in BALB/c vs. 83.9 ± 3.2% in B6; *P=0.29*; n=6 per group), and all mice from both strains achieved complete wound closure by week 2 (100% in both strains). Similar results were observed in the CSS strain (90.4 ± 4.1% at 1 week; n=4; all mice were healed at 2 weeks), suggesting that allelic effect of the B6 allele at *Lsq1* may be specific for recovery after ischemic injury.

Table 4.

Incidence of severity of necrosis in mouse strains following hind-limb ischemia

			Necrosis Grade				
Mouse Strain	N	Total	Grade 0	Grade I	Grade II	Grade III	Grave IV
BALB/c	11	10/11	1/11	4/10	3/10	3/10	None
		(90.1%)	(9%)	(40%)	(30%)	(30%)	
C57BL/6(B/6)	41	1/41	40/41	1/1	None	None	None
		(2.4%)	(97.6%)	(100%)			
B/6 x BALB/cF1	18	3/18	15/18	3/3	None	None	None
		(16.7%)	(83%)	(100%)			
A/J	15	9/15	6/15	1/9	1/9	2/9	5/9
		(60%)	(40%)	(11%)	(11%)	(22%)	(55.5%)
CSS	10	8/10	2/10	1/8	2/8	4/8	None
		(80%)	(20%)	(12.5%)	(25%)	(50%)	

Necrosis grade is from 0-4, as described in the Methods Section.

The "Total" column refers any necrosis, 1 through 4, and the distribution is to the right.

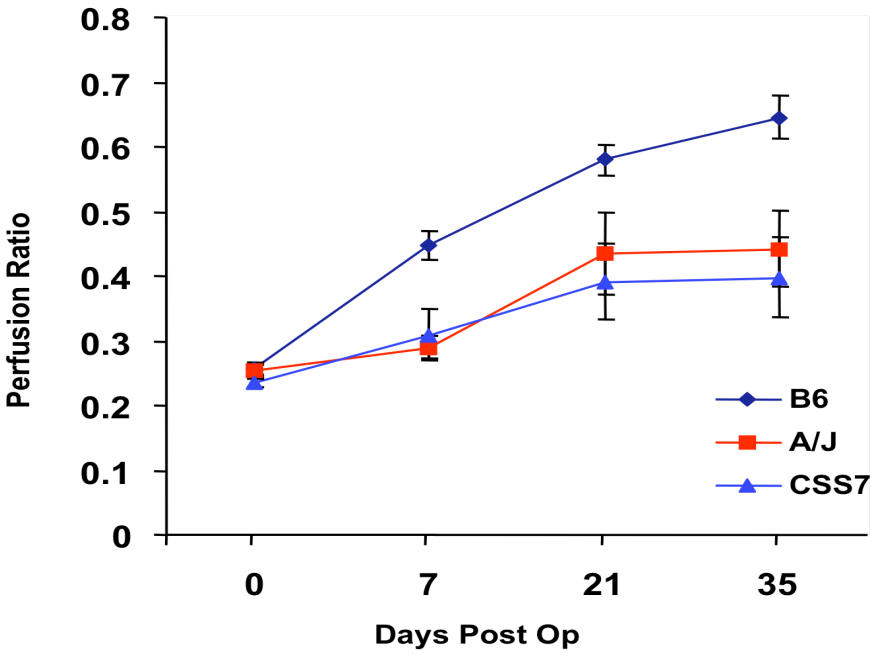

Figure 23. The B6 chromosome 7 confers a strong protective effect on ischemic tissue damage in a chromosome substitution strains. Hindlimb ischemia was induced, and perfusion was measured by laser Doppler perfusion imaging in A/J (n=15), B6 (n=17), and C57BL/6J-Chr7A/J/NaJ (CSS7, n=10) mice. Similar to BALB/c mice, A/J mice display poor recovery after hindlimb ischemia. No difference in perfusion was shown between the 2 strains immediately after induction of hindlimb ischemia ($P>0.05$); however, B6 mice showed better perfusion than A/J strain ($P<0.001$) at later time points. Recovery was similar in CSS7 and A/J strains ($P>0.05$) but different in B6 ($P<0.01$).

3.3 Summary and Discussion

Similar to the studies for focal cerebral ischemia, the works described in this chapter also show that inherited genetic variations strongly influence the ischemic outcome after femoral arterial occlusion, a preclinical animal model of PAD. We found that the genetic background of B6 mice was associated with greater limb perfusion and less limb loss from hindlimb ischemia when compared to the BALB/c strain. Using the two complementary phenotypic measurements, we have provided evidence that the difference in response to blood flow restriction in limbs is under strong genetic control. Through a backcross of F1 (B6XBALB) animals with BALB/c mice, we have identified a significant linkage result mapping to the identical genomic position in chromosome 7 for all quantitative measures of blood flow and limb necrosis as *Civq1* maps.

Insight into a novel genetic factor influencing ischemic outcome in PAD

When occlusions are present in the large arteries to the lower extremity, the result is the most common form of PAD [104-107]. The 2 major clinical manifestations of lower-extremity PAD are (1) intermittent claudication (IC), which is defined as leg pain during exercise that is relieved by rest and the absence of either rest pain or tissue loss, and (2) critical limb ischemia (CLI), which is defined as leg pain at rest with or without tissue loss (non-healing leg ulcers or gangrene). Despite the significant overlap in risk factors leading to the development of both clinical presentations, patients with CLI frequently have ongoing or imminent tissue loss and thus have a higher rate of amputation and mortality. Patients with IC rarely develop tissue loss. Although risk factors include advanced age, diabetes mellitus, hypertension, hypercholesterolemia, and smoking in

patients with lower-extremity PAD, genetic factors and critical pathophysiological pathways modulating ischemic tissue damages (IC vs. CLI) are not fully understood yet.

Previously, several studies have investigated the role of gene polymorphisms in the pathogenesis of PAD in humans; however, in most of these studies, the investigation centered on polymorphisms of genes known to be associated with atherosclerosis or atherothrombosis [104-107]. There is only a single family-based linkage study that identified a genetic locus conferring susceptibility to PAD [108]. Gudmundsson and coworkers identified a locus mapping to human chromosome 1p31 termed PAOD1. One of the strengths of this study is that it took an unbiased approach, starting with the PAD phenotype, to identify novel genetic risk factors rather than starting with a potentially biased list of candidate genes. However, a causative gene underlying this locus has yet to be identified.

In our study, we used a preclinical model of PAD and identified a chromosomal region in mice, termed *Lsq1*, that, when present, was associated with absence of tissue loss. This is the first identification of such a quantitative trait locus in PAD. *Lsq1* is not a region of conserved synteny to human chromosome 1p31. Therefore, the gene for PAOD1 cannot be responsible for *Lsq1*, although it is possible that genes in both species may ultimately be shown to play a role in the same physiological pathway. Our study can serve as a valuable foundation for future studies to identify specific gene(s) involved in PAD in patients. Identification of a gene and responsible mechanism will advance the understanding of the pathophysiology of PAD, as well as new treatment options.

Major physiological mechanisms responsible for *Lsq1*

What is a major physiological mechanism determining these differential ischemic outcomes after hindlimb ischemia? As discussed in chapter 1, pre-existing collateral arteries have been known as a critical anatomic factor responsible for restoration of blood flow after arterial occlusion. Many groups have suggested that anatomic differences in collateral vessel density between B6 and BALB/c strains might result in the difference in the extent of tissue damage from hindlimb ischemia between the two strains [1,91,101-103]. Schaper and colleagues have showed that differences in the extent of pre-existing collateral vessels and arteriogenesis play important roles in perfusion recovery after hindlimb ischemia[103]. Chalothorn *et al.* also reported that the number of pre-existing collaterals in the thigh of BALB/c strain was 35% fewer than in B6 strain, resulting in the different ischemic outcomes [91]. Recently, van Weel *et al.* also showed that collateral artery growth after hindlimb ischemia was severely reduced in BALB/c mice when compared with B6 mice. Intriguingly, the authors further demonstrated that this phenotypic difference in ischemic outcome after hindlimb ischemia was associated with the difference in NK-cells and $CD4^+$ T-cell-mediated arteriogenesis [109].

In agreement with these data, we have identified that *Lsq1* does not affect non-ischemic wound healing, and we showed a correlation between lower perfusion recovery and greater necrosis, indicating that the effect of the chromosome 7 locus may be via a mechanism contributing to restoration of perfusion [1]. This suggests that a causative gene for *Lsq1* may play an important role in the response to ischemia, rather than in generalized tissue regeneration.

As discussed in Chapters 1 and 2, similar phenotypic difference in ischemic outcomes was observed in focal cerebral and hindlimb ischemia between B6 and BALB/c strains. Most significantly, *Lsq1* maps in the identical genomic position of chromosome 7 as *Civq1* for infarct volume and a QTL for collateral vessel number in the brain. Therefore, in support of these genetic evidence, we propose that the observed effect of *Civq1* and *Lsq1* do, in fact, represent different manifestations of the same causal gene that regulates collateral vessel formation. Hence, *Civq1*/ *Lsq1* may confer sensitivity to the effect of ischemia in multiple tissues through restoration of blood flow from collateral circulation.

However, studies by Fukino *et al* and other groups found a differential angiogenic response between the B6 and BALB/c strains after limb ischemia, suggesting a role for angiogenesis in this phenotypic outcome [101,102]. Interestingly, our data showing higher vascular density in B6 tissue at late time points after ligation compared with the CSS7 and A/J strains also supports the role of angiogenesis in strain-specific recovery from hindlimb ischemia. Moreover, the most significant linkage result of *Lsq1* was obtained at day 21 after the complete excision of the femoral artery, also suggesting that a causative gene may be involved in the recovery process following ischemia.

In contrast to cerebral infarction 24 hours post MCA occlusion, an acute ischemic outcome in the brain, multiple pathophysiological mechanisms can be involved in recovery after hindlimb ischemia. This may be one explanation to account for the different observations. These mechanisms may include, but are not limited to, ischemic injury, tissue regeneration, inflammation, angiogenesis, and arteriogenesis. It is potentially possible that a causative gene acts differently between the skeletal muscle and the brain, or that the differential ischemic outcomes from the two different types of

ischemia are determined by different amounts of pre-existing collaterals in the two different tissues between B6 and BALB/c strain. As noted, Chalothorn *et al*. reported that BALB/c strain had 35% fewer collaterals in the thigh than in that of B6 stain, but almost no collateral vessels were observed in the brain of BALB/c mouse [91]. Additionally, we do not rule out the possibility that a potential additional gene on chromosome 7 plays a role in recovery, including adaptation to tissue ischemia, skeletal muscle regeneration, or mechanisms not yet postulated. In Chapter 2, we have shown that *Bag3* exhibits a cytoprotective effect in neuronal cell death induced by OGD. Since the gene is highly expressed in the skeletal muscle, it is potentially possible that a coding SNP between B6 and BALB/c strains that creates an Ile81Met change in *Bag3* protein may confer different sensitivity to ischemic insult in the skeletal muscle.

3.4 Materials and Methods

Hindlimb Ischemia, Perfusion Recovery, Necrosis Score, and Histology

Unilateral femoral artery ligation and excision was performed to induce hindlimb ischemia. Perfusion flow in the ischemic and contralateral nonischemic limbs was measured with the use of a laser Doppler perfusion imaging system [110,111]. Perfusion was expressed as the ratio of the left (ischemic) to right (non-ischemic) hindlimb and was performed immediately after surgery and weekly or biweekly up to 21 or 35 days postoperatively. Perfusion recovery was determined either by the absolute perfusion ratio at follow-up or as the ratio at follow-up minus the ratio immediately after surgery. In mice that developed autoamputation, the perfusion ratio obtained from the limb before autoamputation was used. The extent of necrosis was scored as follows: grade I, involving only toes; grade II, extending to dorsum pedis; grade III, extending to crus; and grade IV, extending to thigh or complete necrosis. In the ischemic and nonischemic gastrocnemius muscles, vascular density was analyzed by immunohistochemistry with a rat anti-mouse CD31 antibody by counting 3 random high-power (magnification x 200) fields for a minimum of 200 fibers and was expressed as the number of CD31 cells per fiber.

Wound Healing

Full-thickness skin punch biopsies were made as described previously [112]. Briefly, mice were anesthetized with ketamine (50 mg/kg) and xylazine (5 mg/kg). The skin over the dorsum surface was shaved, and a 0.7- to 1.0-cm-diameter wound was generated with a disposable 0.8-cm-diameter skin punch biopsy tool. Wound dressing was achieved with the use of a spray-on liquid bandage solution (Nexcare, St Paul, Minn). Wound area was

measured weekly. The healing rate was defined as a percentage of original wound area or totally healed.

Genotyping

A standard high-salt procedure was used to isolate genomic DNA from mouse tails. A total of 105 N2 animals were used to identify quantitative trait locus (QTL) in the linkage scan. Single-nucleotide polymorphism (SNP) genotyping was performed with the use of the GoldenGate genotyping assay and the Illumina Bead Station. The Illumina mouse low-density linkage panel was used, consisting of 377 SNPs covering the entire murine genome, chosen to be maximally informative in crosses between B6 and other inbred strains. In our cross between B6 and BALB/c, 239 autosomal SNP markers were informative. The average spacing per informative SNP was 6.8±1.6 cM, with the largest gap located on chromosome 2 (24.6 cM). Reported genetic map positions for the markers were retrieved from the SNP database (Build 36.1) of the National Center for Biotechnology Information (NCBI).

Linkage Analysis

The MapManager QTX program (version b20) was used to localize the QTL responsible for the variability of recovery phenotypes from surgically induced hindlimb ischemia (necrosis and perfusion ratio). The source codes are available online at http://www.mapmanager.org/mmQTX.html. The significance thresholds for each phenotypic trait were determined empirically by permutation tests performed with all the informative markers and 10,000 permutation tests of data [78]. This logarithmic index can be converted to a logarithm of odds (LOD) score by dividing it by 4.61. Suggestive (*P=0.67*), significant (*P=0.05*), and highly significant (*P=0.001*) thresholds were

established on the basis of the guidelines suggested by Lander and Kruglyak [100]. Single-locus association tests were performed between each marker and the phenotype to identify regions of interest in our initial genome scan. The genome-wide scans were plotted with the use of the J/QTL mapping program (ver. 0.8) obtained from the Jackson Laboratory (http://research.jax.org/faculty/churchill/).

Statistical Analysis

All continuous measures were expressed as mean ± SEM. Statistical comparisons of perfusion or capillary density between multiple strains of mice were performed with the use of 1-way ANOVA; between 2 strains, the independent Student t-test was used. Comparison of perfusion within each strain at different time points was analyzed by repeated-measures ANOVA. Differences in necrosis score between mice with a different genetic background were analyzed by nonparametric Kruskal-Wallis test. In all cases, P=0.05 was considered statistically significant. Correlation of perfusion recovery with necrosis was performed with the use of the Spearman correlation.

4.

Identification of a New Locus Independent of Collateral Number

4.1 Introduction / Rationale

As described in the Chapter 2, our infarct volume data for the multiple inbred strains is correlated inversely with collateral vessel numbers in the brain [92]. However, we have found that one strain of mouse, C3H/HeJ (hereafter C3H), does not follow the correlation. Both B6 and C3H strains exhibit a similarly large number of collateral vessels but the observed infarct volumes were significantly different between the strains (Figure 18). The average infarct volume of C3H mice was 4.3-fold larger (19.1 mm^3) than that of B6 mice (4.4 mm^3). These two additional strains may provide evidence for the presence of additional loci controlling infarct volume. These data allowed us to hypothesize that the difference in infarct volume between B6 and C3H might result from genetic variation in a different locus, independent of collateral vessel number.

4.2 Results

4.2.1 A new locus independent of collateral number mapped to chromosome 4

In order to determine whether the difference in infarct volume between the 2 strains is caused by a different mechanism unrelated to collateral vessel formation and to genetically map a new locus modulating cerebral infarction, we performed an intercross

between B6 and C3H strains. Infarct volumes were measured in both sexes for a total of 30 F2 progeny. F2 mice were genotyped for 178 SNP markers that were informative between the B6 and C3H strains. From this cross, we identified a significant locus (LOD=3.47) that mapped to a new locus (peak LOD at rs3653593) on chromosome 4 (Figure 24). As we hypothesized, *Civq1* on chromosome 7 was not identified in this cross, suggesting that this new locus (*Civq4*) might be associated with a different pathophysiological mechanism, possibly distinct from native collateral vessel formation. Similar to the chromosome 7 locus, *Civq4* explains the majority of the effect (53%) of the total variance of infarct volume observed between B6 and C3H strains. Interestingly, the B6 allele at *Civq4* shows a dominant protective effect on infarct volume. To determine the allelic contribution of the effect of *Civq4*, infarct volumes were evaluated against genotype at the highest LOD score among all of the informative SNP markers (Figure 25). F2 animals homozygous for the C3H allele (n=12) exhibit significantly higher mean infarct volume than mice heterozygous (n=12, $P<0.05$). There was no statistical difference in infarct volume between the F2 animals homozygous for the B6 allele (n=6) and the mice heterozygous (n=12), suggesting that strain B6 harbor a dominantly-acting protective allele(s) at *Civq4*.

4.2.2 Pinworms might interfere with the experimental result after MCAO

Because we first wanted to quickly determine whether *Civq1* on chromosome 7 is responsible for the phenotypic difference between B6 and C3H strain, we carried out a QTL mapping only for a small number of F2 progeny (n=30). In addition to a new locus (*Civq4*) showing a major effect for the observed infarct volume difference, we identified another locus mapping to chromosome 10 that reached the $P=0.63$ suggestive level (Figure 24). Thus, we sought to perform a second mapping analysis with additional F2

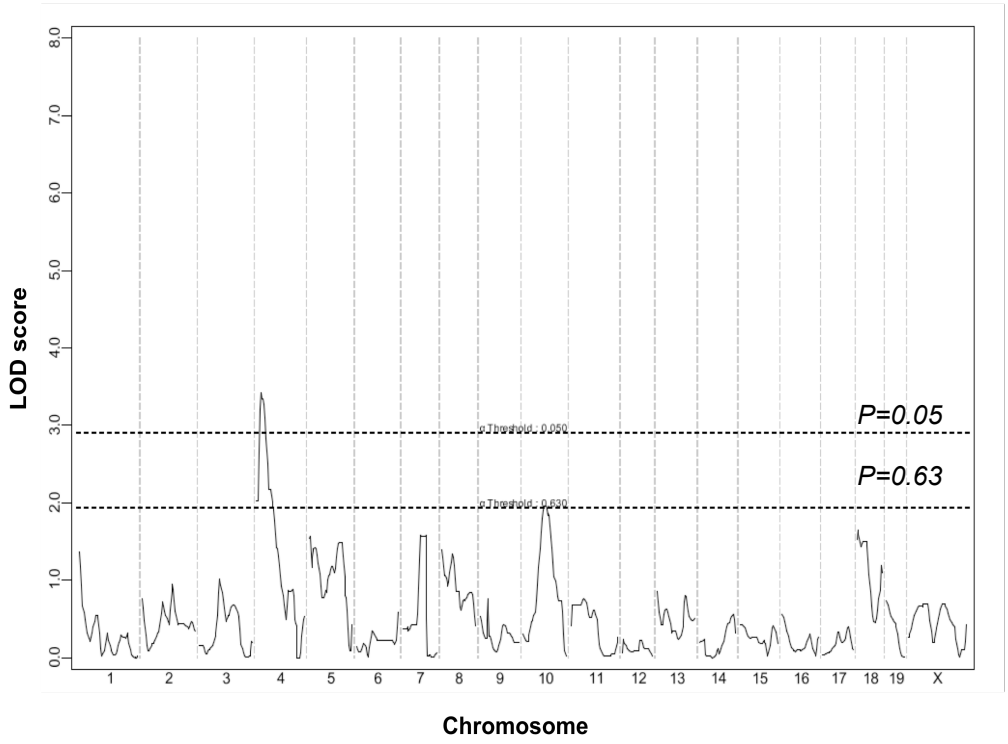

Figure 24. A new infarction is mapped to chromosome 4. The graph presents the results of a genome-wide linkage scan for infarct volume 24 hours after permanent MCAO in 30 (B6xC3H) F2 progeny. Chromosomes 1 through X are represented numerically on the x-axis. One region of the genome, distal chromosome 4, displays significant linkage to the trait, with a LOD score of 3.47. One other locus mapping to chromosome 10 reached the *P=0.63* suggestive level. Chromosome 7 locus was not mapped in this cross.

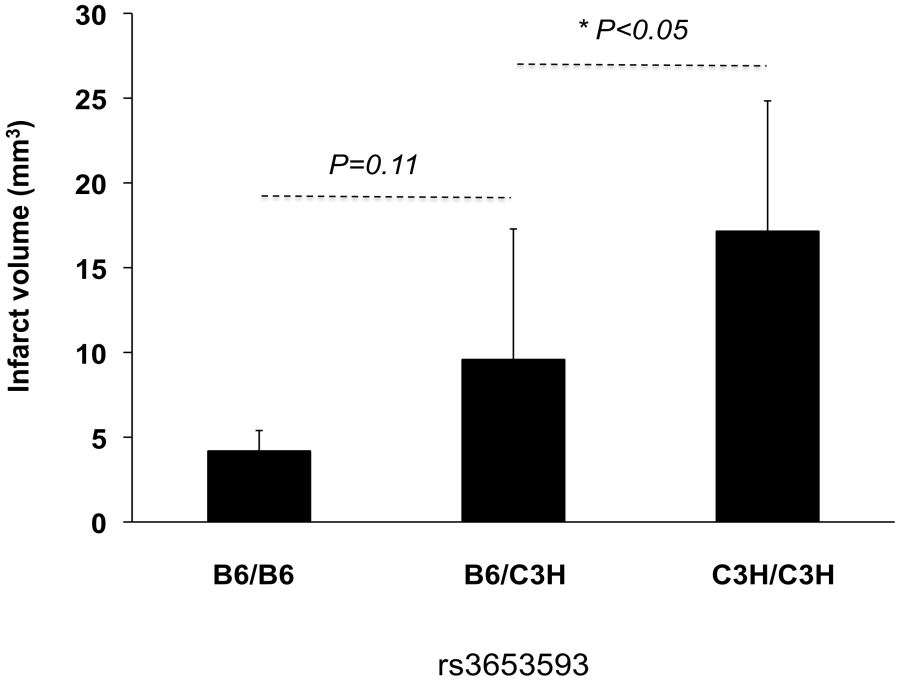

Figure 25. The B6 strain harbors a dominantly-acting protective allele (s) at *Civq4*. The histogram displays the phenotypic effect of the allele at SNP rs3653593 (in parenthesis) on infarct volume in 30 F2 progeny. F2 animals homozygous for the C3H allele (n=12) exhibit higher mean infarct volume than mice homozygous for the B6 allele (n=6) and heterozygous (n=12, *P=0.025*). Infarct volumes were not significantly different between B6 homozygous and heterozygous animals at the marker. Error bars represent SD.

animals not only to validate the existence of the chromosome 10 locus, but also to obtain more significant statistical power for *Civq4*. We generated additional 34 F2 progeny and carried out a mapping analysis. No significant linkage was identified in the second cross (Figure 26). Although the chromosome 10 locus still reached suggestive threshold (*P=0.63*) and two new suggestive loci mapping to chromosome 12 and 17 were identified, *Civq4* was not identified in the second F2 progeny (Figure 26). To determine whether *Civq4* becomes more significant in combined data, we merged the data for the two cohorts and performed a linkage analysis. Surprisingly, a locus mapping to chromosome 8 exhibits significant linkage result (LOD=3.72). We found that the peak of the suggestive chromosome 10 locus was slightly increased, but the linkage value for *Civq4* did not changed (LOD=3.47), indicating that the new 34 F2 animals had no contribution to the chromosome 4 locus (Figure 27). Because *Civq4* exhibited a strong phenotypic effect (53%) on infarct volume for the 30 F2 animals in the first cross, it is less likely that the absence of linkage on chromosome 4 in the second F2 progeny resulted from lack of power.

The only explanation to account for this result was the pinworm infection to the second 34 F2 progeny. During the period of aging, we had been notified that the mice were exposed to rodent pinworm in our animal facility and the drug, Ivermectin, was treated to eradicate the nematodes in the mice. Rodent pinworm has been known to be an environmental agent that may significantly modify the host's immunohematopoietic responses, and, therefore, interfere with the experimental settings and alter the interpretation of the final results [113,114]. It is of course also possible that the drug used to treat the mice influenced the ischemic outcome after MCAO. We do not exclude the possibility that the chromosome 8 and 10 loci are actually present in this cross and

pinworm infection or the drug influenced the physiological mechanism critical for cerebral infarction, resulting in a biased or an interfered ischemic outcome after MCAO. To avoid all these possible interferences, we will start a new intercross when pinworm eradication is confirmed. As an alternative method, we are aware that the parental strain B6 and C3H have been used to construct a series of recombinant inbred lines (BXH) for mapping purposes. We will consider employing subsets of these RI lines that harbor recombination breakpoint on chromosome 4 to help refine the position of the locus. These RI lines also can be used to validate whether the suggestive chromosome 10 locus retains the infarct volume locus.

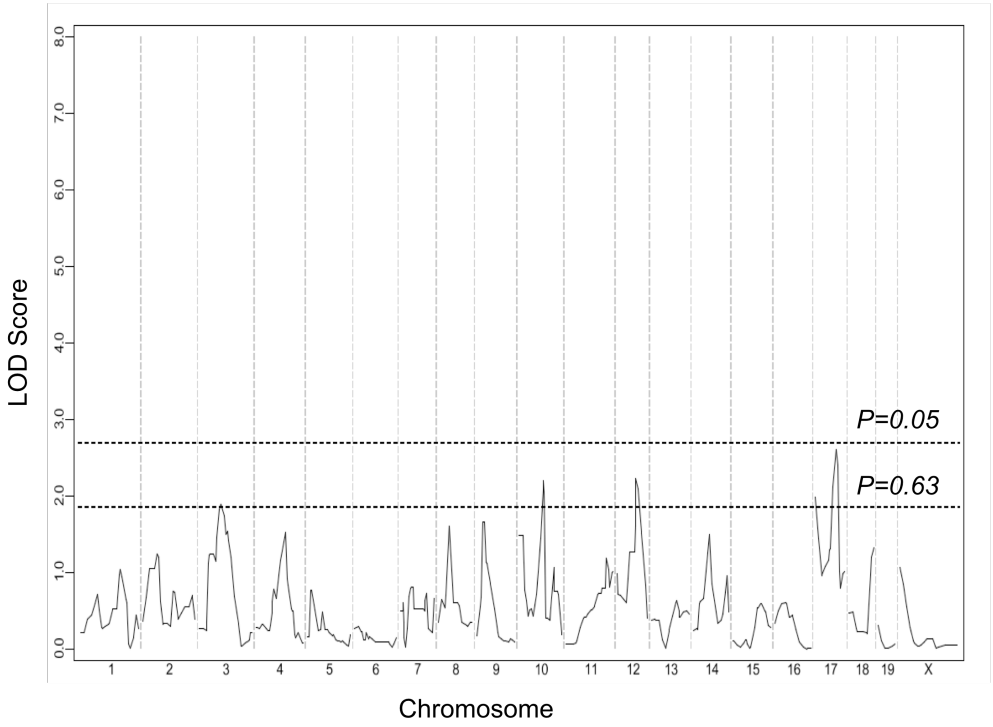

Figure 26. A different genome-wide linkage profile was identified after rodent pinworm infections. The graph presents the results of a genome-wide linkage scan for infarct volume 24 hours after permanent MCAO in 34 (B6xC3H) F2 progeny. Chromosomes 1 through X are represented numerically on the x-axis. No region displays significant linkage to the trait. Three regions on chromosome 10, 12, and 17 reached the *P=0.63* suggestive level. Chromosome 7 (*Civq1*) locus was not mapped in this cross.

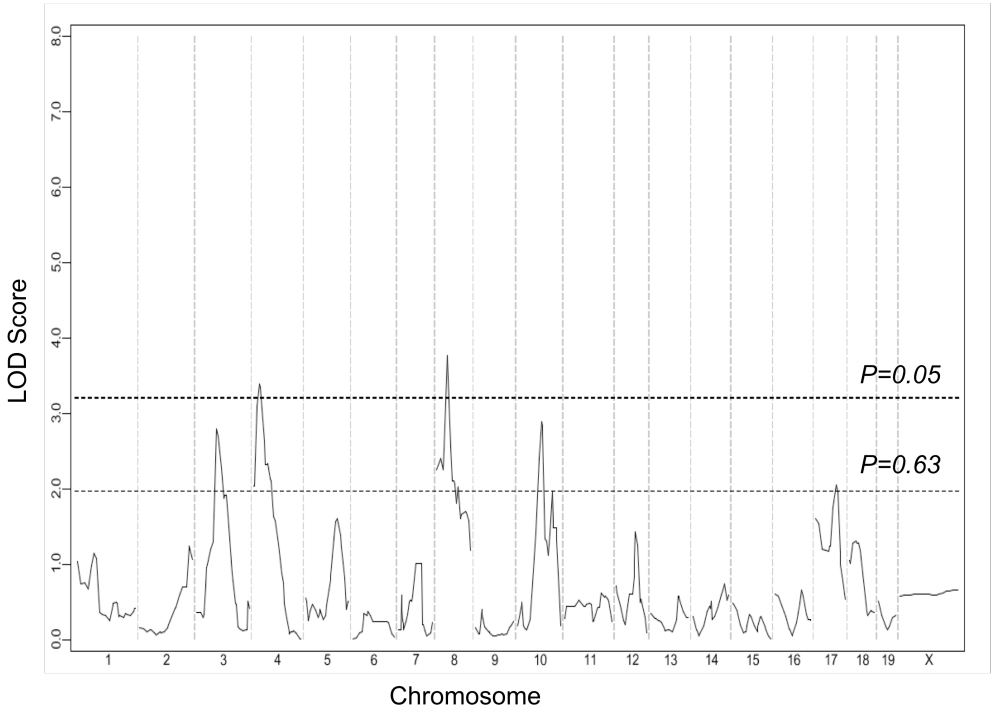

Figure 27. A genome-wide linkage scan for the 64 F2 (B6xC3H) progeny. The graph presents the results of a genome-wide linkage scan for infarct volume 24 hours after permanent MCAO in pinworm-free 30 (B6xC3H) and pinworm-infected 34 (B6xC3H) F2 animals. Chromosomes 1 through X are represented numerically on the x-axis. One new locus mapping to chromosome 8 displays significant linkage value but Civq4 on chromosome 4 shows the unchanged LOD score of 3.47. Two regions on chromosome 3 and 10 reached the *P=0.63* suggestive level. Chromosome 7 (*Civq1*) locus was not mapped in this cross.

4.3 Summary and Discussions

Identification of a new QTL of large effect modulating infarct volume

The work described in this chapter began with the observation that the difference in infarct volume between B6 and C3H strains is not correlated with collateral number in the brain. We have identified a new locus of large effect modulating cerebral infarction, most likely through a mechanism unrelated to collateral circulation. More importantly, because *Civq1*, which is present in multiple inbred strains was not identified in this cross, this new mapping result strongly suggests to us that the causal gene underlying *Civq1* on chromosome 7 may play an important role in collateral vessel formation.

Intriguingly, the *Civq4* interval on chromosome 4 contains the region of conserved synteny for human chromosomal region (8q24.21–8q24.3), which is linked to premature myocardial infarction [115]. Additionally, we have found that a portion of *Civq4* on mouse chromosome 4 is partially overlapping with the region of conserved synteny for the rat chromosome 5 linkage peak that modulates infarct volume in a MCAO study using the spontaneous hypertensive stroke-prone rat (SHR) [17]. However, the width of the rat QTL (>100Mb) and *Civq4* (~30Mb) precludes further conjecture on the relationship between the two loci.

Approaches toward candidate gene(s) identification

As seen previously, the combination of the mapping cross and interval-specific ancestral SNP haplotype analysis for *Civq1* on chromosome 7 has provided us with a short list of candidate genes. However, we will exploit the congenic and nested sub-congenic lines to primarily assist fine mapping of *Civq4* on chromosome 4. Because C3H is the only outlier

strain of the correlation between infarct volume and collateral number among the 15 inbred mouse strains, we hypothesized that the phenotypic variation of C3H strain might be caused by genetic variation unique to that strain, rather than from genetic polymorphisms inherited from the ancestral strains.

Once we genetically isolate the congenic line retaining the infarct volume locus, the line will be used in functional analyses not only to determine the physiological or anatomic mechanism, but also to identify a candidate gene(s) underlying *Civq4*. Since cerebral infarction is the final ischemic outcome from a complex pathophysiological interaction between multiple cell types in the brain, we will test the candidate genes located within the dissected locus of *Civq4* for their mRNA transcript levels in multiple tissues, including the cerebral cortex, leukocytes, and endothelial cells. Independently, candidate genes that harbor functional SNPs (ie. splicing, non-synonymous, or stop codon) will be considered as the highest priority candidate genes.

Pathophysiological mechanisms responsible for *Civq4*

What physiological mechanism may cause the difference in infarct volume between B6 and C3H strains? While the mechanism underlying the chromosome 4 locus is currently unknown, several studies suggested that strain-specific vascular remodeling might cause the difference in vascular injury and atherosclerosis between inbred mouse strains. Specifically, multiple studies in the literature show that strain B6 and C3H mice exhibit differences in inflammation-mediated vascular remodeling and atherosclerosis [116-120]. Of interest, Thurston *et al.* reported that in chronic pulmonary inflammation, B6 mice exhibited new vessel growth (angiogenesis), whereas C3H mice showed vessel enlargement with increased numbers of endothelial cells but without new vessel growth

[116]. Moreover, a recent study further demonstrated that C3H mice showed severe ischemia-reperfusion (I/R) lung injury characterized by increased pulmonary endothelial permeability and edema. By contrast, BALB/c mice that are sensitive to both cerebral and hindlimb ischemia in our studies, exhibited a strong protective phenotype to this lung ischemia [119]. These data suggests that genetic variation underlying *Civq4* might be associated with a different physiological mechanism from collateral circulation.

In this light, the mechanism underlying *Civq4* will be investigated using congenic mouse lines that genetically isolate the locus. We will use sub-congenic mice that have isolated *Civq4* to probe the physiological mechanisms underlying the gene(s) at this locus. Each strain will be investigated for anatomic (vascular), and metabolic (neural) properties to test specific hypotheses. The results will establish the overall physiological mechanism behind *Civq4*. More significantly, the identification of a new gene modulating infarct volume will provide additional insight to the pathways and mechanisms involved in cerebral infarction.

4.4 Materials and Methods

Permanent distal MCAO

Focal cerebral ischemia was induced by direct occlusion of the distal MCA as detailed in previous publications [34-37] with the following modifications. Briefly, mice were anesthetized with ketamine (100 mg/kg) and xylazine (5 mg/kg), and the right MCA was exposed by a 0.5-cm vertical skin incision midway between the right eye and ear. After the temporalis muscle was split, a 2-mm burr hole was drilled at the junction of the zygomatic arch and the squamous bone. While visualizing with a stereomicroscope, the right MCA distal to the lenticulostriate branches was electrocauterized using a microcauterizer. The coagulated MCA segment was then transected with microscissors to verify that the occlusion was permanent. The surgical site was closed with 6-0 sterile nylon sutures, and 4% lidocaine cream was applied. Animals were maintained at 37°C during and after surgery until fully recovered from anesthesia, when they were returned to their cages and allowed free access to food and water. All mice were housed in an air-ventilated room with ambient temperature maintained at 24±0.5°C.

Measurement of Infarct Volume

Twenty-four hours after surgery, the animal was euthanized and the brain was chilled at -70°C for 3 min to slightly harden the tissue. The brain was sliced into 1-mm coronal sections using a brain matrix. Each brain slice was placed in 24 well plates and incubated for 20 min in a solution of 2% TTC in PBS at RT . The sections were then washed twice with PBS and fixed with 10% PBS-buffered formalin. The sections are stored at 4°C. Twenty-four hours after fixation, the caudal face of each section is scanned using a flatbed color scanner. The scanned images are used to determine the infarct volume [98]. ImagePro software is used to calculate the infarcted area of each slice by subtracting the

remaining area of the infarcted hemisphere from the area of the uninfarcted hemisphere to minimize the error that is introduced by edema. The total infarct volumes were calculated by measuring infarct areas on the separate slices, multiplying areas by slice thickness, and summing all slices; this "indirect" morphometric method corrects for edematous swelling [98,99].

Statistical Analysis

Infarct volumes were expressed as mean ± SD and compared among mouse strains using 1-way ANOVA or nonparametric Kruskal–Wallis tests. Heritability H^2 [(genetic (interstrain) variance)/(genetic variance + environmental (intrastrain) variance)] was estimated using 1-way ANOVA.

4.4.4 SNP genotyping

A standard high salt procedure is used to isolate genomic DNA from mouse tails. SNP genotyping is performed using the GoldenGateTM genotyping assay. The Illumina mouse low-density (LD) linkage panel is used, consisting of 377 SNPs covering the entire mouse genome, chosen to be maximally informative in crosses between B6 and other inbred strains. Reported genetic map positions were retrieved from the SNP database (Build 37.1) of NCBI.

Linkage Analysis

Genome-wide scans were plotted using the J/QTL mapping program, version 1.2.1 (http://research.jax.org/faculty/churchill/). Suggestive (*P=0.63*) and significant (*P=0.05*) thresholds were established empirically for each phenotypic trait by 1000 permutation tests using all informative markers [100]. QTL over suggestive threshold value

were named in accordance with the International Committee on Standard Genetic Nomenclature for Mice (http://www.informatics.jax.org/mgihome/nomen). The percentage of total trait variance attributable to each locus was determined using the Fit QTL function provided within the J/QTL software.

5.

Summary and Conclusions

The goal of my dissertation research was to identify natural genetic determinants of cerebral infarction in ischemic stroke. By exploiting the naturally occurring, strain-specific difference in infarct volume through unbiased forward genetic mapping approaches, we aimed to provide insight into novel genetic determinants of ischemic outcomes, as well as to provide insight into understanding of the critical pathophysiological mechanism involved in tissue damage in ischemia. The work described in my dissertation has significantly expanded upon the initial observation on the strain-specific difference in ischemic tissue damage (infarction and limb salvage), by defining and identifying genetic loci, thus providing a new insight into the pathophysiological mechanisms modulating infarction, based on natural, endogenous genetic variation.

Importantly, this work represented clinically relevant phenotype study – infarction in stroke and limb salvage in PAD, with the goal of identifying genes and mechanisms modulating the final outcome of ischemic tissue injury. In the long-term, this work may provide novel targets for therapeutic intervention of ischemic tissue damage associated with human vascular occlusive diseases.

A single locus (*Civq1*/ *Lsq1*) present in multiple inbred strains confers a predominant phenotypic effect on ischemic outcomes

Our studies described in this dissertation have confirmed that the differences in the severity of cerebral infarction after permanent MCAO in the common inbred strains are highly heritable due to natural genetic variation. Through the use of different inbred strains and genetic mapping we provide evidence of 4 distinct QTLs that modulate the volume of cerebral infarction. In particular, a single locus, *Civq1*, mapping to distal chromosome 7 accounts for the major portion of variation in cerebral infarction. These data demonstrate that natural variation in infarct volume is mainly due to DNA sequence variation at a single locus, and possibly at a single gene. These data further suggest the presence of an ancestral allele of the gene determining the outcome of focal cerebral ischemia. The identification of the same QTL in different crosses facilitated the use of ancestral haplotype analysis to greatly reduce the number of potential candidate genes at this locus.

Intriguingly, we have identified that the same locus, *Lsq1*, mapped in the identical position of chromosome 7 also shows a robust phenotypic effect in recovery from hindlimb ischemia. Given the physiological similarities between the two ischemic models and the identical map position, we propose that *Civq*1 and *Lsq1* represent the identical allelic variant in the same causal gene, suggesting that the physiological mechanism behind this particular locus of large effect may be a clinically relevant trait not only to provide insight into pathogenesis of ischemia but also to provide novel targets for therapeutic intervention in human vascular occlusive diseases.

Ancestral haplotype analysis greatly facilitated candidate gene identification

Despite successful detection of many QTLs and the important roles of QTL genes in diseases and traits in rodents and humans, identification of causal genes underlying QTLs has been a major obstacle because of a large confidence interval for the typical QTL. To identify QTL genes, traditional techniques have relied upon genetic methods such as further mapping through the creation of congenic strains [121,122]. However, with the availability of dense SNPs for most of the common inbred strains [123,124], Paigen and colleagues at the Jackson laboratory have demonstrated that the combined cross and complementary bioinformatic analyses based on the assumption that the causal alleles are ancestral significantly narrow down the QTL interval to a few possible candidate genes [79,125].

Similar to these studies, because *Civq1* was identified in 3 different intercrosses and the B6-A/J CSS line, indicating that *Civq1* on chromosome 7 is controlled by ancestral genetic variations common among inbred strains, we were also able to move from a QTL to underlying a few candidate genes. The SNP databases, combined linkage cross, and interval-specific SNP haplotype analysis for *Civq1* provided increased resolution resulting in 5 possible candidate genes. Sequence analysis revealed that 2 of these genes, *Itgal* and *Qprt*, contain coding sequence variants that could explain the QTL. Furthermore, an examination of expression analysis reveals that of the 5 candidate genes, only Itgal is differentially expressed in the brain and there is a consistent pattern whereby the strain with small infarct volume expressed higher *Itgal* mRNA compared with the strains with large infarct phenotype. The differential expression pattern of *Itgal* also co-segregates with the infarct volume phenotypes between relevant strains.

A major physiological mechanism for *Civq1*/ *Lsq1*: Collateral circulation

Our studies described in this dissertation have shown that chromosome 7 (*Civq1*/ *Lsq1*) harbors the major locus for the large difference in infarct volume as well as in limb salvage. The identification of the *Civq1*/ *Lsq1* has raised the question of its associated physiological mechanism and the role of the causative gene in pathophysiology of ischemic diseases. Two broad hypotheses have been put forth to explain the strain-specific effects in infarct volume. The first proposes that differences in infarct volume reflect variation in pre-existing vascular anatomy between the strains. A second suggests that the difference in infarct volume is due to a variation in intrinsic ischemic tolerance or protection pathways in the neural tissue.

Dr. James Faber's group has demonstrated that the extent of pial collateral circulation in the brain is strongly correlated inversely with our infarct volume data for the 15 inbred mouse strains. More importantly, in a F2 intercross between B6 and BALB/c strains, a significant QTL for collateral vessel number was mapped in the identical genomic position of chromosome 7 as *Civq1* maps [92]. Therefore, these data in conjunction with our mapping results for both infarct volume and recovery from hindlimb ischemia strongly suggest that a causative gene for *Civq1*/ *Lsq1* may regulate collateral vessel development and genetic variation in the gene may cause the different extent of blood flow restoration after arterial occlusion, resulting in the differential ischemic outcome.

There is now an extensive body of *in vitro* and *in vivo* evidence that the interaction between circulating blood leukocytes and endothelial cells is a key process of collateral artery growth and development. Collateral vessel growth and proliferation involve endothelial cell activation, basal membrane degradation, leukocyte (ie.

monocytes/macrophages or T lymphocytes) invasion, proliferation of vascular cells, neointima formation (in most species studied), changes of the extracellular matrix and cytokine participation. In line with this, Itgal, thus, represents an attractive candidate gene based on its putative function both in leukocyte migration and in collateral vessel formation. Itgal has been known to be induced by vascular endothelial growth factor (VEGF) and to modulate adhesion of monocytes to collateral endothelium in collateral vessel proliferation. Studies to prove the role of genetic variations in all the candidate genes in the inflammation-mediated vascular remodeling have been planned.

Identification of *Civq4* on chromosome 4 that is not related to the collateral number has provided us with evidence that *Civq1* on chromosome 7 determines infarct volume through the differential collateral circulation after arterial occlusion. However, although it is most likely that a causative gene for *Civq1/Lsq1* may determine collateral artery formation, it is not clear that collateral vessel density ***alone*** can explain the infarct volume difference because other mechanisms contributing to the final outcome of tissue injury could be involved in the locus. Thus, only by genetic dissection of this locus underlying infarct volume and limb salvage can we determine whether *Civq1/Lsq1* regulates collateral vessel density in the tissues. We have generated two reciprocal congenic mouse lines both in B6 and BALB/c backgrounds. The reciprocal congenic lines retaining the infarct volume locus will be used in the analysis of collateral vessel number in order to determine whether *Civq1* for infarct volume regulates collateral vessel formation. These results from using congenic mice will establish the physiological mechanism behind the *Civq1/Lsq1* and confirm the role of the gene underlying the locus in collaterogenesis.

Biomedical significance

Although several therapeutic approaches including reperfusion, neuroprotection, and neuronal regeneration have been proposed, only one treatment is approved for ischemic stroke, the thrombolytic agent tissue plasminogen activator (tPA), but only 2% of ischemic stroke patients receive the benefits from this drug because of the limited administration time and side effects. Over 2 million people worldwide suffer a stroke annually, and it is the leading cause of adult disability in the US and Europe, as well as the third leading cause of death, but for the vast majority of patients, little is done to limit ischemic stroke damage. Besides many issues related to effectiveness and efficiency of the therapeutic approaches, we reasoned that given the multiplicity of mechanisms causing cell death in stroke, perhaps approaches that seek to augment endogenous protective pathways might be more likely to succeed.

In this light, we aimed to investigate genetic factors contributing to this clinically relevant phenotype by exploiting naturally occurring endogenous genetic variations determining ischemic tissue damage. In contrast to the genetic risk factor for stroke susceptibility, our proposal represents a *stroke outcome* study, with the goal of identifying genes and mechanisms modulating the final outcome of ischemic tissue damage. However, it would be very difficult to perform a similar ischemic stroke outcome study in a human cohort. Variation in the anatomic location of the occluded artery, the extent of occlusion, the severity of the ischemia, the duration of time of the stroke until treatment and many other factors are not easily controlled in patients. These variables could seriously confound a genetic study on infarct volume in ischemic stroke patients, and potentially mask genetic risk factors for infarct outcomes. By contrast, these factors are easily controlled using our experimental system in the mouse. By

exploiting natural variation in infarct volume and limb salvage in different mouse strains in the experimental models of ischemia, we identified multiple genetic loci of the highly variable outcome of infarct volume. Importantly, our *Civq* loci do not map to regions of conserved synteny for any of the loci mapped for human stroke susceptibility, illustrating distinct genetic contributions to stroke susceptibility versus stroke outcomes.

Finally, we believe this study will be directly relevant to human ischemic stroke. Despite years of study, the biological events that lead to differences in infarction are not fully understood. The research described in my dissertation will provide insight into the biochemical pathways modulating infarction, based on natural endogenous variation in a genetically tractable mammal. *These genes are not likely to be identified directly in human stroke patients, but the pathways controlling infarction are likely to be conserved across related species.* Identification of the underlying genes will provide a better understanding of the innate processes modulating ischemic tissue damage in the brain, peripheral limbs, and possibly other tissues and organs. The gene underlying *Civq1*/ *Lsq1* may provide novel targets for therapeutic intervention in human vascular occlusive diseases.

Reference

1. Dokun, A.O., *et al.* A quantitative trait locus (LSq-1) on mouse chromosome 7 is linked to the absence of tissue loss after surgical hindlimb ischemia. *Circulation* **117**, 1207-1215 (2008).

2. Thorvaldsen, P., *et al.* Stroke trends in the WHO MONICA project. *Stroke* **28**, 500-506 (1997).

3. McCullough, L.D. & Hurn, P.D. Estrogen and ischemic neuroprotection: an integrated view. *Trends Endocrinol Metab* **14**, 228-235 (2003).

4. Jamrozik, K., Broadhurst, R.J., Anderson, C.S. & Stewart-Wynne, E.G. The role of lifestyle factors in the etiology of stroke. A population-based case-control study in Perth, Western Australia. *Stroke* **25**, 51-59 (1994).

5. Dichgans, M. Genetics of ischaemic stroke. *Lancet Neurol* **6**, 149-161 (2007).

6. Gretarsdottir, S., *et al.* The gene encoding phosphodiesterase 4D confers risk of ischemic stroke. *Nat Genet* **35**, 131-138 (2003).

7. Helgadottir, A., *et al.* The gene encoding 5-lipoxygenase activating protein confers risk of myocardial infarction and stroke. *Nat Genet* **36**, 233-239 (2004).

8. Lohmussaar, E., *et al.* ALOX5AP gene and the PDE4D gene in a central European population of stroke patients. *Stroke* **36**, 731-736 (2005).

9. Rosand, J., Bayley, N., Rost, N. & de Bakker, P.I. Many hypotheses but no replication for the association between PDE4D and stroke. *Nat Genet* **38**, 1091-1092; author reply 1092-1093 (2006).

10. Hata, J., *et al.* Functional SNP in an Sp1-binding site of AGTRL1 gene is associated with susceptibility to brain infarction. *Hum Mol Genet* **16**, 630-639 (2007).

11. Kubo, M., *et al.* A nonsynonymous SNP in PRKCH (protein kinase C eta) increases the risk of cerebral infarction. *Nat Genet* **39**, 212-217 (2007).

12. Liu, Y., *et al.* Apolipoprotein E polymorphism and acute ischemic stroke: a diffusion- and perfusion-weighted magnetic resonance imaging study. *J Cereb Blood Flow Metab* **22**, 1336-1342 (2002).

13. Mori, K., *et al.* L-serine-mediated release of apolipoprotein E and lipids from microglial cells. *Exp Neurol* **185**, 220-231 (2004).

14. Dunn, L.T., Stewart, E., Murray, G.D., Nicoll, J.A. & Teasdale, G.M. The influence of apolipoprotein E genotype on outcome after spontaneous subarachnoid

hemorrhage: a preliminary study. *Neurosurgery* **48**, 1006-1010; discussion 1010-1001 (2001).

15. McCarron, M.O., Delong, D. & Alberts, M.J. APOE genotype as a risk factor for ischemic cerebrovascular disease: a meta-analysis. *Neurology* **53**, 1308-1311 (1999).

16. Rubattu, S., *et al.* Chromosomal mapping of quantitative trait loci contributing to stroke in a rat model of complex human disease. *Nat Genet* **13**, 429-434 (1996).

17. Jeffs, B., *et al.* Sensitivity to cerebral ischaemic insult in a rat model of stroke is determined by a single genetic locus. *Nat Genet* **16**, 364-367 (1997).

18. Hossmann, K.A. Pathophysiology and therapy of experimental stroke. *Cell Mol Neurobiol* **26**, 1057-1083 (2006).

19. Astrup, J., Siesjo, B.K. & Symon, L. Thresholds in cerebral ischemia - the ischemic penumbra. *Stroke* **12**, 723-725 (1981).

20. Ginsberg, M.D. Adventures in the pathophysiology of brain ischemia: penumbra, gene expression, neuroprotection: the 2002 Thomas Willis Lecture. *Stroke* **34**, 214-223 (2003).

21. Lo, E.H. A new penumbra: transitioning from injury into repair after stroke. *Nat Med* **14**, 497-500 (2008).

22. Schaper, W. Collateral circulation: past and present. *Basic Res Cardiol* **104**, 5-21 (2009).

23. Liebeskind, D.S. Collateral circulation. *Stroke* **34**, 2279-2284 (2003).

24. Helisch, A. & Schaper, W. Arteriogenesis: the development and growth of collateral arteries. *Microcirculation* **10**, 83-97 (2003).

25. Gidday, J.M. Cerebral preconditioning and ischaemic tolerance. *Nat Rev Neurosci* **7**, 437-448 (2006).

26. Purcell, J.E., *et al.* Strain-dependent response to cerebral ischemic preconditioning: differences between spontaneously hypertensive and stroke prone spontaneously hypertensive rats. *Neurosci Lett* **339**, 151-155 (2003).

27. Rajdev, S., *et al.* Mice overexpressing rat heat shock protein 70 are protected against cerebral infarction. *Ann Neurol* **47**, 782-791 (2000).

28. Martinou, J.C., *et al.* Overexpression of BCL-2 in transgenic mice protects neurons from naturally occurring cell death and experimental ischemia. *Neuron* **13**, 1017-1030 (1994).

29. Wiessner, C., *et al.* Neuron-specific transgene expression of Bcl-XL but not Bcl-2 genes reduced lesion size after permanent middle cerebral artery occlusion in mice. *Neurosci Lett* **268**, 119-122 (1999).

30. Kermer, P., *et al.* BAG1 over-expression in brain protects against stroke. *Brain Pathol* **13**, 495-506 (2003).

31. Zemke, D., Smith, J.L., Reeves, M.J. & Majid, A. Ischemia and ischemic tolerance in the brain: an overview. *Neurotoxicology* **25**, 895-904 (2004).

32. Carmichael, S.T. Rodent models of focal stroke: size, mechanism, and purpose. *NeuroRx* **2**, 396-409 (2005).

33. Virley, D. Choice, methodology, and characterization of focal ischemic stroke models: the search for clinical relevance. *Methods Mol Med* **104**, 19-48 (2005).

34. Majid, A., *et al.* Differences in vulnerability to permanent focal cerebral ischemia among 3 common mouse strains. *Stroke* **31**, 2707-2714 (2000).

35. Lambertsen, K.L., Gregersen, R. & Finsen, B. Microglial-macrophage synthesis of tumor necrosis factor after focal cerebral ischemia in mice is strain dependent. *J Cereb Blood Flow Metab* **22**, 785-797 (2002).

36. Sugimori, H., Yao, H., Ooboshi, H., Ibayashi, S. & Iida, M. Krypton laser-induced photothrombotic distal middle cerebral artery occlusion without craniectomy in mice. *Brain Res Brain Res Protoc* **13**, 189-196 (2004).

37. Kuraoka, M., *et al.* Direct experimental occlusion of the distal middle cerebral artery induces high reproducibility of brain ischemia in mice. *Exp Anim* **58**, 19-29 (2009).

38. Hossmann, K.A. Genetically modified animals in molecular stroke research. *Acta Neurochir Suppl* **89**, 37-45 (2004).

39. Green, A.R. & Shuaib, A. Therapeutic strategies for the treatment of stroke. *Drug Discov Today* **11**, 681-693 (2006).

40. Barone, F.C., Knudsen, D.J., Nelson, A.H., Feuerstein, G.Z. & Willette, R.N. Mouse strain differences in susceptibility to cerebral ischemia are related to cerebral vascular anatomy. *J Cereb Blood Flow Metab* **13**, 683-692 (1993).

41. Keum, S. & Marchuk, D.A. A locus mapping to mouse chromosome 7 determines infarct volume in a mouse model of ischemic stroke. *Circ Cardiovasc Genet* **2**, 591-598 (2009).

42. Lambertsen, K.L., Meldgaard, M., Ladeby, R. & Finsen, B. A quantitative study of microglial-macrophage synthesis of tumor necrosis factor during acute and late focal cerebral ischemia in mice. *J Cereb Blood Flow Metab* **25**, 119-135 (2005).

43. Frazer, K.A., *et al.* A sequence-based variation map of 8.27 million SNPs in inbred mouse strains. *Nature* **448**, 1050-1053 (2007).

44. Yang, H., Bell, T.A., Churchill, G.A. & Pardo-Manuel de Villena, F. On the subspecific origin of the laboratory mouse. *Nat Genet* **39**, 1100-1107 (2007).
45. Singer, J.B., *et al.* Genetic dissection of complex traits with chromosome substitution strains of mice. *Science* **304**, 445-448 (2004).

46. Belknap, J.K. Chromosome substitution strains: some quantitative considerations for genome scans and fine mapping. *Mamm Genome* **14**, 723-732 (2003).

47. Wang, D. & You, M. Five loci, SLT1 to SLT5, controlling the susceptibility to spontaneously occurring lung cancer in mice. *Cancer Res* **65**, 8158-8165 (2005).

48. Liu, P., *et al.* Candidate lung tumor susceptibility genes identified through whole-genome association analyses in inbred mice. *Nat Genet* **38**, 888-895 (2006).

49. Fenske, T.S., *et al.* Identification of candidate alkylator-induced cancer susceptibility genes by whole genome scanning in mice. *Cancer Res* **66**, 5029-5038 (2006).

50. Pletcher, M.T., *et al.* Use of a dense single nucleotide polymorphism map for in silico mapping in the mouse. *PLoS Biol* **2**, e393 (2004).

51. Manenti, G., *et al.* Mouse genome-wide association mapping needs linkage analysis to avoid false-positive Loci. *PLoS Genet* **5**, e1000331 (2009).

52. DiPetrillo, K., Wang, X., Stylianou, I.M. & Paigen, B. Bioinformatics toolbox for narrowing rodent quantitative trait loci. *Trends Genet* **21**, 683-692 (2005).

53. Flint, J., Valdar, W., Shifman, S. & Mott, R. Strategies for mapping and cloning quantitative trait genes in rodents. *Nat Rev Genet* **6**, 271-286 (2005).

54. Doong, H., *et al.* CAIR-1/BAG-3 forms an EGF-regulated ternary complex with phospholipase C-gamma and Hsp70/Hsc70. *Oncogene* **19**, 4385-4395 (2000).

55. Doong, H., *et al.* CAIR-1/BAG-3 abrogates heat shock protein-70 chaperone complex-mediated protein degradation: accumulation of poly-ubiquitinated Hsp90 client proteins. *J Biol Chem* **278**, 28490-28500 (2003).

56. Homma, S., *et al.* BAG3 deficiency results in fulminant myopathy and early lethality. *Am J Pathol* **169**, 761-773 (2006).

57. Attree, O., *et al.* The Lowe's oculocerebrorenal syndrome gene encodes a protein highly homologous to inositol polyphosphate-5-phosphatase. *Nature* **358**, 239-242 (1992).

58. Zhu, W., *et al.* Inpp5f is a polyphosphoinositide phosphatase that regulates cardiac hypertrophic responsiveness. *Circ Res* **105**, 1240-1247 (2009).

59. Kveiborg, M., Albrechtsen, R., Couchman, J.R. & Wewer, U.M. Cellular roles of ADAM12 in health and disease. *Int J Biochem Cell Biol* **40**, 1685-1702 (2008).

60. Kurisaki, T., *et al.* Phenotypic analysis of Meltrin alpha (ADAM12)-deficient mice: involvement of Meltrin alpha in adipogenesis and myogenesis. *Mol Cell Biol* **23**, 55-61 (2003).

61. Enattah, N.S., *et al.* Identification of a variant associated with adult-type hypolactasia. *Nat Genet* **30**, 233-237 (2002).

62. Lewinsky, R.H., *et al.* T-13910 DNA variant associated with lactase persistence interacts with Oct-1 and stimulates lactase promoter activity in vitro. *Hum Mol Genet* **14**, 3945-3953 (2005).

63. Aznarez, I., *et al.* A systematic analysis of intronic sequences downstream of 5' splice sites reveals a widespread role for U-rich motifs and TIA1/TIAL1 proteins in alternative splicing regulation. *Genome Res* **18**, 1247-1258 (2008).

64. Zheng, Z., Zheng, H. & Yan, W. Fank1 is a testis-specific gene encoding a nuclear protein exclusively expressed during the transition from the meiotic to the haploid phase of spermatogenesis. *Gene Expr Patterns* **7**, 777-783 (2007).

65. Albert, M.L., Kim, J.I. & Birge, R.B. alphavbeta5 integrin recruits the CrkII-Dock180-rac1 complex for phagocytosis of apoptotic cells. *Nat Cell Biol* **2**, 899-905 (2000).

66. Moore, C.A., Parkin, C.A., Bidet, Y. & Ingham, P.W. A role for the Myoblast city homologues Dock1 and Dock5 and the adaptor proteins Crk and Crk-like in zebrafish myoblast fusion. *Development* **134**, 3145-3153 (2007).

67. Yang, S. & Li, Y.P. RGS10-null mutation impairs osteoclast differentiation resulting from the loss of [Ca2+]i oscillation regulation. *Genes Dev* **21**, 1803-1816 (2007).

68. Bender, K., *et al.* A role for RGS10 in beta-adrenergic modulation of G-protein-activated K+ (GIRK) channel current in rat atrial myocytes. *J Physiol* **586**, 2049-2060 (2008).

69. Thomas, P.D. & Kejariwal, A. Coding single-nucleotide polymorphisms associated with complex vs. Mendelian disease: evolutionary evidence for differences in molecular effects. *Proc Natl Acad Sci U S A* **101**, 15398-15403 (2004).

70. Bonelli, P., *et al.* BAG3 protein regulates stress-induced apoptosis in normal and neoplastic leukocytes. *Leukemia* **18**, 358-360 (2004).

71. Rosati, A., *et al.* Apoptosis inhibition in cancer cells: a novel molecular pathway that involves BAG3 protein. *Int J Biochem Cell Biol* **39**, 1337-1342 (2007).

72. Lee, J.H., *et al.* Bis, a Bcl-2-binding protein that synergizes with Bcl-2 in preventing cell death. *Oncogene* **18**, 6183-6190 (1999).

73. Antoku, K., Maser, R.S., Scully, W.J., Jr., Delach, S.M. & Johnson, D.E. Isolation of Bcl-2 binding proteins that exhibit homology with BAG-1 and suppressor of death domains protein. *Biochem Biophys Res Commun* **286**, 1003-1010 (2001).

74. Iwasaki, M., *et al.* BAG3 regulates motility and adhesion of epithelial cancer cells. *Cancer Res* **67**, 10252-10259 (2007).

75. Wang, X., Korstanje, R., Higgins, D. & Paigen, B. Haplotype analysis in multiple crosses to identify a QTL gene. *Genome Res* **14**, 1767-1772 (2004).

76. Park, Y.G., Clifford, R., Buetow, K.H. & Hunter, K.W. Multiple cross and inbred strain haplotype mapping of complex-trait candidate genes. *Genome Res* **13**, 118-121 (2003).

77. Li, R., Lyons, M.A., Wittenburg, H., Paigen, B. & Churchill, G.A. Combining data from multiple inbred line crosses improves the power and resolution of quantitative trait loci mapping. *Genetics* **169**, 1699-1709 (2005).

78. Manichaikul, A., Dupuis, J., Sen, S. & Broman, K.W. Poor performance of bootstrap confidence intervals for the location of a quantitative trait locus. *Genetics* **174**, 481-489 (2006).

79. Burgess-Herbert, S.L., Cox, A., Tsaih, S.W. & Paigen, B. Practical applications of the bioinformatics toolbox for narrowing quantitative trait loci. *Genetics* **180**, 2227-2235 (2008).

80. Wade, C.M., *et al.* The mosaic structure of variation in the laboratory mouse genome. *Nature* **420**, 574-578 (2002).

81. Wiltshire, T., *et al.* Genome-wide single-nucleotide polymorphism analysis defines haplotype patterns in mouse. *Proc Natl Acad Sci U S A* **100**, 3380-3385 (2003).

82. Luo, B.H., Carman, C.V. & Springer, T.A. Structural basis of integrin regulation and signaling. *Annu Rev Immunol* **25**, 619-647 (2007).

83. Arumugam, T.V., *et al.* Contributions of LFA-1 and Mac-1 to brain injury and microvascular dysfunction induced by transient middle cerebral artery occlusion. *Am J Physiol Heart Circ Physiol* **287**, H2555-2560 (2004).

84. Heil, M., *et al.* Vascular endothelial growth factor (VEGF) stimulates monocyte migration through endothelial monolayers via increased integrin expression. *Eur J Cell Biol* **79**, 850-857 (2000).

85. Hoefer, I.E., *et al.* Leukocyte subpopulations and arteriogenesis: specific role of monocytes, lymphocytes and granulocytes. *Atherosclerosis* **181**, 285-293 (2005).

86. Heil, M. & Schaper, W. Influence of mechanical, cellular, and molecular factors on collateral artery growth (arteriogenesis). *Circ Res* **95**, 449-458 (2004).

87. Stone, T.W. & Darlington, L.G. Endogenous kynurenines as targets for drug discovery and development. *Nat Rev Drug Discov* **1**, 609-620 (2002).

88. Ryu, J.K., Jantaratnotai, N. & McLarnon, J.G. Thalidomide inhibition of vascular remodeling and inflammatory reactivity in the quinolinic acid-injected rat striatum. *Neuroscience* **163**, 601-608 (2009).

89. Cowles, C.R., Hirschhorn, J.N., Altshuler, D. & Lander, E.S. Detection of regulatory variation in mouse genes. *Nat Genet* **32**, 432-437 (2002).

90. Yao, H., Cui, Z.H., Masuda, J. & Nabika, T. Congenic removal of a QTL for blood pressure attenuates infarct size produced by middle cerebral artery occlusion in hypertensive rats. *Physiol Genomics* **30**, 69-73 (2007).

91. Chalothorn, D., Clayton, J.A., Zhang, H., Pomp, D. & Faber, J.E. Collateral density, remodeling, and VEGF-A expression differ widely between mouse strains. *Physiol Genomics* **30**, 179-191 (2007).

92. Zhang, H., Prabhakar, P., Sealock, R. & Faber, J.E. Wide genetic variation in the native pial collateral circulation is a major determinant of variation in severity of stroke. *J Cereb Blood Flow Metab* (2010).

93. van Oostrom, M.C., van Oostrom, O., Quax, P.H., Verhaar, M.C. & Hoefer, I.E. Insights into mechanisms behind arteriogenesis: what does the future hold? *J Leukoc Biol* **84**, 1379-1391 (2008).

94. Barres, B.A. The mystery and magic of glia: a perspective on their roles in health and disease. *Neuron* **60**, 430-440 (2008).

95. Lo, E.H. & Rosenberg, G.A. The neurovascular unit in health and disease: introduction. *Stroke* **40**, S2-3 (2009).

96. Tadokoro, S.*, et al.* A Gln747-->Pro substitution in the IIb subunit is responsible for a moderate IIbbeta3 deficiency in Glanzmann thrombasthenia. *Blood* **92**, 2750-2758 (1998).

97. Darlington, L.G.*, et al.* Altered kynurenine metabolism correlates with infarct volume in stroke. *Eur J Neurosci* **26**, 2211-2221 (2007).

98. Wexler, E.J.*, et al.* An objective procedure for ischemic area evaluation of the stroke intraluminal thread model in the mouse and rat. *J Neurosci Methods* **113**, 51-58 (2002).

99. Goldlust, E.J., Paczynski, R.P., He, Y.Y., Hsu, C.Y. & Goldberg, M.P. Automated measurement of infarct size with scanned images of triphenyltetrazolium chloride-stained rat brains. *Stroke* **27**, 1657-1662 (1996).

100. Lander, E. & Kruglyak, L. Genetic dissection of complex traits: guidelines for interpreting and reporting linkage results. *Nat Genet* **11**, 241-247 (1995).

101. Fukino, K., Sata, M., Seko, Y., Hirata, Y. & Nagai, R. Genetic background influences therapeutic effectiveness of VEGF. *Biochem Biophys Res Commun* **310**, 143-147 (2003).

102. Scholz, D., *et al.* Contribution of arteriogenesis and angiogenesis to postocclusive hindlimb perfusion in mice. *J Mol Cell Cardiol* **34**, 775-787 (2002).

103. Helisch, A., *et al.* Impact of mouse strain differences in innate hindlimb collateral vasculature. *Arterioscler Thromb Vasc Biol* **26**, 520-526 (2006).

104. Resnick, H.E., *et al.* Apo E genotype, diabetes, and peripheral arterial disease in older men: the Honolulu Asia-aging study. *Genet Epidemiol* **19**, 52-63 (2000).

105. Flex, A., *et al.* The -174 G/C polymorphism of the interleukin-6 gene promoter is associated with peripheral artery occlusive disease. *Eur J Vasc Endovasc Surg* **24**, 264-268 (2002).

106. Reny, J.L., *et al.* The factor II G20210A gene polymorphism, but not factor V Arg506Gln, is associated with peripheral arterial disease: results of a case-control study. *J Thromb Haemost* **2**, 1334-1340 (2004).

107. Fontana, P., *et al.* P2Y12 H2 haplotype is associated with peripheral arterial disease: a case-control study. *Circulation* **108**, 2971-2973 (2003).

108. Gudmundsson, G., *et al.* Localization of a gene for peripheral arterial occlusive disease to chromosome 1p31. *Am J Hum Genet* **70**, 586-592 (2002).

109. van Weel, V., *et al.* Natural killer cells and CD4+ T-cells modulate collateral artery development. *Arterioscler Thromb Vasc Biol* **27**, 2310-2318 (2007).

110. Hazarika, S., *et al.* Impaired angiogenesis after hindlimb ischemia in type 2 diabetes mellitus: differential regulation of vascular endothelial growth factor receptor 1 and soluble vascular endothelial growth factor receptor 1. *Circ Res* **101**, 948-956 (2007).

111. Li, Y., *et al.* In mice with type 2 diabetes, a vascular endothelial growth factor (VEGF)-activating transcription factor modulates VEGF signaling and induces therapeutic angiogenesis after hindlimb ischemia. *Diabetes* **56**, 656-665 (2007).

112. Jacobi, J., *et al.* Nicotine accelerates angiogenesis and wound healing in genetically diabetic mice. *Am J Pathol* **161**, 97-104 (2002).

113. Ilic, V., *et al.* Syphacia obvelata modifies mitogen-activated protein kinases and nitric oxide synthases expression in murine bone marrow cells. *Parasitol Int* **59**, 82-88 (2010).

114. Bugarski, D., *et al.* Hematopoietic changes and altered reactivity to IL-17 in Syphacia obvelata-infected mice. *Parasitol Int* **55**, 91-97 (2006).

115. Zintzaras, E. & Kitsios, G. Identification of chromosomal regions linked to premature myocardial infarction: a meta-analysis of whole-genome searches. *J Hum Genet* **51**, 1015-1021 (2006).

116. Thurston, G., Murphy, T.J., Baluk, P., Lindsey, J.R. & McDonald, D.M. Angiogenesis in mice with chronic airway inflammation: strain-dependent differences. *Am J Pathol* **153**, 1099-1112 (1998).

117. Korshunov, V.A. & Berk, B.C. Strain-dependent vascular remodeling: the "Glagov phenomenon" is genetically determined. *Circulation* **110**, 220-226 (2004).

118. Harmon, K.J., Couper, L.L. & Lindner, V. Strain-dependent vascular remodeling phenotypes in inbred mice. *Am J Pathol* **156**, 1741-1748 (2000).

119. Dodd-o, J.M., Hristopoulos, M.L., Welsh-Servinsky, L.E., Tankersley, C.G. & Pearse, D.B. Strain-specific differences in sensitivity to ischemia-reperfusion lung injury in mice. *J Appl Physiol* **100**, 1590-1595 (2006).

120. Liu, J., Kershaw, W.C., Liu, Y.P. & Klaassen, C.D. Cadmium-induced hepatic endothelial cell injury in inbred strains of mice. *Toxicology* **75**, 51-62 (1992).

121. Darvasi, A. Interval-specific congenic strains (ISCS): an experimental design for mapping a QTL into a 1-centimorgan interval. *Mamm Genome* **8**, 163-167 (1997).

122. Gale, G.D., *et al.* A genome-wide panel of congenic mice reveals widespread epistasis of behavior quantitative trait loci. *Mol Psychiatry* **14**, 631-645 (2009).

123. Frazer, K.A., *et al.* A second generation human haplotype map of over 3.1 million SNPs. *Nature* **449**, 851-861 (2007).

124. Szatkiewicz, J.P., *et al.* An imputed genotype resource for the laboratory mouse. *Mamm Genome* **19**, 199-208 (2008).

125. Su, Z., *et al.* Four additional mouse crosses improve the lipid QTL landscape and identify Lipg as a QTL gene. *J Lipid Res* (2009).

BIOGRAPHY

Sehoon Keum was born in Seoul, South Korea on January 27, 1976. He graduated from Janghoon High School in Seoul in 1994. In 1998, he graduated *magna cum laude* from Hanyang University in Seoul, South Korea with a Bachelor of Science degree in Biology. In 2000, he earned a Master of Science degree in Neurogenetics from Pohang University of Science and Technology (POSTECH), Pohang, South Korea under the supervision of Dr. Hee-Sup Shin. For the next five years he worked as a researcher in a pharmaceutical research institute of Yuhan Corp., Goonpo, South Korea. In 2005, Sehoon enrolled the University Program in Genetics and Genomics at Duke University, Durham, North Carolina. In 2008, he was awarded an American Heart Association Predoctoral Fellowship for his research in Dr. Douglas A. Marchuk's laboratory where he pursued his Ph.D., awarded in May of 2010.

Publications

Keum S and Marchuk DA. A locus mapping to mouse chromosome 7 determines infarct volume in a mouse model of ischemic stroke. *Circ. Cardiovasc. Genet.* 2009 Dec;2:591-598.

Zhang H, **Keum S**, Marchuk DA, Sealock R, Faber JE. Analysis of 19 mouse strains demonstrates that genetic variations in pial collateral dimensions are the major determinants of severity of infarct volume after middle cerebral artery occlusion (MCAO). *Cardiovasc. Revasc. Med*. 2009 Sept;10(4): 273-274.

Dokun AO*, **Keum S***, Hazarika S, Li Y, LaMonte GM, Wheeler F, Marchuk DA, Annex BH. A QTL (LSq-1) on mouse chromosome 7 is linked to prevention of tissue loss following surgical hind-limb ischemia. *Circulation*. 2008 Mar;117(9):1207-15. *Equal contribution.

Kim D, Song I, **Keum S**, Lee T, Jeong MJ, Kim SS, McEnery MW, Shin HS. Lack of the burst firing of thalamocortical relay neurons and resistance to absence seizures in mice lacking alpha(1G) T-type Ca(2+) channels. *Neuron*. 2001 Jul;31(1):35-45